Chem Soc Rev

REVIEW ARTICLE

View Article Online
View Journal | View Issue

Cite this: *Chem. Soc. Rev.*, 2024, 53, 84

Reactivity of metal–oxo clusters towards biomolecules: from discrete polyoxometalates to metal–organic frameworks

David E. Salazar Marcano, † Nada D. Savić, † Kilian Declerck, † Shorok A. M. Abdelhameed and Tatjana N. Parac-Vogt *

Metal–oxo clusters hold great potential in several fields such as catalysis, materials science, energy storage, medicine, and biotechnology. These nanoclusters of transition metals with oxygen-based ligands have also shown promising reactivity towards several classes of biomolecules, including proteins, nucleic acids, nucleotides, sugars, and lipids. This reactivity can be leveraged to address some of the most pressing challenges we face today, from fighting various diseases, such as cancer and viral infections, to the development of sustainable and environmentally friendly energy sources. For instance, metal–oxo clusters and related materials have been shown to be effective catalysts for biomass conversion into renewable fuels and platform chemicals. Furthermore, their reactivity towards biomolecules has also attracted interest in the development of inorganic drugs and bioanalytical tools. Additionally, the structural versatility of metal–oxo clusters allows for the efficiency and selectivity of the biomolecular reactions they promote to be readily tuned, thereby providing a pathway towards reaction optimization. The properties of the catalyst can also be improved through incorporation into solid supports or by linking metal–oxo clusters together to form Metal–Organic Frameworks (MOFs), which have been demonstrated to be powerful heterogeneous catalysts. Therefore, this review aims to provide a comprehensive and critical analysis of the state of the art on biomolecular transformations promoted by metal–oxo clusters and their applications, with a particular focus on structure–activity relationships.

Received 5th September 2023

DOI: 10.1039/d3cs00195d

rsc.li/chem-soc-rev

1. Introduction

Living organisms are essentially highly complex bioreactors in which many biomolecular reactions take place simultaneously at all times to sustain the processes necessary for life. Therefore, the covalent bonds in biomolecules are regularly being broken and formed, typically using enzymes as catalysts.[1–4] For instance, the biological processes involved in the encoding, decoding, replication, and repair of genetic information rely on the formation and cleavage of phosphoester bonds that form the backbone of nucleic acids.[5,6] Furthermore, during translation of this genetic material, the information contained in messenger RNA is used to combine amino acids into proteins *via* peptide bond formation.[7,8] The amino acid building blocks needed for this process can be obtained by the reverse reaction, through the hydrolysis of peptide bonds in ingested or old proteins.[9,10] Moreover, the energy needed for many biological processes to occur, such as transcription and translation, is obtained through hydrolysis of the phosphoanhydride bond in nucleotides.[11,12] Organisms can also store this energy within polysaccharides, composed of monosaccharides connected by glycosidic bonds, or lipids, such as triglycerides that consist of fatty acids linked to glycerol *via* ester bonds. The glycosidic and ester bonds in carbohydrates and lipids, respectively, can then be broken down to release monosaccharides and fatty acids, which can eventually be converted into energy.[13–15] These are just a few examples of the many biomolecular transformations involving common specific bond types that determine the structural composition of some of the most important biomolecules and their function. Hence, one of the main challenges in (bio)chemistry is being able to reproduce these biomolecular reactions *in vitro*, in order to understand the function, properties, and biochemical transformations of biomolecules. Such knowledge can be further leveraged for the formation of pharmaceuticals, biofuel production, and the synthesis of other industrially relevant products, among many other possible applications.[16–20]

Many biomolecular transformations in living organisms are performed by metalloenzymes, which incorporate metal cofactors within proteins. For instance, most hydrolytic reactions are

Department of Chemistry, KU Leuven, Celestijnenlaan 200F, 3001 Leuven, Belgium. E-mail: tatjana.vogt@kuleuven.be

† These authors contributed equally.

catalyzed by zinc-containing proteins such as the enzyme carboxypeptidase A, which specifically removes C-terminal amino acid residues from a given peptide chain.[21] Furthermore, metalloenzymes can employ single metallic centers or multimetallic clusters depending on the desired reactivity. For example, alkaline phosphatases use a combination of zinc and magnesium centers for dephosphorylation, while the multi-enzyme complex photosystem II contains a unique Mn_4CaO_5 metal–oxo cluster that performs a water-splitting reaction during photosynthesis.[22,23] The presence of these metallic clusters and their composition is often key to achieving the desired reactivity. Hence, this has inspired the study of metallic clusters as biomimetic catalysts for a wide range of reactions.

Metal–oxo clusters (MOCs), which are nanostructures composed of multiple metal centers linked *via* bridging oxygen atoms, have attracted attention for their use as catalysts with promising enzyme-like activity in a wide array of reactions.[24] MOCs can be regarded as discrete units of metal oxides with similar structural and electronic properties, making them interesting model systems for metal oxide nanoparticles and surfaces, especially since they are typically relatively stable in solution as single molecules, and are, therefore, easier to study

David E. Salazar Marcano

David E. Salazar Marcano is a post-doctoral researcher in the Laboratory of Bioinorganic Chemistry at KU Leuven. After obtaining a master's degree in Chemistry in 2018 from the University of Southampton, he completed his PhD in Chemistry at KU Leuven as an FWO fellow under the supervision of Prof. Tatjana N. Parac-Vogt. He is currently developing new hybrid (bio)materials based on polyoxometalates as well as investigating the reactivity of these nanoclusters towards proteins.

Nada D. Savić

Nada D. Savić is an FWO senior researcher in the Laboratory of Bioinorganic Chemistry at KU Leuven. After obtaining her PhD in Serbia in 2019, she moved to the group of Prof. Tatjana N. Parac-Vogt in Belgium. Her research interest is focused on creating regioselective and tunable synthetic proteases based on metal-substituted polyoxometalates and metal–oxo clusters for the hydrolysis of amphiphilic, insoluble and biologically related proteins.

Kilian Declerck

Kilian Declerck received his master's degree in Biochemistry & Biotechnology from KU Leuven in 2022. He is currently a PhD student in the Laboratory of Bioinorganic Chemistry, working on the development of discrete metal–oxo clusters and metal–organic layers as artificial nanozymes for catalysis of biochemical transformations, under the supervision of Prof. Tatjana N. Parac-Vogt.

Shorok A. M. Abdelhameed

Shorok A. M. Abdelhameed obtained her master's degree in Chemistry from KU Leuven. She then completed her PhD as an FWO fellow at KU Leuven in the Laboratory of Bioinorganic Chemistry under the supervision of Prof. Tatjana N. Parac-Vogt in 2022. Her PhD research centered around exploring the redox reactions of metal-substituted polyoxometalates towards proteins.

Tatjana N. Parac-Vogt

Tatjana N. Parac-Vogt is a full Professor of Chemistry and head of the Laboratory of Bioinorganic Chemistry at KU Leuven. She leads an interdisciplinary team performing research at the interface of inorganic chemistry, biochemistry, materials science, and catalysis. She is the recipient of the IUPAC 2023 Distinguished Women in Chemistry/Chemical Engineering award. Tatjana is also a Fellow of the Royal Society of Chemistry and has been elected as a Chemistry Europe Fellow (Class 2020/2021), the highest award given by an association of European chemical societies.

than insoluble and relatively complex MO_x solid materials.[25–27] Moreover, MOCs display significant structural versatility, which can be used to tune their catalytic properties. MOCs are typically categorized based on their charge as these clusters can be anionic, neutral, or cationic depending on their structure and composition.

Anionic MOCs are commonly known as polyoxometalates (POMs), which are typically formed by group V and VI transition metals in their highest oxidation states. POMs can take a wide variety of structures with different shapes and sizes that have distinct chemical and physical properties. Moreover, almost any other element in the periodic table can be incorporated into POM structures allowing for additional versatility in their properties. These anionic nanoclusters are primarily composed of metal centers (typically V^{5+}, Mo^{6+}, or W^{6+}) in octahedral coordination that are bound to terminal and bridging oxo ligands (formally O^{2-}). Some of the most commonly explored POMs, especially for catalytic applications, are the Lindqvist ($[A_6O_{19}]^{n-}$), Keggin ($[EA_{12}O_{40}]^{n-}$), and Wells–Dawson ($[E_2A_{18}O_{62}]^{n-}$) structures (E = P, Si, *etc.*; A = typically V, Mo, or W) shown in Fig. 1. Other transition metals can also be incorporated into POM structures *via* replacement of some of the metal centers and their corresponding oxo ligands to form metal-substituted POMs (M–POMs) *via* lacunary POMs (Fig. 1(d) and (e)). Due to this structural versatility, POMs have been developed as catalysts for a vast range of reactions such as hydrogen evolution, water oxidation, and photoreduction of CO_2, which are key in developing sustainable solutions to climate change.[28] They have also been shown to be particularly suitable as acid catalysts towards a diverse set of molecules, by taking advantage of their Brønsted acidity or by exploiting the Lewis acidity of the metal centers in the POM structure.[29] Moreover, in recent years, the reactivity of POMs towards biomolecules has been increasingly investigated, demonstrating their ability to cleave many biologically relevant bonds such as phosphoester, peptide, phosphoanhydride, and glycosidic bonds.

Cationic MOCs are typically stabilized by organic or inorganic ligands, resulting in neutral structures that can contain a wide range of metal centers.[25,30] Such clusters are mainly reported for group IV metals (Ti, Zr, Hf), which form a wide variety of structures that are highly Lewis acidic as well as less toxic and/or more stable than clusters of other transition metals (*e.g.*, Pt, Pd, Ln, Fe, Cr, *etc.*).[31–36] Hence, group IV clusters have been explored to a greater extent toward biologically relevant reactions. Unlike POMs, Zr and Hf centers in these clusters are typically 7- or 8-coordinated, largely resulting in tetragonal or cubic coordination geometries. These MOCs can drastically vary in size, ranging from the simplest $Zr_4O_2(OOMc)_{12}$ cluster to the much larger $Zr_{70}(SO_4)_{58}(O/OH)_{146}{\cdot}n(H_2O)$ cluster.[37,38] Moreover, MOCs incorporating group IV metals have been extensively investigated as building units of Metal–Organic Frameworks (MOFs).[39–41] These MOFs are typically composed of polydentate carboxylate ligands connecting hexanuclear clusters, $\{M_6O_8\}$, in which each metal center is interconnected *via* four bridging oxo ligands leaving four coordination sites available for binding to other ligands (Fig. 1(f) and (g)).[42] As a result, MOCs have been mainly explored as building units for MOFs in many applications, such as catalysis, sensing, and imaging, while discrete neutral or cationic MOCs have been studied to a lesser extent.[43–46] Similarly to POMs, MOC-based materials have also been investigated as catalysts for promoting biomolecular transformations, with the notable difference of catalyzing these reactions heterogeneously and often with improved efficiency compared to other nanozymes. While a majority of reports on MOC-based materials involve MOFs, other MOC-based hybrid materials have also been investigated, such as POMs immobilized within MOFs or other scaffolds,[47] offering unique opportunities for the development of new heterogeneous catalysts for biomolecular transformations.[48,49]

Despite the significant progress that has been made in the development of metal–oxo clusters as catalysts for a wide range of reactions,[29,45,50–52] their reactivity towards biomolecules and the underlying molecular mechanisms have not been comprehensively reviewed in recent years. Yet, achieving such a mechanistic understanding is crucial due to the important role of the catalytic properties of MOCs in their biological activity as potential inorganic drugs, and in other biomedical applications, as described in multiple reviews.[46,53–57] The reactivity of POMs and MOFs have been recently reviewed by our group, mainly focusing on proteins as substrates.[24,58,59] However, a

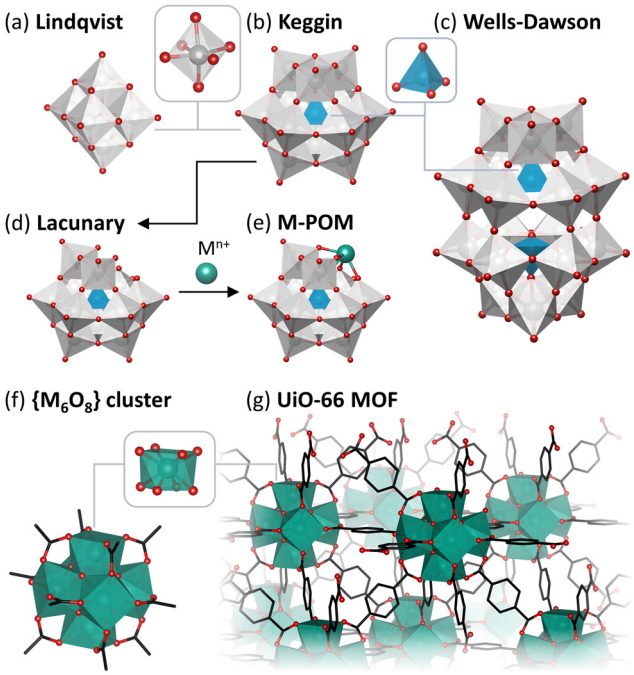

Fig. 1 Mixed ball-and-stick and polyhedral representation of (a) Lindqvist, (b) Keggin, (c) Wells–Dawson, (d) lacunary Keggin, and (e) M–POM Keggin structures as well as of (f) a discrete $\{M_6O_8\}$ cluster capped with carboxylate ligands and (g) the UiO-66 MOF composed of $\{M_6O_8\}$ clusters linked by bidentate carboxylate linkers. POM metal centers in grey, M–POM embedded metal centers and M_6 cluster metal centers in teal, heteroatom in blue, oxygen in red, and carbon in black.

broader discussion of the role of MOCs and MOC-based materials as catalysts in biochemical transformations involving a wide range of biomolecules – such as nucleic acids, nucleotides, sugars, and lipids – is sorely lacking. This is particularly important as there is significant untapped potential regarding their reactivity with other biomolecules that has not been explored, which entails promising avenues for future research. Furthermore, the study of the catalytic activity of MOCs towards specific biomolecules could benefit from the insights gained from other biological systems. Therefore, this review discusses the reactivity of discrete MOCs, largely focusing on clusters formed by group IV to VI transition metals since they have been most extensively investigated. This is followed by a discussion on MOC-based materials, which mainly act as heterogeneous catalysts. For both classes of catalysts, subdivisions are made based on the type of reactivity they exhibit (*e.g.*, hydrolytic, oxidative, *etc.*) and the type of biomolecule involved in the catalytic reaction (*e.g.*, peptides, proteins, nucleic acids, carbohydrates, lipids, *etc.*). In all sections, the biomolecular reactivity of MOCs is discussed in the context of their potential medical, bio-analytical, and environmental applications. Furthermore, particular focus is given to the underlying mechanisms, the structure–activity relationships, and the structural properties of MOCs that can be tuned as a means of optimization towards specific future applications.

2. Reactivity of discrete metal–oxo clusters

2.1. Amino acids, peptides, and proteins

The peptide bond, which connects amino acid residues into complex three-dimensional functional structures to form proteins, is highly stable, the hydrolysis half-life under physiological conditions being estimated at *ca.* 600 years.[60] Therefore, cleaving peptide bonds is an extremely challenging task. Yet, the selective cleavage of peptide bonds is essential in many biological and biomedical studies, particularly in the context of proteomics, which is the large-scale study of the structure, function, and localization of proteins.[61–63] Furthermore, peptide bond hydrolysis is also important in determining enzymatic active sites,[64] mapping metal and ligand binding sites,[65] footprinting,[66] designing therapeutic drugs,[67] and in studying protein folding.[68] Natural enzymes, known as peptidases or proteases, are commonly used to catalyze peptide bond cleavage, with trypsin being the most frequently used. However, these enzymes suffer from several shortcomings as their catalytic activity is mainly preserved under very narrow experimental conditions (temperature and pH)[69] and trypsin especially tends to produce many short peptide fragments, limiting the accurate analysis of the proteins' structural composition.[70] Natural proteases are also prone to self-digestion, thereby contaminating the analyte, resulting in loss of structural information about the protein under study. Considering the importance of peptide bond cleavage, the development of new metal-based catalysts with peptidase-like properties has attracted significant interest.[71–74] In this respect, MOCs, and particularly POMs, have been shown to be a promising class of compounds for the hydrolysis of peptide bonds in a wide range of different substrates.

2.1.1. Hydrolysis of peptides. Studies on protein hydrolysis are often limited to assessing the activity and selectivity of the catalyst since proteins are generally too large and complex to obtain accurate information at a molecular level. Therefore, to investigate the reactivity of MOCs towards peptide bonds, oligopeptides have been used as simpler targets that serve as good model systems.

Initially, molybdate and vanadate oxo-clusters were investigated as catalysts for the hydrolysis of several dipeptides.[75,76] Peptide bond cleavage was determined to be purely hydrolytic in nature since neither the formation of paramagnetic species nor oxidative modifications on the resulting amino acid products were observed. The hydrolysis of dipeptides was investigated under various experimental conditions since the speciation of molybdates and vanadates depends on the concentration, pH, temperature, and ionic strength of the solution.[77] These studies indicated that the monomeric orthovanadate ($[VO_4]^{3-}$) and orthomolybdate ($[MoO_4]^{2-}$) species were the most active in promoting peptide bond hydrolysis (Fig. 2). Furthermore, increasing the ionic strength of the solution increased the rate of hydrolysis in the presence of $[MoO_4]^{2-}$, but the opposite effect was observed when using $[VO_4]^{3-}$. This observation was linked to the different effects of the ionic strength on the speciation of molybdates and vanadates as well as on their interactions with dipeptides. In addition, a detailed mechanistic study revealed that dipeptides bind to $[VO_4]^{3-}$ *via* bidentate coordination of the terminal amino nitrogen and the amide carbonyl oxygen, while tridentate coordination was proposed for $[MoO_4]^{2-}$ *via* the terminal amino nitrogen, amide oxygen, and carboxylate oxygen (Fig. 2). In both cases, coordination-induced polarization of the peptide carbonyl bond activated it towards nucleophilic attack, but the tridentate coordination of the dipeptide to $[MoO_4]^{2-}$ gave rise to better reactivity.[76] The hydrolytic activity is also strongly dependent on the nature of the amino acid side chains of the dipeptides (Table 1) and the greatest reactivity was observed for dipeptides

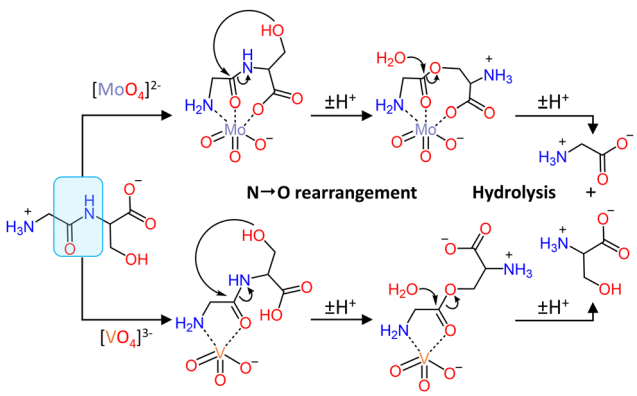

Fig. 2 Proposed mechanism of the hydrolysis of Gly-Ser catalyzed by $[MoO_4]^{2-}$ (top) or $[VO_4]^{3-}$ (bottom) *via* an *N,O*-acyl rearrangement.

Table 1 Selected conditions, percentage conversion, and rate constants (k_{obs}) reported for the hydrolysis of peptides promoted by different (poly)oxometalates catalysts (cat.)

Catalyst	Substrate	Reaction conditions	Conversion/%	$k_{obs}/\times 10^{-6}$ s^{-1}	Ref.
$[MoO_4]^{2-}$	Gly–X (X = Ser, Thr, Ala, Tyr, Gly, Asn, Met)	pD 7, 60 °C, 60 h, 60 eq. cat.	2 (Met)–68 (Ser)	5.9 (X = Ser)	75
	X–Gly (X = Ser, Cys, Asp, Lys)	pD 5–7, 60 °C, 60 h, 60 eq. cat.	2 (Lys)–17 (Cys)	0.84 (Asp; pD 7) 2.34 (Asp; pD 5)	75,78
	His-Ser	pD 7, 60 °C, 60 h, 60 eq. cat.	91		75
	Leu-Ser	pD 7, 60 °C, 60 h, 60 eq. cat.	43		75
	Asp-Ala	pD 7, 60 °C, 60 h, 60 eq. cat.	3		75
	Ala-His	pD 7, 60 °C, 60 h, 60 eq. cat.	5		75
	Gly-Ser-Phe	pD 7, 60 °C, 60 h, 60 eq. cat.	25		75
	Glu-Cys-Gly	pD 7, 60 °C, 60 h, 60 eq. cat.	4		75
$[VO_4]^{3-}$	Gly–X	pD 4.4, 60 °C, 140 h, 12.5 eq. cat.	5 (Ser)–15 (Thr)		76
	(X = Ser, Thr, Ala)	pD 7.4, 60 °C, 140 h, 12.5 eq. cat. pD 7.4, 37 °C, 140 h, 12.5 eq. cat.	7 (Ala)–52 (Ser)	0.07 (Ala)–1.3 (Ser) 0.09 (Ser)	
	Ser-Gly	pD 4.4–7.4, 60 °C, 140 h, 12.5 eq.	3 (pD 7.4)–6 (pD 4.4)	0.05 (pD 7.4)	76
	His-Ser	pD 4.4–7.4, 60 °C, 140 h, 12.5 eq.	25 (pD 4.4)–40 (pD 7.4)	1.2	76
	Leu-Ser	pD 4.4–7.4, 60 °C, 140 h, 12.5 eq.	12 (pD 4.4)–39 (pD 7.4)	1.0	76
	Gly-Ser-Phe	pD 4.4, 60 °C, 140 h, 12.5 eq. cat.	4 (pD 4.4)–16 (pD 7.4)	0.3 (pD 7.4)	76
Zr–WD 1 : 2	Gly–X (X = Gly, Ala, Val, Leu, Ile, Phe, Asp, Asn, Glu, Gln, Ser, Thr, Tyr, Lys, Arg, His)	pD 5, 60 °C, 1 eq. cat.		0.08 (Glu)–3.5 (Ser)	79,80
	X–Gly (X = Ala, His, Ser)	pD 5, 60 °C, 1 eq. cat.		0.34 (Ser)–0.5 (Ala)	79,80
	X-Ser (X = Leu, Ile)	pD 5, 60 °C, 1 eq. cat.		0.35 (Ile) 3.53 (Leu)	79,80
Zr–WD 4 : 2	Gly–X (X = Gly, Ala, Val, Leu, Ile, Phe, Ser, Thr, His, Lys, Arg, Asp, Asn, Gln)	pD 7.4, 60 °C, 1 eq. cat. pD 7.4, 60 °C, 6 eq. cat. pD 5.4, 60 °C, 6 eq. cat.		0.3 (Gly) 0.01 (Ile)–2.3 (Ser) 0.4 (Gly)	81
	Gly-Gly-Gly	pD 7.4, 60 °C, 4 weeks, 6 eq. cat.	45% Gly		82
	Gly-Gly-Gly-Gly	pD 7.4, 60 °C, 4 weeks, 6 eq. cat.	45% Gly		82
	Gly-Ser-Phe	pD 7.4, 60 °C, 10 days, 6 eq. cat.	31% Gly		82
Zr–K 1 : 2	Gly-Ser	pD 5.4, 60 °C, 1 eq. cat.		0.3	83
Zr–K 2 : 2	Gly–X (X = Gly, Ser, Thr, Tyr, Asp, Met, Glu, Asn, Gln, His, Lys, Arg, Ala, Val, Leu, Ile, Phe)	pD 5.4, 60 °C, 1 eq. cat.		0.08 (Ile)–6.3 (Ser)	83,84
	X–Gly (X = Ser, Cys, Asp, His)	pD 5.4, 60 °C, 1 eq. cat.		0.07 (Asp)–0.8 (Ser)	84
	X-Ser (X = Leu, Ile, Tyr)	pD 5.4, 60 °C, 1 eq. cat.		0.5 (Tyr)–4.5 (Leu)	84
	Gly-Gly-Gly	pD 5.4, 60 °C, 4 weeks, 2 eq. cat.	65% Gly	0.7	82
	Gly-Gly-Gly-Gly	pD 7.4, 60 °C, 4 weeks, 2 eq. cat.	55% Gly	0.7	82
	Gly-Ser-Phe	pD 7.4, 60 °C, 10 days, 2 eq. cat.	55% Gly	1.0	82
Ce–K 1 : 2	Gly–X (X = Ser, Gly, Thr)	pD 7.4, 60 °C, 1 eq. cat.		0.8 (Ser)–0.03 (Gly)	85
	X–Gly (X = Cys, His, Ser)	pD 7.4, 60 °C, 1 eq. cat.		0.03	85
	His-Ser	pD 7.4, 60 °C, 1 eq. cat.		1	85
	Leu-Ser	pD 7.4, 60 °C, 1 eq. cat.		0.5	85
Zr–L 1 : 1	Gly–X (X = Ser, Gly, Thr, Ala, Leu, Ile, Tyr)	pD 7.4, 60 °C, 1 eq. cat.		0.02 (Ile)–1.5 (Ser)	86
	Ser-Gly	pD 7.4, 60 °C, 1 eq. cat.		0.1	86
	His-Gly	pD 7.4, 60 °C, 1 eq. cat.		0.5	86
	His-Ser	pD 7.4, 60 °C, 1 eq. cat.		9.5	86
	Leu-Ser	pD 7.4, 60 °C, 1 eq. cat.		1.3	86
	Gly-Gly-Gly	pD 5.4, 60 °C, 4 weeks, 2 eq. cat.	30% Gly		82
	Gly-Gly-Gly-Gly	pD 5.4, 60 °C, 4 weeks, 2 eq. cat.	30% Gly		82
	Gly-Ser-Phe	pD 5.4, 60 °C, 2 eq. cat.	20% Gly		82

with a serine residue downstream of the peptide bond (X-Ser where X = an amino acid residue). This is due to the intramolecular nucleophilic attack of the hydroxyl group of serine on the peptide bond, which leads to an *N,O*-acyl rearrangement and the formation of a more hydrolytically labile ester bond (Fig. 2).[75,76] Therefore, hydrolysis of dipeptides by vanadates and molybdates depends on several factors: (i) the speciation, (ii) the nature of the metal and its binding to the dipeptide, and (iii) the amino acid sequence. However, the kinetic lability of molybdate and vanadate oxo-clusters in solution limits their broader applicability and complicates their investigation in catalytic reactions.

Further research into the hydrolytic activity of POMs shifted towards polyoxotungstate clusters since they are less labile compared to vanadates and molybdates in solution. However, the lower lability of tungsten centers also hinders their ability

to effectively coordinate to dipeptides. This problem can be overcome by using M–POMs that contain other transition metal centers incorporated into the POM structure (Fig. 1(e)). Therefore, Wells–Dawson polyoxotungstate M–POMs with different embedded metals (M = Mn^{3+}, Fe^{3+}, Co^{2+}, Ni^{2+}, Cu^{2+}, Y^{3+}, Eu^{3+}, Yb^{3+}, Ce^{4+}, Zr^{4+}, and Hf^{4+}) were investigated toward peptide bond hydrolysis of several dipeptides (Ala-Gly and Gly-X where X = Gly, Ala, Val, Leu, Ile, Phe, Ser, Thr, Tyr, Glu, Gln, Asn, Asp, His, Lys, Arg, Met, and Cys).[79,80] The Zr^{4+}- and Hf^{4+}-substituted Wells–Dawson M–POMs were shown to be considerably more catalytically active towards peptide bond hydrolysis in comparison to all other M–POMs (Table 1) due to the high Lewis acidity of Zr^{4+} and Hf^{4+}, as well as their high coordination number, redox inactivity, and oxophilicity.[80] The importance of Lewis acidic metal ions in the hydrolytic process was confirmed by the addition of different carboxylic acid inhibitors, which competitively bind to the embedded metal center and, therefore, decreased the rate of peptide bond hydrolysis. The POM framework also plays an essential role since it prevents the formation of insoluble gels, which typically occurs when using Zr^{4+} and Hf^{4+} salts.[70,80] Hence, polyoxotungstate M–POMs are promising catalysts for peptide bond hydrolysis that exploit the high Lewis acidity of the embedded metal center and the aqueous stability of the POM framework as an inorganic ligand.

Zr^{4+} and Hf^{4+} M–POMs are often present in solution as dimers (Fig. 3(a)) where two POM units bind to one metal center (*e.g.*, $[M(\alpha_2\text{-}P_2W_{17}O_{61})_2]^{16-}$; M–WD 1 : 2) or two M–POMs are linked *via* μ-OH ligands (*e.g.*, $[\{M(\mu\text{-}OH)(H_2O)(\alpha_2\text{-}P_2W_{17}O_{61})\}_2]^{16-}$; M–WD 2 : 2). In these dimers the embedded metal center in the dimer with a 1 : 2 metal : POM ratio has no free coordination sites, while each metal center in the 2 : 2 dimer only has one free coordination, which is typically occupied by a labile water ligand that can be exchanged with the incoming substrate. However, the dimeric POMs are typically in equilibrium with a monomeric POM species ($[M(\alpha_2\text{-}P_2W_{17}O_{61})]^{6-}$; M–WD 1 : 1), which forms upon dissociation of the dimers (Fig. 3(a)). This monomeric species is believed to be the catalytically active species since it has four free coordination sites on Zr^{4+}/Hf^{4+}.[80] Interestingly, the dimeric tetrazirconium-substituted Wells–Dawson M–POM ($[Zr_4(\mu_3\text{-}O)_2(OH)_2(H_2O)_4(P_2W_{16}O_{59})_2]^{14-}$; Zr–WD 4 : 2), composed of two Wells–Dawson POM units linked by a $\{Zr_4(\mu_3\text{-}O)_2(OH)_2(H_2O)_4\}^{10+}$ cluster (Fig. 3(b)), was also shown to have considerable activity towards Gly–X dipeptides (Table 1) although its dissociation into a monomer has not been reported.[81] This is likely due to the ability of dipeptides to coordinate in a bidentate fashion to Zr^{4+} centers bearing two water ligands, $\{Zr(H_2O)_2\}$, by displacing those labile waters without affecting the overall structure of the POM.

The proposed mechanism of peptide bond hydrolysis promoted by M–POMs involves coordination of the terminal amine nitrogen and the peptide carbonyl oxygen to a metal center, resulting in activation of the carbonyl carbon towards nucleophilic attack by solvent water.[80,87] Furthermore, it was found that the uncoordinated terminal carboxylic acid has an important role in the hydrolytic process since it acts as a general base that can remove a proton from the attacking water nucleophile.[81,87] Hence, although M–POMs have a tendency to form dimeric structures, for them to be catalytically active there needs to be several free coordination sites that allow for bidentate binding of the dipeptide, which may be achieved through dissociation of the dimer in solution.

The hydrolytic activity of Lindqvist and Keggin Zr–POMs towards dipeptides has also been investigated. The Keggin Zr–POMs were shown to effectively catalyze the hydrolysis of glycylserine (Gly-Ser) and glycylglycine (Gly-Gly) dipeptides to produce single amino acids as the main products (Fig. 4(a)), along with small amounts of cyclic dipeptide side-products (cGly-Ser and cGly-Gly).[83] The cyclization reaction was shown to be reversible as the Zr–POMs hydrolyzed cGly-Ser and cGly-Gly back into the dipeptides, which were further hydrolyzed to give amino acid products (Fig. 4(a)). Comparison of two dimeric Keggin M–POMs (Table 1), showed that the rate constant for the hydrolysis of Gly-Ser was 20 times higher for $[\{Zr(\mu\text{-}OH)(H_2O)(\alpha\text{-}PW_{11}O_{39})\}_2]^{8-}$ (Zr–K 2 : 2) compared to $[Zr(\alpha\text{-}PW_{11}O_{39})_2]^{10-}$ (Z–K 1 : 2). This demonstrates the importance of the Zr^{4+} centers for the hydrolysis reaction, since dissociation of Zr–K 2 : 2 gives two hydrolytically active monomeric POMs ($[Zr(\alpha\text{-}PW_{11}O_{39})]^{3-}$; Zr–K 1 : 1) while only one Zr–K 1 : 1 is formed from dissociation of Z–K 1 : 2 together with a catalytically inactive lacunary POM.[83] Furthermore, Zr–K 1 : 1 was confirmed to be the catalytically active species since binding to Zr–K 2 : 2, which could in principle occur *via* replacement of coordinated H_2O, was found to be thermodynamically unfavorable by Density Functional Theory (DFT) calculations.[87] However, even though the formation of Zr–K 1 : 1 is favored at lower pH, the rate constant of Gly-Gly hydrolysis catalyzed by Zr–K 2 : 2 was observed to vary with the pH following a bell-shaped profile reaching a maximum at around pH 5.5. This is because, at higher pH, Zr–K 2 : 2 was converted to Zr–K 1 : 2 or formed an inactive complex with the dipeptide, while at lower pH protonation of the amine nitrogen hindered effective peptide

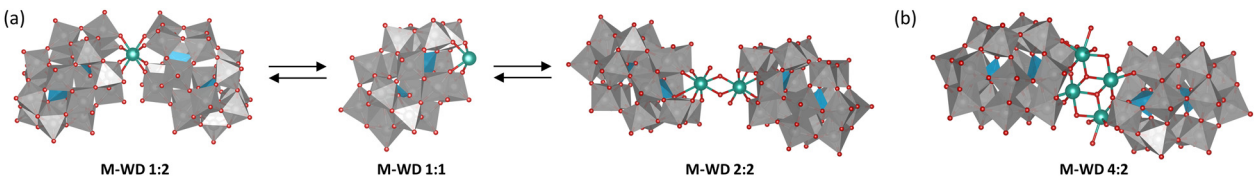

Fig. 3 (a) Equilibrium between the dimeric $[M(\alpha_2\text{-}P_2W_{17}O_{61})_2]^{16-}$ (M–WD 1 : 2), the monomeric $[M(\alpha_2\text{-}P_2W_{17}O_{61})]^{6-}$ (M–WD 1 : 1), and the dimeric $[\{M(\mu\text{-}OH)(H_2O)(\alpha_2\text{-}P_2W_{17}O_{61})\}_2]^{16-}$ (M–WD 2 : 2) Wells–Dawson M–POMs (M = Zr^{4+} or Hf^{4+}). (b) Structure of the dimeric tetrazirconium-substituted Wells–Dawson M–POM ($[Zr_4(\mu_3\text{-}O)_2(OH)_2(H_2O)_4(P_2W_{16}O_{59})_2]^{14-}$; Zr–WD 4 : 2). Tungsten in gray, oxygen in red, phosphorus in blue, zirconium/hafnium in teal.

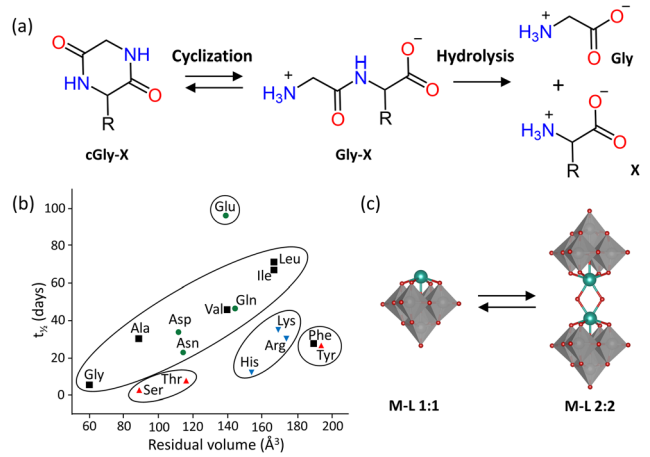

Fig. 4 (a) Hydrolysis and cyclization of a Gly–X dipeptide. (b) Plot of the half-life ($t_{1/2}$) of the hydrolysis of Gly–X dipeptides catalyzed by Zr–WD 1 : 2 with respect to the residue volume of amino acid X with different side chains containing: aliphatic (■), hydroxyl (▲), carbonyl (●), or charged (▼) groups. Adapted from ref. 79 with permission from the Royal Society of Chemistry. (c) Equilibrium between the monomeric $[W_5O_{18}Zr(H_2O)_3]^{2-}$ (Zr–L 1 : 1) and the dimeric $[\{Zr(\mu\text{-}OH)(W_5O_{18})\}_2]^{6-}$ (Zr–L 2 : 2) Lindqvist M–POMs.

coordination.[83] Increasing the concentration of Zr–K 2 : 2 also resulted in a decrease in the rate of Gly-Gly hydrolysis due to the conversion of Zr–K 2 : 2 into Zr–K 1 : 2. Therefore, while the speciation of polyoxotungstates is less complex in comparison to molybdates and vanadates, the equilibria between monomeric and dimeric species, which is affected by the solution conditions, still plays an important role in their reactivity and needs to be carefully considered.

In order to circumvent the equilibrium between dimeric and monomeric species observed for the Wells–Dawson and Keggin Zr–POMs, the hydrolytic activity of the monomeric Lindqvist Zr–POM (Fig. 4(c)), $[W_5O_{18}Zr(H_2O)_3]^{2-}$ (Zr–L 1 : 1), was also investigated towards dipeptides, since this M–POM was reported to be more stable as a monomer in solution.[86] Zr–L 1 : 1 displayed good hydrolytic activity towards a range of dipeptides (Table 1), with the fastest reaction rate observed for the histidylserine dipeptide (His-Ser). Interestingly, the pH dependence of the hydrolysis of His-Ser by Zr–L 1 : 1 gave a similar bell-shaped curve to that of Zr–K 2 : 2, but with a maximum at pH 7.5. The lower rate at higher pH was attributed to the formation of the dimeric form (Fig. 4(c)): $[\{Zr(\mu\text{-}OH)(W_5O_{18})\}_2]^{6-}$ (Zr–L 2 : 2). Furthermore, the role of Zr–L 1 : 1 as a catalyst was demonstrated through the successful hydrolysis of His-Ser added after completion of the initial His-Ser hydrolysis, which could be repeated for three consecutive cycles, but its overall hydrolytic activity was not significantly higher compared to the Keggin Zr–POMs.

In accordance with the results obtained for the molybdate and vanadate oxoanions, the hydrolytic activity of M–POMs was found to depend on the side chain of the amino acid residues in the hydrolyzed dipeptides (Fig. 4(b) and Table 1).[79–81,84] Similarly, hydrolysis was observed to be fastest for X-Ser dipeptides due to the *N,O*-acyl rearrangement discussed above.[79,84,86,88] The rate of hydrolysis was also faster for dipeptides with positively charged amino acid side chains due to their favorable electrostatic interactions with negatively charged M–POMs.[84] For peptides with aliphatic residues, the reaction rate decreased with increasing molecular volume of the side chains, due to steric effects.[79,84,86,87] Additionally, out of a series of Gly–X dipeptides, the glycine dipeptide containing glutamate (Gly-Glu) gave the lowest rate constant for peptide bond hydrolysis catalyzed by Zr–WD 2 : 2, which was proposed to be due to the competing coordination of the carboxylate group of Glu to Zr^{4+}.[79] However, the Gly–X dipeptide containing aspartate (Gly-Asp), which also has a carboxylate group in the side chain, was hydrolyzed faster due to weaker coordination of the carboxylate as a result of the shorter side chain of Asp.[79] Interestingly, deamination of Asn to Asp and Gln to Glu was also observed during the hydrolysis of Gly-Asn or Gly-Gln catalyzed by Zr–K 2 : 2.[84] The sequence of the amino acids in the dipeptides also influenced the rate of hydrolysis. The rate of Ser-Gly hydrolysis was lower compared to Gly-Ser due to a less favorable four-membered ring transition state.[79,84] On the other hand, the rate of Ala-Gly hydrolysis was faster than that of Gly-Ala due to Ala-Gly being less prone to cyclization, which slows down the reaction as the cyclic side products need to be hydrolyzed back to the dipeptides to afford the individual amino acids as the final reaction products.[79,86] Hence, this demonstrates the potential selectivity of M–POMs towards the preferential peptide bond hydrolysis of certain combinations of amino acids in a specific order. These early studies with dipeptides have proven to be valuable as they provided molecular insight into factors that could influence the selectivity of M–POMs, as observed from their tendency to preferentially hydrolyze a particular sequence of amino acids in a polypeptide chain.

Following studies on dipeptides, the hydrolysis of larger oligopeptides – triglycine (Gly_3), tetraglycine (Gly_4), pentaglycine (Gly_5), glycylglycylhistidine (Gly-Gly-His), glycylserylphenylalanine (Gly-Ser-Phe-Ala), and insulin chain B (30 amino acid polypeptide) – promoted by Zr–WD 1 : 2, Zr–WD 4 : 2, Zr–K 2 : 2, and Zr–L 1 : 1 was also investigated.[80,82,89,90] In the presence of Zr–WD 1 : 2, Gly_4 was hydrolyzed to form Gly, but intermediate products, Gly_3 and Gly-Gly, were observed as well, indicating that the reaction likely proceeds *via* sequential hydrolysis of the peptide bonds in the tetrapeptide, tripeptide, and dipeptide.[89] Out of all explored POMs, Zr–WD 1 : 2 displayed the best hydrolytic activity towards tri- and tetrapeptides. Moreover, NMR studies revealed that Keggin and Lindqvist POMs interact with Gly_3, Gly_4, and Gly-Ser-Phe-Ala through the amine nitrogen and the *N*-terminal amide oxygen, while Gly-Gly-His interacts *via* a different binding mode due to additional coordination of the imidazole nitrogen atom to Zr^{4+}.[82] Slower hydrolysis was observed in the presence of Zr–L 1 : 1 and Zr–WD 4 : 2 species, which was attributed to the formation of less-active complexes in solution.[82] The hydrolytic rate was fastest in the case of the tetrapeptide Gly-Ser-Phe-Ala, where the Gly-Ser peptide bond was preferentially hydrolyzed thanks to the intramolecular

Table 2 Conditions and cleavage sites of selected reports on the hydrolysis of proteins promoted by different MOCs

MOC	Protein[c]	Reaction conditions	No. of cleavages	Cleavage sites[a]	Ref.
Zr–WD 1 : 2	HSA	pH 7.4, 60 °C, 10 eq. POM	4	Arg114–Leu115, Ala257–Asp258, Lys313–Asp314, Cys392–Glu393	106
		pH 7.4, 60 °C, 50 eq. POM + CHAPS	7	Cys62–Asp63, Gly71–Asp72, Asp107–Asp108, Lys313–Asp314, His367–Glu368, Ser470–Asp471, Ala511–Asp512	114
Hf–WD 1 : 2	HEWL	pH 5.0, 60 °C, 100 eq. POM	6	Asp18–Asn19, Asp48–Gly49, Thr51–Asp52, Asp52–Tyr53, Asp66–Gly67, Asp101–Gly102	96
	Ova	pH 7.4, 60 °C, 100 eq. POM	8	Phe13–Asp14, Arg85–Asp86, Asn95–Asp96, Ala139–Asp140, Ser148–Trp149, Ala361–Asp362, Asp362–His363, Pro364–Phe365	98
Zr–K 1 : 2	Ova	pH 7.4, 60 °C, 50 eq. POM (+ SDS, CHAPS, or Zw3–12)	6		115
	Cyt *c*	pH 4.1, 60 °C, 40 eq. POM	3	Asp3–Val4, Asp51–Ala52, Gly78–Thr79	95
		pH 7.4, 60 °C, 50 eq. POM + SDS, CHAPS, or Zw3–12	3		116
Zr–K 2 : 2	HHM	pH 5, 60 °C, 100 eq. POM	6	Asp4–Gly5, Asp20–Ile21, Asp44–Lys45, Asp60–Leu61, Asp126–Ala127, Asp141–Ile142	70
		pH 5.5, 60 °C, 100 eq. POM + SDS + CHAPS or Zw3–12	8 6		117
	Hb	pH 5, 60 °C, 100 eq. POM	11	α-subunit: Asp6–Lys7, Asp74–Asp75, Asp75–Leu76, Asp85–Leu86, Asp94–Pro95, Asp116–Phe117 β-subunit: Asp46–Leu47, Asp51–Ala52, Asp68–Ser69, Asp78–Asp79, Asp98–Pro99	97
	Cyt *c*	pH 4.1, 60 °C, 40 eq. POM	3	Asp3–Val4, Asp51–Ala52, Gly78–Thr79	95
Ce–K 1 : 2	Cyt *c*	pH 4.1–7.4, 37–60 °C, 40 eq. POM	2	Trp60–Lys61, Gly78–Thr791	95
		pH 7.4, 60 °C, 50 eq. POM + SDS or CHAPS + Zw3–12	2 None		116
	HEWL	pH 7.4, 37 °C, 10 eq. POM	2	Trp28–Val29, Asn44–Arg45	85
	Hb	pH 5, 60 °C, 100 eq. POM	7	α-subunit: Asp75–Leu76, Asp94–Pro95 β-subunit: Asp51–Ala52, Asp68–Ser69, Asp78–Asp79, Asp98–Pro99, Asp128–Phe129	93
Hf_{18}	HHM	pH 7.4, 60 °C, 2 μmol cluster	6	Asp5, Asp21, Asp45, Asp110, Asp123, Asp142[b]	118

[a] Determined by Edman degradation. [b] Both Asp–X and X–Asp cleavage were observed at all sites. [c] HSA = Human Serum Albumin; HEWL = Hen Egg White Lysozyme; Ova = Ovalbumin; Cyt *c* = Cytochrome *c*; HHM = Horse Heart Myoglobin; Hb = Hemoglobin.

nucleophilic attack of the peptide carbonyl carbon by the hydroxyl group in the side chain of Ser, as observed for dipeptides. This highlights the beneficial role of Ser in peptide bond hydrolysis, even in larger peptides.[82]

2.1.2. Hydrolysis of proteins. The hydrolysis of proteins into peptide fragments is of particular importance in the field of proteomics as peptide fragments can be more easily characterized by mass spectrometry.[91,92] The data obtained from peptide fragments can then be combined to determine the amino acid sequence of a protein, including its post-translational modifications. Hence, based on the promising hydrolytic activity of POMs towards di-, tri-, and tetra- peptides discussed in Section 2.1.1., the catalytic activity of POMs was further investigated towards the hydrolysis of a wide range of proteins that differ in terms of isoelectric point (pI), structure, and size including hen egg white lysozyme (HEWL), human serum albumin (HSA), human serum holo-/apo-transferrin, ovalbumin, bovine blood hemoglobin, horse heart myoglobin, and bovine/horse heart cytochrome *c* (Table 2).[70,85,88,90,93–99] All reactions were performed under mild reaction conditions in acetate or phosphate buffer at 37 or 60 °C, and were followed by sodium dodecyl sulfate-polyacrylamide gel electrophoresis (SDS-PAGE). In some cases, SDS-PAGE was coupled with Edman degradation and liquid chromatography tandem mass spectrometry (LC-MS/MS) to determine the position of the hydrolyzed peptide bond in the protein sequence (Table 2). These studies have shown that POMs can be particularly interesting as artificial proteases for middle-down proteomics, which focuses on analyzing peptide fragments of around 3–15 kDa. Fragments of this size are ideal because they preserve structural information about the protein and reduce the complexity of the proteolytic mixture that is often obtained when using natural enzymes, such as trypsin, that produce many smaller fragments.[100,101] In order to understand the driving forces behind the hydrolytic activity, the interactions of POMs with proteins have also been investigated *in silico* by DFT calculations and molecular dynamics simulations, as well as experimentally using a range of complementary techniques, including multinuclear NMR, fluorescence, circular dichroism, and UV-Vis spectroscopy, along with Isothermal Titration Calorimetry (ITC) and Single Crystal X-ray Diffraction (SC-XRD).[102–110] These interaction studies have shown that POM-protein binding is mainly driven by charge-charge and H-bonding interactions, although hydrophobic interactions and coordinative binding can also occur, especially with POMs functionalized with organic moieties and with M–POMs, respectively.[110–113] However, since POM-protein interactions and the hydrolytic activity of POMs towards proteins have been

recently reviewed by our group,[24,58,111] this section will only briefly discuss the main conclusions obtained from these studies.

Similarly to peptides, studies on the hydrolytic activity of POMs towards proteins initially focused on using molybdates and then moved on to investigate M–POMs as catalysts.[78] These studies showed that $[MoO_4]^{2-}$ was the catalytically active species in the hydrolysis of HEWL, which occurred preferentially at Asp–X peptide bonds. This was an intriguing finding because studies with dipeptides showed that X-Ser dipeptides were hydrolyzed the fastest. However, similar selectivity was also observed for the hydrolysis of different proteins catalyzed by Zr^{4+} and Hf^{4+} Wells–Dawson, Keggin, and Lindqvist M–POMs, regardless of the structure of the POM framework (Table 2).[70,88,90,95–97] Based on DFT calculations, this selectivity towards Asp–X bonds in proteins was proposed to result from the intramolecular attack of the metal-activated carbonyl carbon of the peptide bond by the carboxylate group in the side chain of Asp, leading to the formation of a five-membered cyclic hemiaminal that is then hydrolyzed (Fig. 5). Interestingly, such selectivity towards Asp–X bonds in proteins is extremely rare in nature, which makes POMs unique alternatives to natural enzymes. Furthermore, this shows that the reactivity towards simpler model systems is not always entirely representative of more complex biomolecules.

Ce^{4+} M–POMs generally displayed slightly different selectivity than Zr^{4+} and Hf^{4+} M–POMs under the same conditions (Table 2).[88,93–95] Although the reasons for this are not yet fully understood, it was hypothesized that this difference originates from the redox properties of Ce^{4+} as the reduction of Ce^{4+} to Ce^{3+} was observed to occur in the presence of proteins, resulting in loss of the hydrolytic activity due to the lower Lewis acidity of Ce^{3+}.[85,88,93,95] Hence, the properties of the catalytically active metal center embedded in the POM cluster affect the overall reactivity.

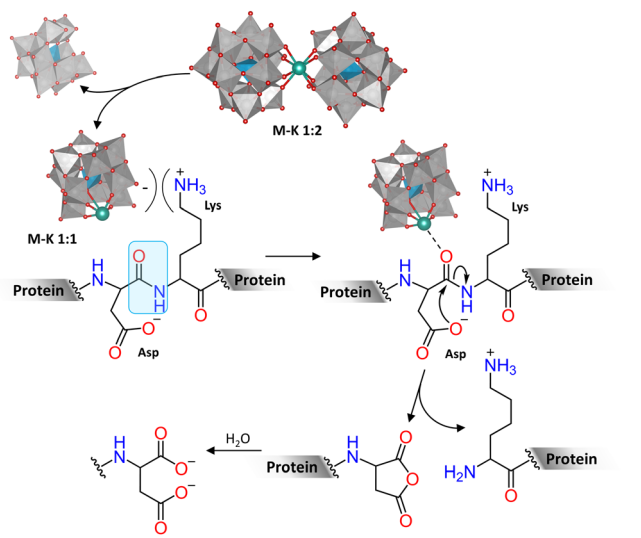

Fig. 5 Example mechanism of hydrolysis of an Asp–Lys peptide bond in a protein catalyzed by M–K 1:2, which dissociates into M–K 1:1 and a monolacunary Keggin POM at the protein surface.

Besides the crucial role of the Lewis acidic metal ion in the hydrolytic process, electrostatic interactions between negatively charged POMs and positively charged regions of proteins also have a significant influence on the outcome of the hydrolytic reaction. M–POM catalyzed hydrolysis typically occurs in positive regions of the protein due to favorable electrostatic interactions with the negatively charged POM, and, therefore, M–POMs with higher net negative charge have generally been reported to give rise to higher hydrolytic efficiencies. However, the catalytic activity of POMs has been found to also depend on the protein structure, as smaller proteins (*e.g.*, myoglobin and cytochrome *c*) displayed stronger interactions with smaller Keggin M–POMs, while larger proteins (*e.g.*, HSA and transferrin) interact more favorably with larger POMs, such as the Wells–Dawson M–POMs.[70,88,95,99] In addition, SC-XRD and DFT calculations indicated that the low dielectric constant at the surface of proteins facilitates the dissociation of M–POM dimers into the catalytically active monomeric species with more available coordination sites (Fig. 5).[96] Therefore, the interplay between the structure of the POM and that of the protein (*i.e.*, charge and size) is a determining factor in the hydrolysis reaction.

The reaction conditions also have an influence on the reactivity of M–POMs.[58] Acetate buffer (pH 5.5) has been determined to be more suitable for protein hydrolysis catalyzed by M–POMs than phosphate buffer (7.4) due to its lower pH and because of the inactivation of M–POMs by binding of phosphate to the embedded metal center.[70,119] Furthermore, the electrostatic nature of POM-protein interactions means that they are significantly affected by the pH, ionic strength, and temperature.[58,111] The reactivity also depends on the speciation of M–POMs, which in turn depends on the ionic strength, concentration, temperature, dielectric constant, and pH of the medium.[58] Hence, the conditions used need to be carefully considered to optimize the hydrolytic activity.

Recently, our group also demonstrated that M–POMs are mostly stable in the presence of surfactants and preserve their catalytic activity towards peptide bonds.[114–116,120–123] This is noteworthy since surfactants are essential in the study of many disease-related proteins and naturally water-insoluble proteins, such as membrane proteins. Studying these proteins is challenging and requires the use of surfactants to solubilize them. However, the presence of surfactants typically leads to denaturation of natural proteases causing them to lose their catalytic activity. In contrast, studies have shown that, even in the presence of surfactants, Zr–POMs are able to hydrolyze proteins such as β-casein, an unstructured and poorly soluble protein, and zein, a fully water-insoluble protein.[120,122] Therefore, M–POMs could aid in bridging the current gap in the study of disease-related proteins and naturally water-insoluble proteins that are difficult to hydrolyze with natural proteases.

Hydrolysis in the presence of surfactants can also be used to probe the structure of soluble proteins since protein unfolding induced by surfactants can lead to certain cleavage sites becoming more accessible to the POM catalyst depending on the protein structure. This was indeed observed for the hydrolysis

of myoglobin and HSA in the presence of anionic and/or zwitterionic surfactants as the addition of surfactants enhanced the hydrolytic efficiency of the M–POM and/or increased the number of peptide fragments (Table 2).[114,117] However, the presence of surfactant molecules interacting with residues on the surface of the protein may also hinder the binding of the POM to the protein surface. Therefore, compared to the reaction in the absence of surfactants, a decrease in the hydrolytic activity was observed in the presence of surfactants for the hydrolysis of ovalbumin, which has a high number of hydrophobic residues that can interact strongly with the hydrophobic tails of surfactants. Similarly, cytochrome *c* was hydrolyzed with a lower efficiency in comparison to the structurally similar myoglobin. This was attributed to the high pI of cytochrome *c*, which carries a higher overall positive charge compared to myoglobin, thus inducing stronger electrostatic interactions with zwitterionic and anionic surfactants, thereby blocking interactions between the protein and the M–POM. Accordingly, the hydrolytic activity of M–POMs towards proteins was observed to generally decrease with increasing concentration of surfactants, which hinders the exchange of surfactants with the M–POM at the protein surface and may induce dissociation of the M–POM.[114,120,122] In addition, the interaction of M–POMs with the ammonium groups of zwitterionic surfactants and their incorporation into micelles disrupted the equilibria between the dimeric and catalytically active monomeric species, which can negatively affect the hydrolytic activity of the M–POM.[117] Overall, these studies have shown that surfactants can be used as additives to tune the hydrolytic activity of POMs and the number of obtained peptide fragments. Moreover, the surfactant-protein interactions play an important role in the outcome of the hydrolytic reaction and depend on the structure of both the employed surfactant and the protein.

Despite the promising hydrolytic activity of POMs towards peptide bond cleavage, other MOCs have not been as extensively investigated for this type of reactivity. Nevertheless, a recent study by our group has shown that a water-insoluble neutral Hf^{4+} cluster (Fig. 6(a)), $Hf_{18}O_{10}(OH)_{26}(SO_4)_{13}(H_2O)_{33}$ (Hf_{18}), acted as an effective heterogeneous catalyst towards the hydrolysis of myoglobin in water and several buffers.[118] Interestingly, Hf_{18} hydrolyzed the protein at Asp–X and X–Asp cleavage sites in both positively and negatively charged regions of the protein (Table 2), in contrast to the selectivity of M–POMs for Asp–X peptide bonds in positively charged protein regions. This was attributed to the synergistic effect of both Lewis and Brønsted acidity of the cluster. The Brønsted acidity due to labile water ligands bound to Hf^{4+} centers is distinct from the purely Lewis acidic POM catalysts and was essential for the hydrolytic activity of Hf_{18}. However, the protein was observed to adsorb strongly onto the solid MOC catalyst, especially at lower pH, and, as a result, the protein and peptide fragments could not be easily separated after the reaction without deactivating the solid catalyst. Therefore, further optimization of the separation protocol or the structure of the cluster is necessary in order to obtain a recyclable heterogeneous MOC catalyst for the hydrolysis of proteins.

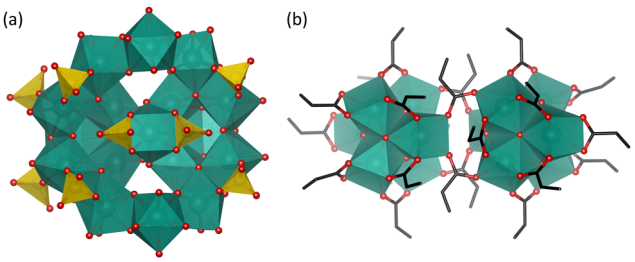

Fig. 6 Structures of (a) $Hf_{18}O_{10}(OH)_{26}(SO_4)_{13}(H_2O)_{33}$ (Hf_{18}) and (b) $[Zr_6(OH)_4O_4(OAcr)_{12}]_2$ (Acr = acrylate). Hafnium in teal, oxygen in red, sulfur in yellow, carbon in black.

2.1.3. Peptide bond formation. The cyclic by-products that were observed during the hydrolysis of dipeptides due to intramolecular peptide bond formation suggested that these POMs can also promote peptide bond formation. The formation of peptide bonds is important for producing many synthetic materials, such as pharmaceuticals and polymers, but remains relatively challenging as the removal of water and the use of additives to facilitate the reaction are often necessary.[124,125] Hence, the ability of Zr–POMs to promote amide bond formation in aqueous solutions is remarkable, and has been further explored by our group using POMs and Zr-oxo clusters to catalyze peptide bond formation. M–POMs were shown to effectively catalyze the cyclization of several different dipeptides in dimethyl sulfoxide (DMSO), with better activity being observed for Zr^{4+} and Hf^{4+} M–POMs than for M–POMs with other embedded metal centers (Fe^{3+}, Ni^{2+}, Co^{2+}, Cu^{2+}, Ce^{3+}, and Ce^{4+}), similarly to peptide bond hydrolysis.[126] Zr^{4+} and Hf^{4+} M–POMs have also been shown to catalyze direct intermolecular amide bond formation in different organic solvents.[127,128] The catalytic activity of M–POMs towards both intra- and intermolecular peptide bond formation was found to depend on the POM structure and number of embedded metal centers.[126,129] Additionally, neutral hexanuclear and dodecanuclear Zr^{4+} clusters ($[Zr_6(OH)_4O_4(OMc)_{12}]$ where Mc = methacrylate and $[Zr_6(OH)_4O_4(OAcr)_{12}]_2$ where Acr = acrylate) have also shown promising catalytic activity towards direct intermolecular amide bond formation (Fig. 1(f) and 6(b)).[127,128] These findings highlight the potential of both M–POMs and neutral Zr^{4+} clusters as highly promising water-tolerant catalysts for peptide bond formation that do not require harsh conditions or the use of additives.[126–129]

2.1.4. Oxidative modifications and cleavage. Investigating the POM-promoted oxidation of amino acids, peptides, and proteins is essential for potential biomedical applications of POMs as it can provide valuable insights into the underlying mechanisms behind their biological activity. While the biological activity of POMs is largely believed to be linked to their redox activity, the mechanism of action is still not well understood.[130] Furthermore, oxidative modifications of proteins have been linked to many diseases, such as Alzheimer's and cancer. Therefore, selectively reproducing similar modifications *in vitro* using POMs would provide a better

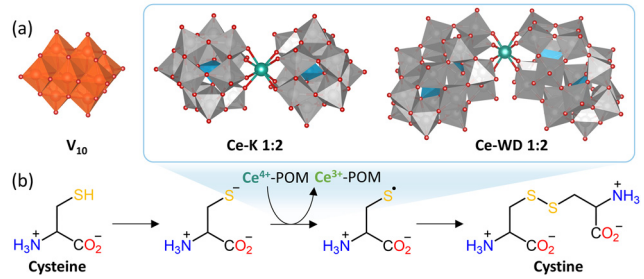

Fig. 7 (a) POM structures that have been reported to induce the oxidation of discrete amino acids or amino acids in peptides and/or proteins. (b) Proposed mechanism of the oxidation of cysteine to cystine *via* homocoupling of cysteinyl radicals.

understanding of the role of oxidation in the onset of these diseases.[130–133] Hence, the redox activity of POMs towards biomolecules could enable interesting opportunities in biomedicine.

POMs with redox-active metal centers have been shown to induce oxidative modifications in redox-active amino acids. Decavanadate ($[H_xV_{10}O_{28}]^{(6-x)-}$; V_{10}) has been proposed to oxidize certain cysteine (Cys) residues in actin proteins (Fig. 7(a)), which are present in muscle filaments, and in the Ca^{2+}-ATPase enzyme responsible for Ca^{2+} homeostasis and muscle relaxation.[134,135] This redox activity is likely linked to both the structure of V_{10} and the ease of V^{5+} reduction to V^{4+}. Vanadates with lower nuclearity did not oxidize Cys residues in actin and the isostructural decaniobate ($[Nb_{10}O_{28}]^{6-}$; Nb_{10}), which is kinetically inert and redox inactive, did not induce oxidation of Cys in Ca^{2+}-ATPase.[134,135] Furthermore, the redox activity of V_{10} is believed to be in part responsible for its ability to inhibit actin-stimulated myosin ATPase and Ca^{2+}-ATPase activity, which is of interest for the investigation and regulation of muscle function among other possible biomedical applications.[134,136] This illustrates how the redox activity of POMs likely plays an important role in their biological activity, which is especially relevant when exploring POMs as potential inorganic drugs.[57]

Our group has also recently shown that Ce^{4+}-substituted Keggin and Wells–Dawson POMs (Ce–POMs) displayed redox activity towards certain amino acids (Fig. 7(a)), which is likely driven by coordination of free carboxylate or amino groups to Ce^{4+}, as well as electrostatic and/or H-bonding interactions.[137] As with V_{10}, Cys was shown to be particularly susceptible to undergo oxidation into cystine in the presence of Ce–POMs, resulting in a concomitant reduction of Ce^{4+} to Ce^{3+}. Other redox-active amino acids – tryptophan (Trp), tyrosine (Tyr), histidine (His), and phenylalanine (Phe) – were also observed to cause reduction of Ce^{4+} in the M–POM to Ce^{3+}, but no oxidation products were detected.[137] This suggests that oxidation takes place *via* a radical mechanism in which the amino acids can be regenerated by the solvent or, in the case of Cys, cystine can form through homocoupling of cysteinyl radicals (Fig. 7(b)).

The rate of Ce^{4+} reduction in Ce–POMs by amino acids was found to depend on the nature of the amino acid side chain according to the following order: Cys ≫ Trp > Tyr > Phe ≈ His.[137] This corresponds to an inverse correlation with the redox potential of the amino acids, which means that amino acids that are oxidized more easily caused faster reduction of Ce^{4+}. The reaction rate of Cys oxidation was also observed to increase with the pH, temperature, and ionic strength. This suggests that cysteinyl radicals are formed from cysteinyl anions, which are favored at higher pH and whose coordination to the anionic M–POM is more favorable at higher ionic strengths due to shielding of repulsive electrostatic interactions. A similar influence of pH and ionic strength was also noted for Trp and Tyr, which can be attributed to a decrease in redox potential with increasing pH. In addition, due to the influence of the POM scaffold on the redox potential of Ce^{4+}, the rate of the reaction was also found to depend on the POM framework, with the Keggin Ce–POM giving a faster rate by one order of magnitude in comparison to the Wells–Dawson Ce–POM. Hence, several factors influence the ability of M–POMs to oxidize amino acids in solution, and the redox potential of both the amino acids and the Ce^{4+} center in the POM play an important role.

Oxidation of peptides was also observed in the presence of Ce–POMs, but the rate of reaction was affected by the incorporation of the amino acid into the peptide due to changes in the redox potential and additional steric effects.[137] Interestingly, the oxidation of peptides occurred at room temperature in the absence of any hydrolysis, indicating that the oxidation reaction is faster and the resulting formation of the Ce^{3+}–POM further prevents hydrolysis from occurring due to its lower Lewis acidity. In contrast, proteins have only been observed to induce reduction of the Ce^{4+} center in Ce–POMs upon incubation at higher temperatures. This was proposed to be due to amino acid residues within proteins being less accessible towards electron transfers, which makes reduction of Ce^{4+} by proteins less favorable at room temperature compared to peptides.[93] As a result, only partial reduction of Ce^{4+} to Ce^{3+} has been reported as a side-reaction during the hydrolysis of proteins by Ce–POMs.[85,116]

The redox activity of Ce^{4+} in Ce–POMs was found to have an impact on the efficiency and selectivity of the hydrolytic cleavage of hemoglobin, a tetrameric protein composed of two α-chains and two β-chains (Fig. 8(a) and Table 2).[93] It was observed that, at pH 5, Asp–X peptide bonds were hydrolyzed on both the α-chain (2 cleavage sites) and the β-chain (5 cleavage sites), but at pH 7.4 hydrolysis only occurred on the β-chain (1 cleavage site). This reduction in hydrolytic activity with increasing pH corresponds to weaker electrostatic interactions between the M–POM and the protein (pI = 6.8) and a higher rate of reduction of Ce^{4+} into the hydrolytically inactive Ce^{3+} at higher pH. Furthermore, the higher hydrolytic activity of the M–POM towards the β-chain is likely due to the higher number of redox-active residues on the α-chain, particularly His, which are able to reduce hydrolytically active Ce^{4+} into the hydrolytically inactive Ce^{3+}. This was confirmed by the hydrolytic activity of the redox-inactive Zr^{4+}–POM towards the α-chain (6 cleavage sites), which was higher compared to the Ce^{4+}–POM and did

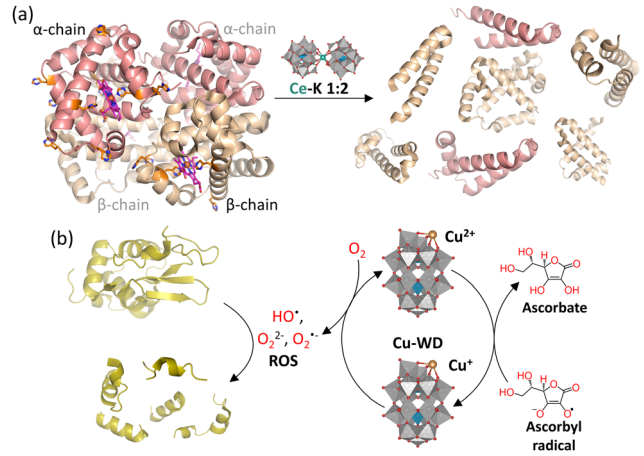

Fig. 8 (a) Hydrolysis of hemoglobin promoted by Ce–K 1 : 2 preferentially at the β-chain (beige) due to the higher number of redox active amino acids, such as histidine (orange), in the α-chain (pink) that cause reduction of Ce^{4+} to the less hydrolytically active Ce^{3+}. Adapted from ref. 93 with permission from the Royal Society of Chemistry. (b) Oxidative cleavage of lysozyme due to the production of reactive oxygen species (ROS) induced by Cu–WD in combination with ascorbate.

not decrease as significantly upon increasing the pH.[97] Therefore, the redox activity of certain M–POMs can be leveraged to tune their hydrolytic activity and selectivity. In addition, fragmentation of proteins catalyzed by redox-active POMs can occur in a stepwise manner first involving oxidation of amino acid residues followed by rearrangement and hydrolytic cleavage. This was observed for the cleavage of Ca^{2+}-ATPase enzyme into two fragments catalyzed by V_{10} under UV irradiation, which occurred presumably *via* photo-oxidation of certain amino acid residues, such as serine.[138] Hence, the oxidation of amino acid residues by POMs may play an integral role in protein fragmentation that can be leveraged for bioanalytical applications.

Another strategy to achieve protein fragmentation is through oxidative cleavage of the peptide bond. Our group has recently demonstrated that a Cu^{2+}-substituted Wells–Dawson POM (Fig. 8(b)), $[Cu(H_2O)(\alpha_2\text{-}P_2W_{17}O_{61})]^{8-}$ (Cu-WD), can selectively cleave HEWL in the presence of ascorbate (Asc) *via* the formation of reactive oxygen species (ROS).[130] The proposed mechanism involves the Asc-induced reduction of Cu^{2+} to Cu^+, which then reduces O_2 in the solution to form ROS in the vicinity of the protein (Fig. 8(b)), thereby producing radicals on the protein that subsequently break the peptide chain. Furthermore, as with the previously discussed hydrolytic reactions, binding of the POM to specific positively charged regions of the protein imposes the selectivity of the oxidative cleavage. However, protein fragmentation by oxidative cleavage is much faster than hydrolytic cleavage since fragments were obtained under physiological pH and temperature (37 °C; pH 7.5) after just 1 h. The cleavage efficiency was also observed to increase at more acidic pH, which was attributed to the enhanced production of ROS at lower pH. Hence, oxidative cleavage induced by POMs is a promising avenue for the selective oxidative modification and fragmentation of proteins, with many potential industrial, biomedical, and bioanalytical applications, such as in redox proteomics.[139]

2.2. Nucleic acids and nucleotides

2.2.1. Hydrolysis of nucleic acids and their model systems. The phosphoester bond, which forms the backbone of nucleic acids, is one of the most stable bonds present in biomolecules, with a half-life of ~100 000 years for DNA, which allows for the preservation of genetic material.[140] Nevertheless, the cleavage of phosphoester bonds is an essential step in a wide range of cellular processes, including DNA repair and excision.[141,142] In living organisms this is typically performed by metalloenzymes known as phosphatases or nucleases, most of which catalyze the hydrolysis of phosphoester bonds through two or more adjacent metal ions. These metal ions are typically positioned in such a way that activation of both the phosphate substrate and the water nucleophile is possible, which is necessary for the hydrolytic process to occur.[143] Hence, due to their inherent multinuclear composition, metallic clusters such as POMs, are particularly interesting for the development of artificial phosphatases. Investigating the hydrolytic activity of MOCs towards phosphoester bonds may also provide insights into the structure–activity relationships of metallic clusters in natural phosphatases. In addition, natural phosphatases are not easy to obtain in high purity and their enzymatic activity is often affected by the presence of other species in solution, such as amino acids. Therefore, there is a need for more accessible artificial phosphatases, which are of crucial importance in biology and medicine for the development of new therapeutic agents and biochemical tools.[144,145] In this respect, POMs have been shown to have promising antiviral, antibacterial, and antitumor activity that has often been linked to their phosphatase-like activity, making them attractive candidates for medical applications.[56,57,146–149] Hence, in order to better understand the biological activity of POMs and to develop them as artificial phosphatases, interaction and reactivity studies with nucleic acids and their model systems are of substantial interest.

Initial efforts to develop POMs as artificial phosphatases focused mostly on heptamolybdate ($[Mo_7O_{24}]^{6-}$; Mo_7), in part because this POM has shown considerable antitumor activity against different tumor cell lines, displaying comparable activity *in vivo* to some commercially used drugs.[150–156] Additionally, DNA fragmentation was detected for tumor cells treated with this POM.[150] In agreement with these observations, Mo_7 was shown to catalyze the hydrolysis of (*p*-nitrophenyl)phosphate (NPP) and bis(*p*-nitrophenyl)phosphate (BNPP), which are commonly used as model systems for DNA, as well as 2-hydroxypropyl-4-nitrophenyl phosphate (HPNP), an RNA model substrate (Fig. 9).[151–153,157] Although multiple oxomolybdate clusters that differ in structure and nuclearity can form in aqueous solution depending on the pH and the presence of other species in solution (*e.g.*, templating phosphate ions),[77] Mo_7 was proposed to be the catalytically active species since the rate of hydrolysis was highest at the pH where Mo_7 is the major component (pH 5–6).[151,153,157] In contrast, hydrolysis was

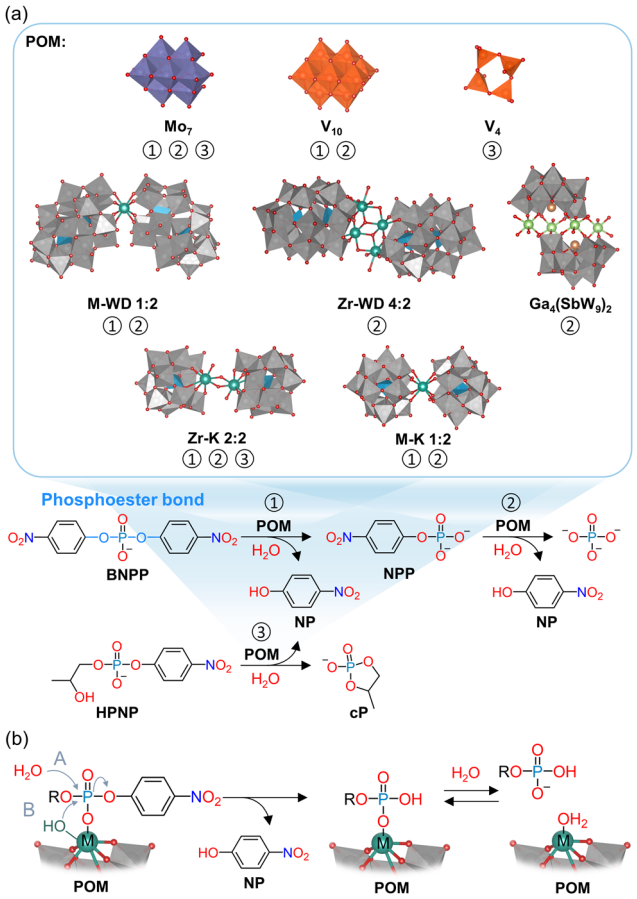

Fig. 9 (a) Hydrolysis of the phosphoester bond of DNA model systems, NPP and BNPP, catalyzed by $[Mo_7O_{24}]^{6-}$ (Mo_7), $[H_xV_{10}O_{28}]^{(6-x)-}$ (V_{10}), $[M(\alpha_2\text{-}P_2W_{17}O_{61})_2]^{16-}$ (M–WD 1 : 2), $[Zr_4(\mu_3\text{-}O)_2(OH)_2(H_2O)_4(P_2W_{16}O_{59})_2]^{14-}$ (Zr–WD 4 : 2), $[Ga_4(H_2O)_{10}(\beta\text{-}SbW_9O_{33})_2]^{6-}$ ($Ga_4(SbW_9)_2$), $[\{Zr\text{-}(\mu\text{-}OH)(H_2O)\alpha\text{-}PW_{11}O_{39}\}_2]^{8-}$ (Zr–K 2 : 2), and $[M(\alpha\text{-}PW_{11}O_{39})_2]^{10-}$ (M–K 1 : 2) as well as of the RNA model system HPNP by Mo_7, $[V_4O_{12}]^{4-}$ (V_4), and Zr–K 2 : 2. (b) Generalized mechanism of the hydrolysis of phosphate model systems by POMs through activation of the phosphoester bond towards nucleophilic attack by (A) solvent water or (B) metal-coordinated HO^-/H_2O.

barely observed at lower pH, where $[Mo_8O_{26}]^{4-}$ (Mo_8) is the main species (pH 2–6), or at higher pH (pH 8), where monomeric $[MoO_4]^{2-}$ predominates.[151,157] Therefore, this demonstrates that the specific multimetallic structure of Mo_7 is important for its catalytic activity towards phosphoester bond cleavage.

Even though the biological activity of POMs is often attributed to their redox properties, the cleavage of the phosphoester bond by Mo_7 was established to be purely hydrolytic and not oxidative in nature since the reduction of Mo^{6+} to Mo^{5+} was not observed.[151,153] The ability of Mo_7 to hydrolyze the phosphoester bond was suggested to be due to its lability and the partial detachment of at least one $\{MoO_4\}$ unit.[152,153] This allows for the incorporation of a phosphate group into the POM structure, which can induce bond strain and polarization of the P–O ester bond, thereby activating it towards nucleophilic attack by water.[152,153] Hence, the isostructural heptatungstate POM ($[W_7O_{24}]^{6-}$) was reported to be hydrolytically inactive as it is less labile.[157,158] Therefore, both the POM's structure and the composition of the POM in terms of the metal centers present have a large impact on its ability to promote the reaction.

Based on the proposed mechanism, the reaction of Mo_7 with phosphate substrates should result in the formation of an intermediate complex consisting of an oxomolybdate species with the bound phosphate substrate. In the case of the hydrolysis of NPP, these intermediate structures were proposed to be $[(NPP)_2Mo_5O_{21}]^{4-}$ and $[(NPP)_2Mo_{12}O_{36}(H_2O)_6]^{4-}$ based on diffusion ordered spectroscopy (DOSY) NMR.[152] These proposed structures are in agreement with the formation of a catalytically inactive phosphomolybdate species, $[(PO_4)_2Mo_5O_{15}]^{6-}$ (P_2Mo_5), after the hydrolysis of NPP and BNPP by Mo_7, as determined by both NMR and Extended X-ray Absorption Fine Structure (EXAFS) spectroscopy.[152,153] However, only a small amount of P_2Mo_5 was formed after the hydrolysis of HPNP by Mo_7.[151] This is likely because the reaction does not result in the formation of phosphate as the cyclic phosphate ester is produced instead (Fig. 9(a)). More recently, DFT calculations and electrospray ionization mass spectrometry (ESI-MS) have suggested that Mo_7 dissociates to form $[Mo_2O_8]^{4-}$ (Mo_2) and $[Mo_5O_{15}]^{0}$ (Mo_5). The binding of NPP to Mo_2, forming $[Mo_2O_4(OH)_4(NPP)]^{2-}$, was proposed to be responsible for promoting the cleavage of the phosphoester bond while the role of Mo_5 is to capture the phosphate resulting from the phosphoester bond cleavage leading to the formation of P_2Mo_5.[158] Overall, these results highlight the challenging nature of identifying the intermediate species that can form in reactions catalyzed by highly dynamic POM structures.

The hydrolysis of phosphoester bonds was observed to be catalyzed by vanadates as well. The reaction was determined to also be hydrolytic in nature and to proceed *via* incorporation of the phosphate substrate into the POM framework to activate the P–O bond.[159] This was supported by the fact that the rate of hydrolysis of NPP and BNPP increased with the ionic strength of the solution due to shielding of repulsive electrostatic interactions between the negatively charged substrate and the anionic POM catalyst.[160] Interestingly, based on the pH dependence of the rate constant, V_{10} was identified to be the main catalytically active species in the hydrolysis of NPP and BNPP, while $[V_4O_{12}]^{4-}$ (V_4) was proposed to be responsible for promoting the hydrolysis of HPNP (Fig. 9(a)).[159,160] This difference could be attributed to the formation of vanadate ester intermediates with HPNP, which was determined to be deprotonated under the employed reaction conditions. However, the exact nature of the intermediate species formed upon binding of the phosphate substrate to V_{10} or V_4 is unknown. Furthermore, the characterization of the species in solution is complicated by the dynamic exchange between oxovanadate species and/or the rapid association–dissociation equilibrium with the phosphate substrate in solution as observed by NMR.[159,160] Nevertheless, the catalytic activity of V_{10} and V_4 could also be attributed to their lability, which allows for the incorporation of the substrate into a polyoxovanadate cluster thereby activating it towards nucleophilic attack.

Overall, these studies on the reactivity of molybdates and vanadates towards DNA and RNA model systems showcase that due to the dynamic and complex speciation of these POMs in aqueous solutions, the exact structures of the intermediate species formed upon binding of the substrate are difficult to determine.[152,153,158–160] Hence, a multi-technique approach is necessary to elucidate the nature of the species present throughout a reaction.

Tungstate M–POMs were also investigated as catalysts towards the hydrolysis of the phosphoester bond since they are less dynamic in solution. Moreover, the embedded Lewis acidic metal centers in M–POMs can also activate the phosphoester bond as well as coordinate H_2O and/or HO^-, which can serve as a nucleophile that attacks the phosphoester bond (Fig. 9(b)). Several Wells–Dawson M–POMs with different metal ions were screened and the Zr^{4+} and Hf^{4+} M–POMs ($[M(\alpha_2\text{-}P_2W_{17}O_{61})_2]^{16-}$ where M = Zr^{4+} or Hf^{4+}) were found to display better hydrolytic activity towards both NPP and BNPP while M–POMs with other embedded metal ions (M = Mn^{3+}, Fe^{3+}, Co^{2+}, Ni^{2+}, Y^{3+}, La^{3+}, Eu^{3+}) displayed either no hydrolytic activity or were only able to hydrolyze NPP (Fig. 9). The better activity of Zr^{4+} or Hf^{4+} (Table 3) is due to their higher Lewis acidity, oxophilicity, redox-inactivity, fast ligand exchange as well as their ability to form complexes with high coordination numbers and flexible geometries.[161] In addition, similarly to the hydrolysis of peptide bonds (Section 2.1.1), it was determined that the 1 : 1 and 2 : 2 M–POM species were responsible for the hydrolytic activity since these species have vacant coordination sites that are available for the phosphate substrate to coordinate. This was confirmed by the faster rate of hydrolysis at lower pH values, which favors the formation of the monomeric 1 : 1 M–POM. The reaction was determined to proceed through a similar mechanism to that observed for molybdates and vanadates, involving activation of the P–O bond towards

Table 3 Conditions and rate constants (k_{obs}) of selected reports on the hydrolysis of phosphoester/phosphoanhydride bonds catalyzed by different POMs

POM	Substrate	Reaction conditions	Conversion & $k_{obs}/\times10^{-6}$ s^{-1}	Ref.
Mo_7	NPP	pD 5.5, 50 °C, 1 eq. POM	78.0	152
		pD 5.1, 50 °C, 7 eq. POM	27.3	153
	BNPP	pD 5.5, 50 °C, 1 eq. POM	2.3	157
	HPNP	pD 5.7, 50 °C, 0.1–1.0 eq. POM	3.9 (0.1 eq.)–6.4 (1 eq.)	151
	ATP	pH 2–6, r.t., 20 eq. Na_2MoO_4	3.7 (pH 6)–5.5 (pH 2) mM h^{-1}	162
	ADP	pH 4, r.t., 5 h, 20 eq. Na_2MoO_4	12% yield of AMP	162
Mo_8Pro	ATP	pH 3.4, r.t., 12 h, 3 eq. POM	100% conversion	163
		pH 7, r.t., 48 h, 3 eq. POM	75% conversion	
$Mo_{12}(Mo_4)$	ATP	pH 5, 25 °C, 10 days, 1 eq. POM	10% conversion	164
		pH 5, 40 °C, 10 days, 1 eq. POM	72% conversion	
		pH 5, 40 °C, 10 days, 1 eq. POM, K^+	86% conversion	
		pH 7.5, 40 °C, 10 days, 1 eq. POM	41% conversion	
	ADP	pH 5, 40 °C, 10 days, 1 eq. POM	26% conversion	164
		pH 7.5, 40 °C, 10 days, 1 eq. POM	6% conversion	
V_{10}	NPP	pD 5.0, 50 °C, 10 eq. of Na_3VO_4	17.0	160
	BNPP	pD 5.0, 70 °C, 10 eq. of Na_3VO_4	3.3	160
	ATP	pH 2, 25 °C, 10 eq. Na_3VO_4	1130.0 (k_1; ATP → ADP)	165
			46.7 (k_2; ADP → AMP)	
		pH 2, 50 °C, 10 eq. Na_3VO_4	10730.0 (k_1; ATP → ADP)	
			383.3 (k_2; ADP → AMP)	
		pH 7, 50 °C, 10 eq. Na_3VO_4	4.3 (k_1; ATP → ADP)	
			4.3 (k_2; ADP → AMP)	
V_4	HPNP	pD 7.0, 37 °C, 0.66 eq. Na_3VO_4	1.9	159
M–WD 1 : 2 (M = Y^{3+}, La^{3+}, Eu^{3+})	NPP	pD 7.2, 50 °C, 1 eq. POM	0.3 (M = Y^{3+})	161
		pD 7.2, 50 °C, 1 eq. POM	0.8 (M = La^{3+}, Eu^{3+})	
Zr–WD 1 : 2	NPP	pD 7.2, 50 °C, 1 eq. POM	12.8	161
	BNPP	pD 7.2, 50 °C, 1 eq. POM	0.7	161
Hf–WD 1 : 2	NPP	pD 7.2, 50 °C, 1 eq. POM	19.7	161
	BNPP	pD 7.2, 50 °C, 1 eq. POM	1.1	161
Zr–WD 4 : 2	NPP	pD 6.4, 50 °C, 0.2 eq. POM	84.4	166
	BNPP	pD 6.4, 50 °C, 0.2 eq. POM	0.3	166
	HPNP	pD 6.4, 50 °C, 0.2 eq. POM	5.1	166
$Al_4(SbW_9)_2$	NPP	pD 6–7, 60 °C, 0.5 eq. POM	6.9 (pD 7)–12.2 (pD 6)	167
$Ga_4(SbW_9)_2$	NPP	pD 4–8, 60 °C, 0.5 eq. POM	0.9 (pD 8)–23 (pD 4)	167
	ATP	pD 5, 50 °C, 20 h, 0.1 eq. POM	75% conversion	167
Zr–K 1 : 2	BNPP	pD 6.4, 60 °C, 1 eq. POM	1.1	143
	HPNP	pD 6.4, 50 °C, 1 eq. POM	9.2	168
Zr–K 2 : 2	BNPP	pD 6.4, 60 °C, 1 eq. POM	4.8	143
	HPNP	pD 6.4, 50 °C, 1 eq. POM	115.0	168
	ATP	pD 6.4, 50 °C, 1 eq. POM	10.4	144
		pD 6.4, 50 °C, 0.15 eq. POM	1.97	
Ce–K 1 : 2	NPP	pD 6.4, 50 °C, 1 eq. POM	5.3	169

r.t. = room temperature.

nucleophilic attack by a water molecule through coordination of the phosphate substrate to the embedded metal center, but without any structural rearrangement of the POM (Fig. 9(b)). Although the rate of hydrolysis was slower compared to Mo_7 (Table 3), the M–POMs could be used in catalytic amounts and under physiological pH conditions.[161]

The reactivity of M–POMs with multiple substituted metal centers was also investigated since the hydrolysis of phosphoester bonds is usually favored through adjacent metal centers, as observed in natural phosphatases. Accordingly, $[Zr_4(\mu_3\text{-}O)_2(OH)_2(H_2O)_4(P_2W_{16}O_{59})_2]^{14-}$ (Zr–WD 4 : 2), which has four Zr^{4+} centers, gave rise to faster hydrolysis of NPP in comparison to Zr–WD 1 : 2 (Table 3), which has only one Zr^{4+} center, and the catalyst remained active after at least 3 cycles.[166] For this reaction, it was proposed that NPP coordination occurs *via* the replacement of one of the waters coordinated to two Zr^{4+} centers, $\{Zr(H_2O)_2\}$, and the phosphoester bond could be hydrolyzed by nucleophilic attack of the second coordinated water or solvent water (Fig. 9(b)). Furthermore, since there are two Zr^{4+} centers with coordinated water ligands, coordination and hydrolysis of NPP can potentially occur simultaneously at both sites. Moreover, Zr–WD 4 : 2 was found to be active towards BNPP and HPNP as well.[166] Similarly, the sandwich-type Krebs M–POMs ($[M_4(H_2O)_{10}(\beta\text{-}SbW_9O_{33})_2]^{6-}$ where M = Ga^{3+} or Al^{3+}; $M_4(SbW_9)_2$), containing four metallic centers with available coordination sites, also showed hydrolytic activity towards NPP (Fig. 9).[167] However, due to the poor solubility of these Krebs M–POMs, the mechanism of action could not be investigated.

The reaction mechanism for the hydrolysis of NPP, BNPP, and HPNP by M–POMs was investigated in more detail for the dimeric Keggin M–POM with two adjacent Zr^{4+}, Zr–K 2 : 2, due to its higher solubility (Fig. 9).[143,168] Hydrolysis of BNPP was 5 times faster with Zr–K 2 : 2 in comparison to Zr–K 1 : 2 (Table 3) due to the presence of more Zr^{4+} centers with free coordination sites in Zr–K 2 : 2 that allow for easier nucleophilic activation. However, the monomeric Zr–K 1 : 1, which is in equilibrium with both Zr–K 1 : 2 and Zr–K 2 : 2, was proposed to be the catalytically active form, in agreement with the results for peptide bond hydrolysis. The reaction mechanism for the hydrolysis of BNPP involves monodentate coordination of BNPP to Zr–K 1 : 1 followed by intramolecular nucleophilic attack of the phosphate group by an OH group coordinated to the Zr^{4+} center, which leads to the release of *p*-nitrophenol (NP) and the formation of NPP (Fig. 9(b)). The formed NPP can also coordinate to Zr–K 1 : 1 and undergo hydrolysis *via* nucleophilic attack of a solvent water molecule. A similar reaction mechanism was also suggested for the hydrolysis of HPNP catalyzed by Zr–K 2 : 2.[168]

The reactivity of the dimeric Ce^{4+} Keggin M–POM ($[Ce\{\alpha\text{-}PW_{11}O_{39}\}_2]^{10-}$; Ce–K 1 : 2) towards NPP was also investigated *via* NMR experiments and DFT calculations to determine the influence of the embedded metal ion on the hydrolysis reaction (Fig. 9).[168,169] The monomeric Ce–K 1 : 1 species was suggested to be responsible for the hydrolytic activity in a comparable manner to what was established for Zr–POMs, even though Ce^{4+} has a higher coordination number than Zr^{4+} and Ce–K 1 : 2 is not coordinatively saturated. Due to the higher coordination number of Ce^{4+}, two NPP molecules were proposed to coordinate to Ce^{4+} at once, while only one coordinated NPP substrate was proposed for Zr^{4+}. However, it was determined that only one of the coordinated NPP molecules can be hydrolyzed at a time during the reaction process. Therefore, changing the metal center to Ce^{4+} did not have a major effect on the mechanism.

Based on the understanding gained from the studies on the model systems, the hydrolysis of supercoiled plasmid pUC19 DNA catalyzed by Zr–K 2 : 2 at physiological pH and temperature was also investigated.[170] Hydrolysis of one strand of DNA led to the relaxed form while hydrolysis at both strands was shown to result in the linear form (Fig. 10). Hydrolysis of calf thymus DNA (ctDNA) with the same M–POM was also attempted, but characterization of the fragmentation products was not successful since ctDNA is a complex mixture of linear

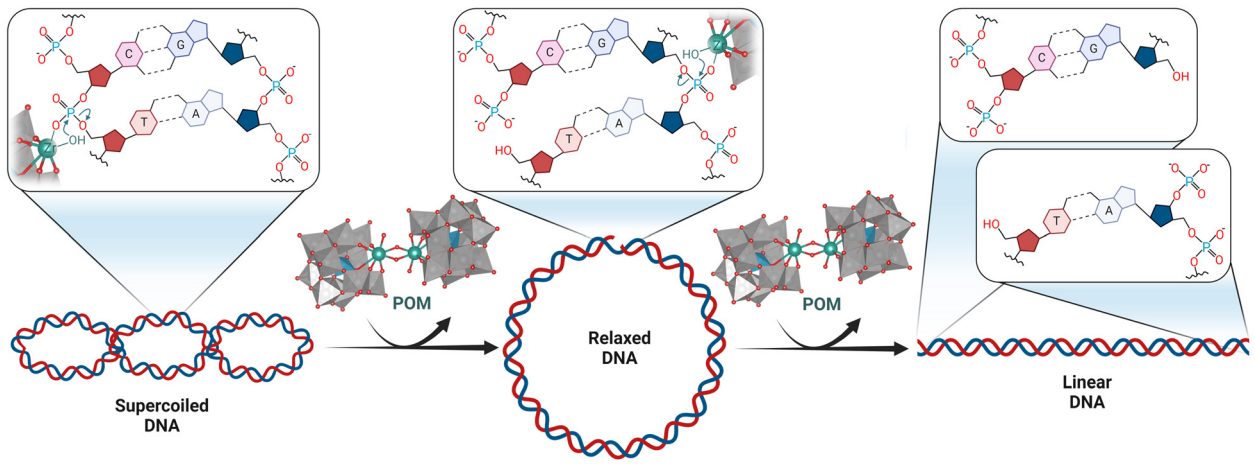

Fig. 10 Schematic representation of the proposed mechanism for phosphoester bond hydrolysis of supercoiled plasmid pUC19 DNA catalyzed by Zr-K 2:2, resulting in the relaxed form after cleavage of one strand of DNA and in the linear form after cleavage of both strands.

DNA fragments of different lengths.[170] To date, this remains the only reported study specifically on the hydrolysis of DNA catalyzed by POMs and no reports on the hydrolysis of RNA promoted by POMs have been published so far. Nevertheless, the antitumor activity of cyclopentadienyltitanium substituted Keggin M–POMs was proposed to be potentially linked to DNA hydrolysis, since agarose gel electrophoresis indicated that fragmentation of plasmid DNA occurred upon incubation with $K_4H_3[(CpTi)_3SiW_9O_{37}]$.[171] However, to the extent of our knowledge, this was not investigated further and the nature of the catalytically active species has not been confirmed since the stability of this M–POM after incubation with DNA was not reported. Therefore, the insights gained from the model systems still need to be implemented more extensively in the design of effective catalysts for the controlled hydrolysis of nucleic acids. This is essential in order to bridge the gap between simple model systems and more complex biomolecules, and, in doing so, gain a deeper understanding of the biological activity of POMs from a molecular point of view. Furthermore, this is also necessary for the development of POMs as genomic tools or therapeutic agents, with potential impact in biomedical sciences, biotechnology, and pharmacology.

2.2.2. Hydrolysis of nucleotides. Adenosine triphosphate (ATP) is an essential molecule in living organisms that provides the energy needed to drive many of the biochemical processes of life.[143] This transfer of energy is achieved through the energy released from the hydrolysis of the phosphoanhydride bond within the triphosphate group of ATP, to form adenosine diphosphate (ADP), which can be hydrolyzed further to form adenosine monophosphate (AMP) as shown in Fig. 11. In addition, ATP serves as a precursor for other important biomolecules such as RNA and DNA.[172] Furthermore, ATP is also a therapeutic target in diseases such as cancer which are known to result in consumption of ATP at a much higher unregulated rate than normal.[173] Therefore, catalysts that can hydrolyze ATP are of interest for biomedical applications.

As with phosphoester bond hydrolysis, initial studies into the hydrolysis of the phosphoanhydride bond catalyzed by POMs were in part inspired by the antitumor activity of Mo_7, which has also been attributed to the ability of molybdates to inhibit the formation of ATP.[150,163] At pH 6 and 4, ATP was hydrolyzed by Mo_7 into ADP as the main product, whereas AMP was obtained as the major species at pH 2 and no hydrolysis was observed at pH 14.[162] The reaction mechanism was proposed to involve the incorporation of the phosphate groups into an oxomolybdate structure, resulting in different phosphomolybdate intermediate species as well as P_2Mo_5, $[(O_3POPO_3)Mo_6O_{18}(H_2O)_4]^{4-}$ (P_2Mo_6), and Keggin-type phosphomolybdates as side-products. P_2Mo_5 was mainly observed as a side product of the reactions where ADP was the major product, while only P_2Mo_6 formed at lower pH when AMP was the main product. Hence, it was proposed that binding of ATP to a species similar to P_2Mo_5 results in ADP while binding of ATP to a P_2Mo_6-like species results in the direct formation of AMP, with the speciation being determined by the pH. Interestingly, unlike in phosphoester bond hydrolysis, ATP hydrolysis was observed in the presence of excess P_2Mo_5. Therefore, the speciation in solution should be further investigated to determine the reaction mechanism, which may differ from phosphoester bond hydrolysis.

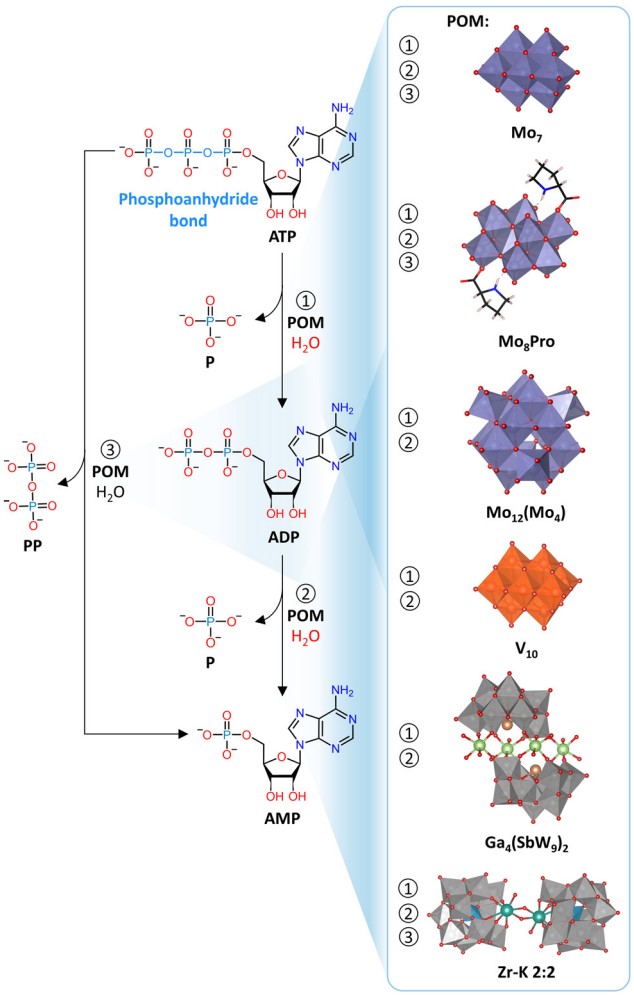

Fig. 11 Hydrolysis of the phosphoanhydride bond to form ADP from ATP (1) as well as AMP stepwise from ADP (1–2) or directly from ATP (3) catalyzed by Mo_7, Mo_8Pro, $Mo_{12}(Mo_4)$, V_{10}, $Ga_4(SbW_9)_2$, or Zr–K 2 : 2.

Since octamolybdate POMs functionalized with amino acids have been shown to inhibit the growth of cancer cell lines,[147] the hydrolysis of ATP catalyzed by γ-octamolybdate covalently functionalized with two proline moieties ($[Mo_8O_{24}(OOCC_4H_8N)_2]^{4-}$; Mo_8Pro) was also investigated (Fig. 11).[163] A similar pH dependence and intermediate speciation to that observed with Mo_7 was reported, with ADP and AMP being formed in equal amounts at pH 3.4, while ADP was favored at higher pH. This was linked to a structural rearrangement of Mo_8Pro to form Mo_7 when the pH was increased to 5.7 and its decomposition into $[MoO_4]^{2-}$ at physiological pH. Nevertheless, even at physiological pH hydrolysis of *ca.* 75% of ATP into ADP was still observed but at a lower rate (Table 3), which was suggested to be due to the small amount of the (rearranged) Mo_8Pro still present at this pH since $[MoO_4]^{2-}$ is hydrolytically inactive. However, after 24 h at pH 3.4, $[Mo_8O_{26}]^{4-}$ fully converted ATP to AMP while with Mo_8Pro significant

amounts of ADP were still present, suggesting that the proline functionality hinders the reactivity in this case. Nevertheless, this is one of the very few reported examples of the reactivity of an organic–inorganic hybrid POM towards a biomolecule. Therefore, further research should be performed to determine the role of the organic functionality and, in doing so, optimize the reactivity.

Another polyoxomolybdate with anticancer activity that has also been investigated as a catalyst for ATP hydrolysis is $[H_2Mo^{5+}{}_{12}O_{28}(OH)_{12}(Mo^{4+}O_3)_4]^{6-}$ ($Mo_{12}(Mo_4)$), which consists of a 12-electron reduced ε-Keggin core capped at four triangular faces with $\{Mo^{4+}O_3\}$ moieties and can be obtained from Mo_7 by photoreduction (Fig. 11).[164] At 40 °C and pH 5 or pH 7.5, $Mo_{12}(Mo_4)$ hydrolyzed ATP into ADP as the major product while producing AMP and P_2Mo_5 as minor products, which remained present in low concentrations even after 10 days without any other byproducts. Furthermore, the rate of hydrolysis was faster at pH 5 than at pH 7.5 (Table 3). However, the rate of hydrolysis of ADP was much slower than for ATP, with only 26% conversion after 10 days at 40 °C (pH 5), and there was barely any hydrolysis of AMP, demonstrating the selectivity of $Mo_{12}(Mo_4)$ for phosphoanhydride bond hydrolysis of ATP. Interestingly, the rate of hydrolysis was found to increase in the presence of K^+ ions, which can shield repulsive interactions between the two negatively charged species (Table 3). In addition, the POM core remained relatively unchanged throughout the reaction as only partial release of $\{Mo^{4+}O_3\}$ moieties was detected, which suggests that a P_2Mo_5-like species is not formed as an intermediate and the small amounts of P_2Mo_5 are formed from the released $\{Mo^{4+}O_3\}$ moieties. However, the exact mechanism has not been investigated further. Like for Mo_8Pro, this study stands out because it is one of the very few examples of the use of a reduced POM to promote biomolecular transformations and, therefore, incites further study of the reactivity of reduced POMs.

In addition to molybdates, several other POMs that were investigated as catalysts for phosphoester bond hydrolysis have been shown to be catalytically active towards ATP. For instance, the hydrolytic activity of vanadates has been recently reported.[165] In contrast to the results obtained for molybdates, the hydrolysis of ATP into ADP and AMP was seen to occur in succession, with AMP being formed from the hydrolysis of ADP rather than directly from ATP.[165] The mechanism was proposed to also involve complexation of the phosphate substrate to form an intermediate phosphovanadate species of unknown structure and composition. Furthermore, the rate of hydrolysis was highest at pH 2 (Table 3), where protonated V_{10} (Fig. 11) is the main species in solution. Therefore, it was proposed that V_{10} is more active than other vanadate species present at higher pH due to the lower negative charge of protonated V_{10} ($[H_3V_{10}O_{28}]^{3-}$), resulting in less electrostatic repulsion towards ATP, as well as the higher kinetic lability of the oxo ligands of vanadates at lower pH.

M–POMs have also been reported to hydrolyze ATP. The Krebs-type M–POM $Ga_4(SbW_9)_2$ was shown to catalyze the hydrolysis of ATP in a stepwise manner to produce ADP and then AMP (Fig. 11).[167] However, although NMR indicated that complexation of the terminal phosphate of ATP to the M–POM likely occurred, the exact mechanism and the intermediate species formed are not known. A more detailed investigation into the mechanism was performed for the hydrolysis of ATP catalyzed by Zr–K 2 : 2 (Fig. 11).[144] It was proposed that Zr^{4+} coordinates to either the terminal or the central phosphate groups of ATP, thereby activating them towards nucleophilic attack by coordinated OH^- or free H_2O. Hence, either stepwise formation of ADP and then AMP or direct formation of AMP could take place depending on where Zr^{4+} coordinates. Interestingly, phosphoester bond cleavage in AMP that would result in the formation of free triphosphate was not observed. Therefore, this illustrates the powerful selective nature of M–POM catalysts.

Overall, these studies provide valuable insights into the interactions and reactivity of POMs towards ATP. However, they mainly rely on NMR spectroscopy to obtain mechanistic insights. Therefore, additional studies employing complementary techniques, such as ESI-MS, and theoretical studies are necessary in order to gain a deeper understanding of how POMs catalyze the hydrolysis of ATP and how the selectivity of hydrolysis can be controlled.

2.3. Carbohydrates

Polysaccharides are polymeric chains of monosaccharides that are linked together *via* glycosidic bonds (Fig. 12) and are used by organisms for energy storage (*e.g.*, starch) or as structural elements (*e.g.*, cellulose).[174] Since polysaccharides represent a major component of biomass, their breakdown into monosaccharides, such as glucose, is the first step in the conversion of biomass into renewable and sustainable fuels.[175,176] This is an important type of reactivity to address since the environmentally damaging effects of the overconsumption of fossil fuels have led to the exploration of sustainable alternatives, and the conversion of biomass is a particularly attractive option because it is the only renewable carbon reservoir for the

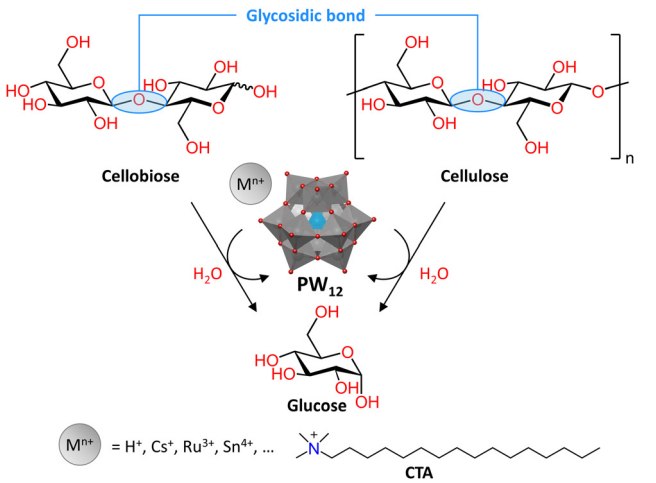

Fig. 12 Hydrolysis of the glycosidic bond in cellobiose and cellulose into glucose catalyzed by $(M^{n+})_{3/n}[PW_{12}O_{40}]^{3-}$ (PW_{12}) with different counter-cations.

production of fuels and chemicals.[177] However, commonly employed techniques for biomass valorization (*i.e.*, thermochemical, enzymatic, and bacterial degradation) suffer from several drawbacks.[178–181] Therefore, the development of efficient catalysts is critical for the synthesis of biofuels as well as bulk and commodity chemicals, altogether contributing to the development of a sustainable chemical industry.

2.3.1. Hydrolysis of biomass sugars. Cleavage of glycosidic bonds in the polysaccharides that compose cellulosic biomass is typically achieved by employing mineral acids or natural enzymes.[182–184] However, both methods have disadvantages. Controlling the selectivity, rate, and efficiency of the hydrolysis reaction in the presence of mineral acids is very challenging, and the subsequent separation of the obtained products is difficult.[176,185,186] Moreover, corrosion of the reactor and high equipment cost associated with using mineral acids, together with waste disposal problems, represent major obstacles.[185] Additionally, such processes require very high pressures and temperatures (100–300 °C), which can result in side reactions and degradation of the obtained products.[176,185,186] Enzymatic processes, on the other hand, are less harmful and operate under very mild reaction conditions, but the high cost of the currently used enzymes and their limited recyclability, stability, and substrate selectivity hinder their use in industry.[176,186] Therefore, there is a great need for developing more environmentally conscious and cost-effective biomass conversion catalysts that can operate under mild reaction conditions.

Heteropolyacids (HPAs), a subclass of protonated POMs, have been investigated as homogeneous and heterogeneous catalysts due to their potential reusability, strong Brønsted acidity, proton mobility, and excellent stability at high temperatures, making them potentially very effective catalysts for biomass conversion, as has been recently reviewed in detail.[175,187–189] For instance, the Keggin-type HPAs $H_3[PW_{12}O_{40}]$ and $H_4[SiW_{12}O_{40}]$ were shown to catalyze the selective hydrolysis of cellobiose – a glucose disaccharide model for cellulose – as well as the more complex polysaccharides cellulose and lignocellulose (Fig. 12).[175,185] These studies showed that HPAs give better yields than traditional mineral acids due to their higher Brønsted acidity, with $H_3[PW_{12}O_{40}]$ displaying slightly better reactivity than $H_4[SiW_{12}O_{40}]$ (Table 4).[185] Brønsted acidity is needed for the hydrolysis of carbohydrates since the reaction mechanism proceeds first *via* protonation of the ether oxygen in the glycosidic bond, making it a good leaving group. This is in contrast to the hydrolysis of peptides/proteins, nucleic acids, and nucleotides where the mechanism involves Lewis acidic activation of C=O or P=O bonds towards nucleophilic attack. As a result, HPAs rather than M–POMs have been predominantly investigated for the hydrolysis of sugars.

In order to optimize the hydrolytic activity of $H_3[PW_{12}O_{40}]$, different parameters have been investigated, such as the catalyst loading, reaction time, and temperature. In doing so, better selectivity was observed at elevated temperatures, which could be exploited due to the high hydrothermal stability of the HPA.[175] However, extended hydrolysis at higher temperatures resulted in reduced glucose yield due to the formation of by-products.[175,202] Additionally, due to their high thermal stability and high Brønsted acidity, HPAs ($H_3[PW_{12}O_{40}]$, $H_3[PMo_{12}O_{40}]$, $H_4[SiW_{12}O_{40}]$, $H_4[SiMo_{12}O_{40}]$, $H_4[PVMo_{11}O_{40}]$, $H_5[PV_2Mo_{10}O_{40}]$) were also shown to be suitable catalysts for the thermal decomposition of lignocellulosic biomass in pine wood as they lowered the required temperature by 100 °C.[203] Furthermore, the reusability of $H_3[PW_{12}O_{40}]$ through extraction with diethyl ether or recrystallization was also reported.[175] More recently, it was found that microwave-assisted conversion of cellulose to glucose can be performed in the presence of a Wells–Dawson HPA, $H_6[P_2W_{18}O_{60}]$.[190] However, Keggin-type HPAs have shown better performance (Table 4).[190] Therefore, $H_3[PW_{12}O_{40}]$ has been identified as a promising catalyst for biomass conversion.

The reactivity and selectivity of $H_3[PW_{12}O_{40}]$ can be tuned through the replacement of the protons by counter-cations. A systematic study of 11 different metal counter-cations ($M_{3/n}[PW_{12}O_{40}]$; M^{n+} = Ag^+, Ca^{2+}, Co^{2+}, Y^{3+}, Sn^{4+}, Sc^{3+}, Ru^{3+}, Fe^{3+}, Hf^{4+}, Ga^{3+}, and Al^{3+}) established that the Lewis acidity of the counter-cation has an influence on the hydrolytic activity of the POM towards cellobiose and cellulose. POMs with counter-cations having moderate Lewis acidities, such as Sn^{4+} and Ru^{3+}, gave higher conversion rates and even better turnover frequencies for the formation of glucose compared to $H_3[PW_{12}O_{40}]$.[185] Furthermore, in order to develop HPAs as suitable heterogeneous catalysts with a high-surface area, the hydrolytic activity of microporous and insoluble Cs^+ salts of $H_3[PW_{12}O_{40}]$ ($Cs_xH_{3-x}[PW_{12}O_{40}]$; x = 1–3) towards cellulose has also been investigated.[192,204] By varying the number of available surface acid sites through the partial substitution of protons by Cs^+, $Cs_1H_2[PW_{12}O_{40}]$ was shown to have the best catalytic activity due to its higher Brønsted acidity (Table 4). Contrastingly, $Cs_{2.2}H_{0.8}[PW_{12}O_{40}]$ showed the highest selectivity, which was attributed to its microporous structure.[192] Similar results were reported for the hydrolytic activity of $H_3[PW_{12}O_{40}]$ with the cationic surfactant cetyltrimethylammonium ($C_{16}H_{33}N(CH_3)_3^+$; CTA), which forms a supramolecular micellar assembly with the POM that was shown to efficiently and selectively hydrolyze sucrose, starch, and cellulose.[193] By varying the ratio of protons to CTA ($(CTA)_xH_{3-x}[PW_{12}O_{40}]$), the conversion and selectivity of the hydrolysis of the disaccharide sucrose into glucose and fructose was found to be highest for $(CTA)_1H_2[PW_{12}O_{40}]$ due to its greater Brønsted acidity (Table 4). Furthermore, $(CTA)_1H_2[PW_{12}O_{40}]$ produced relatively higher yields of the monosaccharides compared to $H_3[PW_{12}O_{40}]$, which was attributed to the accumulation of sucrose around the POM due to the formation of micelles. Moreover, the micellar catalyst could be removed through centrifugation and reused without any significant loss of catalytic activity. These reports are noteworthy since, although the hydrolytic activity is mainly accredited to the Brønsted acidity of the HPA, they tackle reaction optimization through the structure–activity relationship of the counter-cation rather than that of the POM framework itself. This is in stark contrast to many of the previously mentioned studies on the reactivity of POMs towards biomolecules, where the role of the counter-cation has been scarcely discussed.

Table 4 Selected conditions and percentage conversion of various sugars catalyzed by different POMs

POM	Substrate	Reactivity	Reaction conditions	Conversion/%	Ref.
$H_3[PW_{12}O_{40}]$	Cellulose	Hydrolysis	H_2O, 180 °C, 2 h, 0.08 mmol POM	51% glucose	175
			H_2O, 120 °C, 24 h, 6 mol% POM	18	185
			H_2O, 160 °C, 0.25 h, 0.14 mmol POM	90 (77% glucose)	190
	Cellobiose	Hydrolysis	H_2O, 120/150 °C, 24 h, 0.07 mmol POM	53 (51% glucose)	185
	Lignocellulose	Hydrolysis	H_2O, 120/150 °C, 24 h, 6 mol% POM	39	185
$H_4[SiW_{12}O_{40}]$	Cellobiose,	Hydrolysis	H_2O, 120 °C, 24 h, 0.07 mmol POM	61 (53% glucose)	185
	Cellulose	Hydrolysis	H_2O, 120 °C, 24 h, 6 mol% POM	17	185
	Chitin	Hydrolysis, isomerization & dehydration	DMSO : H_2O (1 : 3), 200 °C, 3 min 0.2 mmol POM	23% HMF	191
$H_6[P_2W_{18}O_{60}]$	Cellulose	Hydrolysis	H_2O, 160 °C, 5 min, 0.1 mmol POM	47 (37% glucose)	190
$Cs_1H_2[PW_{12}O_{40}]$	Cellulose	Hydrolysis, isomerization & dehydration	H_2O, 160 °C, 6 h, 0.06 mmol POM	27% glucose	192
$(CTA)_1H_2[PW_{12}O_{40}]$	Sucrose	Hydrolysis, isomerization & dehydration	H_2O, 80 °C, 1 h, 0.08 mmol POM	100	193
	Starch	Hydrolysis, isomerization & dehydration	H_2O, 120 °C, 5 h, 0.07 mmol POM	96 (82% glucose)	193
	Cellulose	Hydrolysis, isomerization & dehydration	H_2O, 170 °C, 8 h, 0.07 mmol POM	44	193
$Cr((DS)H_2[PW_{12}O_{40}])_3$	Cellulose	Hydrolysis, isomerization & dehydration	H_2O, 150 °C, 2 h, 0.06 mmol POM	77 (53% HMF)	194
$Sn_{0.1}H_{2.6}[PW_{12}O_{40}]$	Cassava starch	Hydrolysis, isomerization & dehydration	DMSO/THF/NaCl, 160 °C, 1 h, 0.1 mmol POM	91 (54% HMF)	195
$KH_3[CrPW_{11}O_{39}]$	Glucose	Dehydration	H_2O, 130 °C, 2 h, 0.1 mmol POM	76 (33% HMF)	196
	Fructose	Dehydration	H_2O, 130 °C, 1.5 h, 0.1 mmol POM	91 (33% HMF)	196
$(CTA)H_3[CrPW_{11}O_{39}]$	Glucose	Dehydration	H_2O, 130 °C, 2 h, 0.1 mmol POM	84 (42% HMF)	196
	Fructose	Dehydration	H_2O, 130 °C, 1.5 h, 0.1 mmol POM	90 (41% HMF)	196
$Fe[PW_{12}O_{40}]$	Fructose	Dehydration	DMSO, 120 °C, 2 h, 6.9 μmol POM, 0.1 MPa	100 (97% HMF)	197
$Cs_{2.5}H_{0.5}[PW_{12}O_{40}]$	Fructose	Dehydration	MIBK, 115 °C, 2 h, 0.45 mmol POM	95 (78% HMF)	198
$Ag_3[PW_{12}O_{40}]$	Fructose	Dehydration	H_2O/MIBK, 120 °C, 1 h, 0.02 mmol POM	78% HMF	199
	Glucose	Isomerization & dehydration	H_2O/MIBK, 130 °C, 4 h, 0.1 mmol POM	76% HMF	199
$[MimAM]H_2[PW_{12}O_{40}]$	Glucose	Dehydration	THF/H_2O/NaCl, 160 °C, 7.5 h, 30 μmol POM	100 (54% HMF)	200
$TBA_6[P_2W_{17}–SO_3H]$	Fructose	Dehydration	1,4-Dioxane, 100 °C, 2 h, 150 mg POM	99% HMF	201

Hence, inspiration can be drawn from these results to apply the same strategies of systematic counter-cation variation to the optimization of reactivity in other areas.

2.3.2. Dehydration of sugars into platform chemicals. POMs have been shown to be effective catalysts not only in the hydrolysis of polysaccharides into monosaccharides but also for their conversion into platform chemicals such as 5-hydroxymethylfurfural (HMF). HMF is a useful, versatile, and key intermediate platform in the formation of industrially relevant value-added chemicals such as levulinic acid (LA), γ-valerolactone (GVL), caprolactam, adipic acid, and furan derivatives, such as 2,5-furandicarboxylic acid (Fig. 13). These value-added chemicals can in turn be used for manufacturing fuel additives, biofuels, polymers, and pharmaceuticals.[191,193,195,204,205] HMF can be obtained directly from fructose *via* an acid-catalyzed dehydration process. However, due to the high cost of fructose, glucose is a more attractive starting material for the synthesis of HMF due to its higher abundance in lignocellulosic biomass.[205] Hence, HMF can be obtained from cellulosic biomass through its hydrolysis into glucose, usually followed by isomerization to fructose, which is further followed by dehydration (Fig. 13). HPAs can catalyze all these reactions allowing for the one-pot conversion of biomass into HMF.

Conversion of cellulose, as well as more complex mixtures of holocellulose and lignocellulose, into HMF under relatively mild conditions has been reported using $H_3[PW_{12}O_{40}]$ and a micellar HPA, $Cr((OSO_3C_{12}H_{25})H_2[PW_{12}O_{40}])_3$ ($Cr(DS)H_2PW_{12}$ where DS = dodecyl sulfate), which has both Brønsted and Lewis acidic sites due to the Cr^{3+} counter-cation.[194,203] This synergistic combination of Brønsted and Lewis acidity is key for biomass conversion to HMF since Lewis acid sites favor the isomerization of glucose to fructose while the Brønsted acid sites promote the dehydration of fructose to HMF (Fig. 13). As discussed above, these micellar catalysts display enhanced reactivity due to the accumulation of the substrate onto the micellar catalyst. Therefore, $Cr(DS)H_2PW_{12}$ promoted higher conversion into HMF than $Cr(H_3[PW_{12}O_{40}])_3$, $Cr(OSO_3C_{12}H_{25})_3$, $CrCl_3$, or $H_3[PW_{12}O_{40}]$ (Table 4). It also selectively produced HMF due to its Lewis acidity and micellar structure, as the decomposition of HMF into LA and furfural was slower compared to $Cr(H_3[PW_{12}O_{40}])_3$. Moreover, the catalyst was highly

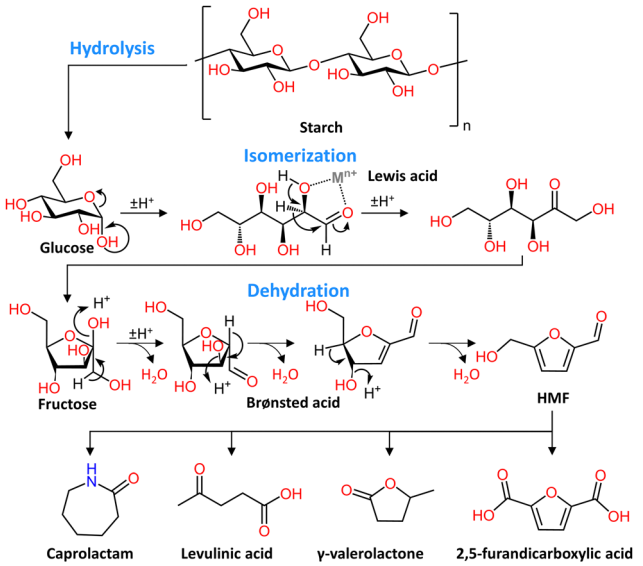

Fig. 13 Proposed mechanism for the conversion of cellulose to HMF *via* hydrolysis to glucose, which is then isomerized to fructose (catalyzed by a Lewis acid) that in turn then undergoes dehydration to HMF (catalyzed by a Brønsted acid). Some of the value-added chemicals that can be made from HMF are also shown at the bottom.

stable under the examined reaction conditions and could be reused for up to 6 reaction cycles with minimal leaching. In addition, HPAs generally lowered the decomposition temperature of pine wood by 100 °C for its conversion into furfural, thereby making the formation of feedstock chemicals from non-edible sources more accessible.[203]

More recently, it has been shown that HPAs also have promising catalytic activity for the conversion of other sources of biomass into HMF. Chitin, an abundant aminopolysaccharide composed of *N*-acetylglucosamines that is present in the exoskeleton of crustaceans, has been converted into HMF *via* a microwave-assisted process employing different Keggin HPAs ($H_3[PW_{12}O_{40}]$, $H_3[PMo_{12}O_{40}]$, $H_4[SiW_{12}O_{40}]$, and $H_4[SiMo_{12}O_{40}]$) after pre-treatment of chitin with acid/base followed by ball milling to break the H-bond network and decrease its crystallinity.[191] Among all tested HPAs, $H_4[SiW_{12}O_{40}]$ displayed the best catalytic performance (Table 4), which even surpassed all previously reported catalysts for chitin conversion into HMF. This was attributed to the greater softness of this HPA, which may enable the stabilization of organic intermediates. Cassava starch has also been transformed into HMF by using Brønsted–Lewis acid bifunctional catalysts ($Sn_xH_{3-4x}[PW_{12}O_{40}]$, x = 0.10–0.75).[195] The mechanism was proposed to first involve hydrolysis of starch to form glucose, followed by isomerization into fructose, which undergoes dehydration by elimination of three water molecules to form HMF (Fig. 13). Hydrolysis of starch to glucose and the dehydration of fructose to HMF are promoted by the Brønsted acidity of the POM while the isomerization of glucose to fructose is favored by the Lewis acidity of Sn^{4+}. $Sn_{0.1}H_{2.6}[PW_{12}O_{40}]$ presented the best selectivity and HMF yield compared to $H_3[PW_{12}O_{40}]$ and $Sn_xH_{3-4x}[PW_{12}O_{40}]$ for $x > 0.1$ due to the presence of Lewis acid sites without significantly decreasing the Brønsted acidity. Therefore, these results show the tunability that can be achieved through changing the composition of POMs or the counter-cation.

Although biomass is a more accessible source of platform chemicals, the formation of HMF directly from fructose and glucose *via* dehydration catalyzed by heterogeneous and homogeneous POM catalysts has also been investigated. Similarly to the reports for biomass sources, this has been achieved using a micellar and Brønsted–Lewis acidic catalyst. More specifically, a Cr^{3+}-substituted Keggin M–POM with CTA as a counter-cation ($((CTA)_xH_{4-x}[CrPW_{11}O_{39}]$ where x = 1 or 2) was prepared and characterized.[196] Although the incorporation of CTA as a counter-cation resulted in a decrease in the conversion of fructose, the selectivity towards the formation of HMF increased, which was proposed to be due to the formation of micelles preventing decomposition of HMF as previously discussed for $Cr((DS)H_2PW_{12}$. In addition, when starting from glucose, purely Brønsted acid catalysts, such as $H_3[PW_{12}O_{40}]$, typically produce LA and formic acid instead of HMF. However, $KH_3[CrPW_{11}O_{39}]$ and $(CTA)H_3[CrPW_{11}O_{39}]$ produced HMF with yields of around 30% and 40%, respectively (Table 4).[196] This demonstrates how the reactivity can be tuned by embedding a Lewis acid metal center and using a cationic surfactant as counter-cation. Furthermore, these catalysts were active in water, while heterogeneous catalysts that have also been shown to catalyze the dehydration of fructose to HMF are typically less active in water due to undesired side reactions and poisoning of active sites.[197–199] However, high yields of HMF have also been reported using $Fe[PW_{12}O_{40}]$ and $Cs_{2.5}H_{0.5}[PW_{12}O_{40}]$ in dimethyl sulfoxide (DMSO) while removing water by continuous mild evacuation (Table 4).[197] Additionally, it was found that using a biphasic system of water and methyl isobutyl ketone (MIBK) significantly increased the conversion and selectivity for HMF catalyzed by $Cs_{2.5}H_{0.5}[PW_{12}O_{40}]$ or $Ag_3[PW_{12}O_{40}]$, due to MIBK preventing decomposition of HMF (Table 4).[198,199] $Cs_{2.5}H_{0.5}[PW_{12}O_{40}]$ in this biphasic system even gave a higher conversion and selectivity for HMF than other heterogeneous catalysts, such as Amberlyst-15, sulfated zirconia, and zeolites.[198,199] In addition, all of the above-mentioned catalysts could be recycled and their catalytic activity was generally preserved over several cycles.

The incorporation of ionic liquid (IL) cations with HPAs has also been explored to produce heterogeneous catalysts for the formation of HMF from sugars. Such catalysts can be obtained by simply combining HPAs with an IL cation. This has mainly been reported for HPAs with SO_3H-functionalized IL cations, such as 1-(3-sulfonic acid)propyl-3-methyl imidazolium ([MIMPS]) or poly(1-vinyl-3-propane sulfonate imidazolium) (poly(VMPS)), which have been demonstrated to act as effective heterogeneous catalysts for the dehydration of fructose to HMF.[202,206,207] Furthermore, HPAs with SO_3H-functionalized IL cations have been shown to catalyze the one-pot formation of HMF as well as levulinic acid and alkyl levulinates, which are also important platform chemicals.[202,208,209] This was achieved not only from fructose but also from sucrose and inulin, a polysaccharide typically obtained from chicory, as well as from

glucose, cellobiose, and cellulose. However, the conversion of glucose, cellobiose, and cellulose generally gave lower yields, which is likely due to the lack of Lewis acidic sites needed for the effective formation of HMF directly from glucose and its derivatives. A yield of only 26% was obtained for the conversion of glucose to HMF using $H_3[PW_{12}O_{40}]$ and poly(VMPS) under optimized conditions.[202,206] However, conversion of glucose into HMF in good yields (Table 4) has been recently reported using HPA-IL catalysts formed through combining $H_3[PW_{12}O_{40}]$ with the IL cation 1-aminoethyl-3-methylimidazolium ($[MimAM]^+$): $[MimAM]_xH_{3-x}[PW_{12}O_{40}]$ (x = 1–3).[200] The reaction mechanism was proposed to involve (i) ring opening of glucose due to protonation of the bridging oxygen along with (ii) formation and stabilization of a 1,2-enediol intermediate followed by (iii) dehydration of the 1,2-enediol in a series of chain reactions *via* synergistic contributions of $[MimAM]^+$ and the HPA (Fig. 14). Hence, the mechanism does not involve isomerization to fructose due to the formation of the HPA-stabilized 1,2-enediol intermediate. Interestingly, this suggests that amino-functionalized IL cations, such as $[MimAM]^+$, may serve as alternatives to using toxic Lewis acidic metal centers (*e.g.*, Cr^{3+}). In addition, while $[MimAM]H_2[PW_{12}O_{40}]$ displayed a slightly higher yield of HMF than $H_3[PW_{12}O_{40}]$, increasing the amount of $[MimAM]^+$ counter-cations decreased the yield of HMF. This is due to the importance of the synergy between $[MimAM]^+$ and the Brønsted acidity of the HPA, as evidenced by the low catalytic activity of [MimAM]Br and of the HPA with 1-ethyl-3-methylimidazolium ($[EMim]H_2[PW_{12}O_{40}]$ where $[EMim]^+$ lacks the amino functionality). Likewise, lower activity was observed for $[MimAM]H_2[PMo_{12}O_{40}]$, $[MimAM]H_3[SiW_{12}O_{40}]$, and $[MimAM]_3H_2[PV_2Mo_{10}O_{40}]$. Furthermore, the catalytic activity decreased according to their Brønsted acid strength: $H_3[PW_{12}O_{40}] > H_3[PMo_{12}O_{40}] > H_4[SiW_{12}O_{40}] > H_5[PV_2Mo_{10}O_{40}]$. However, while a similar trend has also been observed for the dehydration of fructose with different ILs, the influence of the structure of the IL cation has not been extensively investigated. Nevertheless, the differences in the reactivity of HPAs with SO_3H-functionalized IL cations *vs.* with amino-functionalization indicate a promising possible avenue for tuning the catalytic activity and selectivity of HPAs.

Phase transfer catalysts, which combine the benefits of both homogenous and heterogeneous catalysts, have also been recently proposed as an alternative to heterogeneous catalysts, which often suffer from reduced acidity with respect to homogeneous HPAs. Exceptionally, a tetrabutylammonium (TBA) salt of a Wells–Dawson POM covalently functionalized with sulfonic acid groups ($TBA_6[P_2W_{17}$-$SO_3H]$) has been recently reported as a phase transfer catalyst for the conversion of fructose to HMF with 99% yield after 2 h at 100 °C in 1,4-dioxane (Table 4).[201] It was shown to also catalyze the conversion of glucose, sucrose, and inulin into HMF in reasonable yields, but failed to convert cellulose. Moreover, this is one of the few examples where a covalently functionalized hybrid POM was used as a catalyst in biomolecular transformations. Hence, phase transfer catalysts and hybrid POMs should be investigated further to obtain better catalysts for biomass conversion.

2.3.3. Hydrolysis of glycosidic bonds in glycoproteins. As well as being important sources of energy and added-value chemicals, monosaccharides can also form shorter glycan chains that are typically attached to glycolipids or glycoproteins. As such, they serve as ligands in receptor-mediated intracellular interactions as part of several key processes such as cell recognition, adhesion, communication, proliferation, differentiation, and even viral infection.[210] Sugars known as sialic acids (Fig. 15) are often found at the terminal position of glycan chains, and they play particularly important roles in these biological processes.[211] Hence, sialic acids are used as biomarkers for several diseases, including cancer, and their

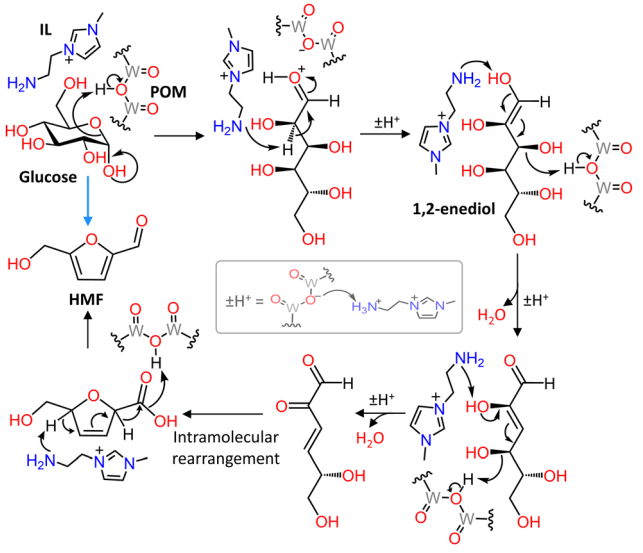

Fig. 14 Proposed mechanism for the conversion of glucose to HMF catalyzed by an HPA with an IL cation *via* formation of a 1,2-enediol intermediate that then undergoes dehydration to HMF through synergistic contributions of the IL cation and the HPA.

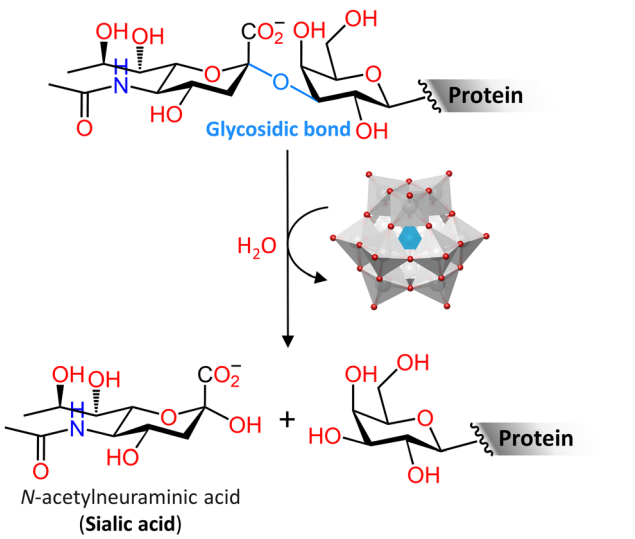

Fig. 15 Hydrolysis of the terminal glycosidic bond of an example glycan chain of a glycoprotein resulting in the release of a sialic acid catalyzed by $M_3[EA_{12}O_{40}]^{3-}$ (M = H^+, Na^+, or K^+; E = P^{5+} or Si^{4+}; A = W^{6+} or Mo^{6+}).

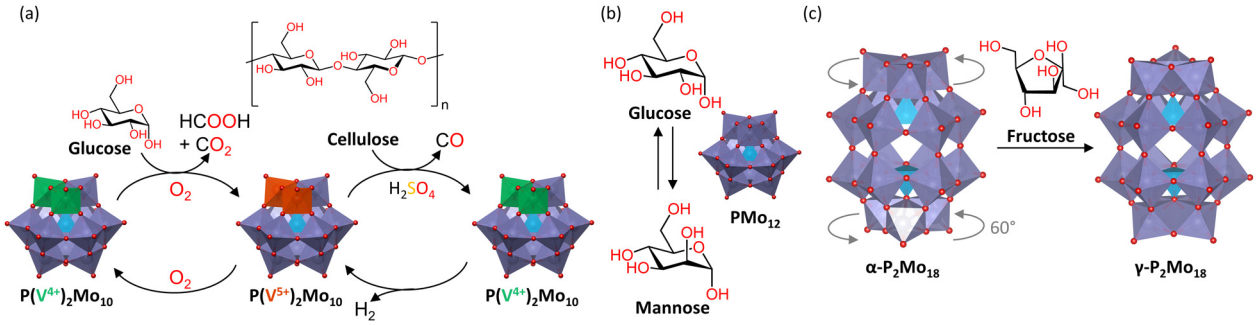

Fig. 16 (a) Catalytic activity of $H_5[PV_2Mo_{10}O_{40}]$ (PV_2Mo_{10}) towards the decomposition of glucose into HCOOH and CO_2 under an O_2 pressurized atmosphere (left) or towards the decomposition of cellulose into CO and H_2 (right). (b) Epimerization reaction between glucose and mannose catalyzed by $[PMo_{12}O_{40}]^{3-}$ (PMo_{12}). (c) Isomerization and reduction of $[\alpha\text{-}P_2Mo_{18}O_{62}]^{6-}$ ($\alpha\text{-}P_2Mo_{18}$) into 6-electron reduced $[\gamma\text{-}P_2Mo_{18}O_{62}]^{12-}$ ($\gamma\text{-}P_2Mo_{18}$), with its top and bottom $\{Mo\}_3$ caps rotated by 60°, catalyzed by fructose.

inclusion in therapeutic agents has a large impact on their efficacy.[210–212] Therefore, being able to monitor the sialic acids on glycan chains is of crucial importance. This typically requires hydrolysis of the glycosidic bond using enzymes or acid hydrolysis, both of which face similar problems to those discussed for the hydrolysis of biomass polysaccharides.[213] Moreover, the less expensive acid hydrolysis method often leads to the destruction of the protein and the sialic acids, thereby complicating the interpretation of the obtained hydrosylates.[213] By leveraging the hydrolytic activity of HPAs, our research group recently explored the application of Keggin and Wells–Dawson type HPAs ($H_3[PW_{12}O_{40}]$, $H_4[SiW_{12}O_{40}]$, $H_3[PMo_{12}O_{40}]$) and metal salts ($Na_3[PW_{12}O_{40}]$, $Na_6[H_2W_{12}O_{40}]$, $K_6[P_2W_{18}O_{62}]$) towards the cleavage of glycosidic bonds in glycoproteins (Fig. 15). The release of sialic acids under mild reaction conditions was investigated on two glycoproteins with a high content of sialic acids: α-2-HS-glycoprotein (fetuin) from bovine fetal serum and 1-acid glycoprotein (AGP) from bovine plasma.[214,215] The obtained results have shown that all investigated HPAs enable the selective release of sialic acids with minimal incubation time and protein destruction in comparison with conventional acids (*e.g.*, HCl, H_2SO_4, CH_3COOH, CF_3COOH) under the same reaction conditions. Although the composition, size, shape, and charge of the POM did not seem to have any major influence on the reactivity, their enhanced activity has been proposed to result from their negative charge which can stabilize the positively charged glycosyl cation and oxocarbenium ion intermediates.[214] Moreover, the structure of sialic acids during the hydrolytic process is preserved, which facilitates the structural analysis of sialic acids.[214,215] Hence, HPAs are promising catalysts that could facilitate the monitoring of sialic acids in glycoproteins for diagnostic and therapeutic applications. However, since only a limited number of studies have been performed so far, further research is required in order to determine the feasibility of their implementation and widespread use across different types of glycoproteins.

2.3.4. Redox activity towards sugars. The combined redox activity and Brønsted acidity of certain HPAs make them particularly suitable for the conversion of biomass into biofuels and industrially relevant chemicals, such as formic acid.[216] For example, $H_5[PV_2Mo_{10}O_{40}]$ has been shown to catalyze the selective decomposition of sugars (*e.g.*, glucose, cellobiose, sucrose, *etc.*) into formic acid and CO_2 under a pressurized O_2 atmosphere (Fig. 16(a)).[217,218] This has been proposed to take place *via* an electron transfer-oxygen transfer mechanism, whereby the HPA catalyzes the oxidative cleavage of carbon–carbon bonds in vicinal diols and primary alcohols through the insertion of oxygen.[217,219] The fully oxidized POM is then regenerated by O_2, which was proposed to be the rate-limiting step at low O_2 pressures.[220] A systematic study of V^{5+}-substituted Keggin-type phosphomolybdate HPAs ($H_{3+n}[PV_nMo_{12-n}O_{40}]$ where n = 0–6) showed that $H_8[PV_5Mo_7O_{40}]$ had better selectivity for formic acid, which was attributed to the formation of VO_2^+ with increasing V^{5+} centers.[220] In addition, when the decomposition of cellulose and hemicellulose was performed with $H_5[PV_2Mo_{10}O_{40}]$ and H_2SO_4 under anaerobic conditions, HCOOH was dehydrated into CO and the oxidized POM could be regenerated by electrolysis with the release of H_2 (Fig. 16(a)).[217] The resulting mixture of CO and H_2, known as synthesis gas, can be used for the formation of hydrocarbon fuels as well as other compounds.[217] Nb- and Ta-substituted Keggin polyoxomolybdates have also been shown to catalyze the oxidation of glucose into formic acid as the major liquid-phase product, with their effective activation energy (55 kJ mol^{-1}) being lower compared to the non-substituted $H_3[PMo_{12}O_{40}]$ (80 kJ mol^{-1}).[216] Therefore, these studies show that by varying the POM's composition and the reaction conditions, it is possible to optimize the reaction and even alter its outcome. However, although mechanistic studies have been performed, the mode of interaction of these POMs with sugars remains unclear.

In a different study, structurally related Keggin-type phosphomolybdates ($H_3[PMo_{12}O_{40}]$, $Ag_3[PMo_{12}O_{40}]$ and $Sn_{0.75}[PMo_{12}O_{40}]$) were demonstrated to catalyze the epimerization of D-glucose to D-mannose (Fig. 16(b)), as well as the reverse reaction (at a slower rate), which is a relevant process in the production of certain pharmaceuticals.[217] This was proposed to occur due to binding of the sugar to molybdate, resulting in an electron transfer from glucose to the POM and a C1–C2 intramolecular carbon shift. The

counter-cation did not seem to have any influence on the reaction and no conversion was observed with the more inert isostructural phosphotungstate ($H_3[PW_{12}O_{40}]$). However, the structure of the sugar-bound molybdate intermediate remains unknown and the role of the electron transfer event resulting in reduction of Mo^{6+} into Mo^{5+} is not well understood. Therefore, further research must be performed to shed light on this type of reactivity. Nevertheless, the use of ^{13}C-labeled glucose in this study provided valuable insights into the reaction mechanism. This approach is noteworthy since it is not often used for investigating the reactivity of POMs towards biomolecules, but could potentially be applied to other systems to reveal additional mechanistic details.

In contrast to most of the reactions described in the literature, where the aim is the controlled modification of a biomolecule, the redox activity of sugars towards POMs has also been exploited to reduce and modify a POM structure. This is of interest because reduced POM species have been shown to have potential applications in several fields, but their controlled synthesis can be challenging.[221] Hence, fructose was used as a reducing agent in the selective conversion of $[\alpha\text{-}P_2Mo_{18}O_{62}]^{6-}$, the most stable isomer of the Wells–Dawson phosphomolybdate structure, into the less stable 6-electron reduced γ-isomer (Fig. 16(c)).[222] In contrast, glucose was less effective, which was ascribed to its weaker bidentate coordination to Mo^{6+}, while fructose can act as a tridentate ligand due to having three OH groups in close proximity that could promote better interaction and efficient reduction.[222] This binding is potentially responsible for the selectivity since a mixture of isomers was obtained with standard reducing agents. However, further studies are required to determine the exact role of the sugar and the nature of the sugar-bound intermediate. Furthermore, whether or not the sugars are transformed in the process was not reported, even though this reactivity suggests that phosphomolybdates may be of interest for the selective oxidation of sugars. Moreover, this study appears to be the other side of the coin to the previously discussed study on the epimerization of glucose and, therefore, highlights the importance of approaching the investigation of reactivity from both the point of view of the catalyst and that of the substrate.

2.4. Lipids

Lipids are a vast family of hydrophobic and amphiphilic biomolecules that, are typically used by living organisms as essential components of cell membranes, for signal transduction, and for energy storage as an alternative to carbohydrates.[223] Several studies have been reported on the interactions of POMs with lipid mono- and bi-layers in the context of the effect of POMs on cell membranes for biomedical applications, such as the development of antimicrobial drugs.[224–228] However, the reactivity of POMs towards lipids has mainly been investigated in the context of biodiesel production, which typically consists of fatty methyl or ethyl esters formed by transesterification of triglycerides in oils, such as vegetable oil and waste cooking oil, using mineral acids or bases.[229–233] Although base catalysts (*e.g.*, KOH, NaOH, $NaOCH_3$) are commonly used due to their higher activity, they are corrosive and prone to form soaps if the oil contains a significant amount of water or free fatty acids, which leads to loss of catalyst and requires expensive isolation of the desired biodiesel products.[234–236] On the other hand, mineral acids (*e.g.*, HCl, H_2SO_4) can catalyze the transesterification of triglycerides and the esterification of free fatty acids simultaneously, but they are also highly corrosive and give rise to waste-disposal problems.[234–236] Therefore, alternative acid catalysts are needed to make the production of biodiesel more viable while also ensuring it is environmentally safe.

As previously discussed, the high Brønsted acidity and stability of HPAs make them good alternatives to mineral acids. Accordingly, it was shown that anhydrous Keggin-type HPAs ($H_x[EA_{12}O_{40}]^{(n-x)-}$ where E = P^{5+} or Si^{4+} and A = Mo^{6+} or W^{6+}) could catalyze the transesterification of rapeseed oil with methanol or ethanol resulting in better percentage conversion compared to H_2SO_4 and H_3PO_4 (Table 5).[232] Interestingly, greater triglyceride conversion was obtained with ethanol over methanol, and also when using anhydrous over hydrated HPAs, or when using polyoxomolybdates over polyoxotungstates (Table 5). The latter is contrary to the expected trend based on HPA acid strength, which is highest for $H_3[PW_{12}O_{40}]$, and this discrepancy was proposed to stem from the easier loss of crystallization waters from polyoxomolybdates as the presence of water affects the progress of the reaction. On the other hand, the transesterification of Macauba oil, a type of palm oil, was found to follow the expected trend according to the Brønsted acidity: $H_3[PW_{12}O_{40}] > H_3[PMo_{12}O_{40}] > H_4[SiW_{12}O_{40}] > H_2SO_4$ (Table 5).[237] A more recent study has also shown that for the methanolic esterification of palmitic acid, one of the most commonly found saturated fatty acids in animal and vegetable oil,[238] $H_5[BW_{12}O_{40}]$ was significantly more active as a catalyst than $H_3[PW_{12}O_{40}]$ under the same conditions (Table 5).[239] This was attributed to the higher proton number and, therefore, higher Brønsted acidity of $H_5[BW_{12}O_{40}]$.[239] Nevertheless, the Keggin-type HPA $H_3[PW_{12}O_{40}]$ has been most extensively investigated in the context of biodiesel production, which is likely due to both its relatively high Brønsted acidity and its commercial availability.[239] For instance, this HPA was shown to be an effective and recyclable catalyst for the methanolic and ethanolic esterification of palmitic acid and of other saturated and unsaturated fatty acids (*e.g.*, myristic, stearic, oleic, and linoleic acids), resulting in similar or increased activity towards all fatty acids in comparison to H_2SO_4 (Table 5).[230,233,240] $H_3[PW_{12}O_{40}]$ was also shown to be active in the methanolic transesterification of triglycerides in waste cooking oil, which is particularly unsuitable for base-catalyzed transesterification due to its high content of free fatty acids and water.[230,241,242] In these esterification and transesterification reactions, HPAs have been proposed to catalyze the reaction through protonation of the ester carbonyl group, thereby activating it towards nucleophilic attack by an alcohol (Fig. 17).[230,243] In the case of triglycerides this proceeds in a stepwise manner *via* di- and mono-glycerides to produce fatty acid esters and glycerol (Fig. 17).[230,243] Hence, the high Brønsted

Table 5 Selected conditions and percentage conversion reported for the esterification of free fatty acids (FA) and triglycerides (TG) catalyzed by different POMs

POM	Substrate	Reaction conditions	Conversion/%	Ref.
$H_3[PW_{12}O_{40}]$	Palmitic acid	2.5 : 1 MeOH : FA, 65 °C, 12 h, 0.1 mmol POM	97	230
		50 : 1 MeOH : FA, reflux, 10 h, 0.4 mmol POM	97	233
		12 : 1 MeOH : FA, 90 °C, 3 h, 6 wt% POM	87	229
		10 : 1 MeOH : FA, 65 °C, 3 h, 10.9 mM POM	52	239
		20 : 1 MeOH : FA, 65 °C, 6 h, 243 : 1 FA : POM	94	244
	Myristic, stearic, oleic, linoleic acids	50 : 1 MeOH : FA, reflux, 10 h, 0.4 mmol POM	93 (linoleic), 95 (oleic), 97 (myristic & stearic)	233
	Waste cooking oil	70 : 1 MeOH : oil, 65 °C, 14 h, 10 wt% POM	87–89	230,241
	Rapeseed oil	MeOH, 80 °C, 5 h, 3 mol% POM,	11	232
		6 : 1 EtOH : oil, 85 °C, 3 h, 1.7 mol% POM	27	
	Macauba oil	12 : 1 EtOH : oil, 90 °C, 8 h, 2 mol% POM	68	237
$H_3[PMo_{12}O_{40}]$	Rapeseed oil	6 : 1 EtOH : oil, 85 °C, 3 h, 1.6 mol% POM	55	232
	Macauba oil	12 : 1 EtOH : oil, 90 °C, 8 h, 2 mol% POM	65	237
$H_4[SiW_{12}O_{40}]$	Rapeseed oil	6 : 1 EtOH : oil, 85 °C, 3 h, 2 mol% POM	20	232
	Macauba oil	12 : 1 EtOH : oil, 90 °C, 8 h, 2 mol% POM	68	237
$H_4[SiMo_{12}O_{40}]$	Rapeseed oil	6 : 1 EtOH : oil, 85 °C, 3 h, 2 mol% POM	45	232
$H_5[BW_{12}O_{40}]$	Palmitic acid	10 : 1 MeOH : FA, 65 °C, 3 h, 10.9 mM POM	99	239
$H_5[TiPW_{11}O_{40}]$	Palmitic acid	20 : 1 MeOH : FA, 65 °C, 6 h, 243 : 1 FA : POM	94	244
$[CTA]H_4[BW_{12}O_{40}]$	Palmitic acid	18 : 1 MeOH : FA, 65 °C, 5 h, 4.48 mM POM	99	239
		18 : 1 EtOH : FA, 65 °C, 5 h, 4.48 mM POM	91	
		18 : 1 ButOH : FA, 65 °C, 5 h, 4.48 mM POM	72	
	Oleic & stearic acid	18 : 1 MeOH : FA, 65 °C, 5 h	94 (stearic) & 97 (oleic)	239
$[CTA]H_4[TiPW_{11}O_{40}]$	Palmitic acid	20 : 1 MeOH : FA, 65 °C, 6 h, 243 : 1 FA : POM	95	244
$[GlyH]_xH_{3-x}[PW_{12}O_{40}]$	Palmitic acid	12 : 1 MeOH : FA, 90 °C, 3 h, 6 wt% POM	81% (x = 3)–93% (x = 1) yield	229
$Cs_xH_{3-x}[PW_{12}O_{40}]$	Palmitic acid	30 : 1 MeOH : FA, 60 °C, 6 h, 50 mg POM	9 (x = 3)–100 (x = 2.3)	234
	Tributyrin	30 : 1 MeOH : TG, 60 °C, 6 h, 50 mg POM	3 (x = 0.9)–50 (x = 2.3)	234
	Palmitic acid + tributyrin (50 : 1)	30 : 1 MeOH : TG, 60 °C, 6 h, 50 mg POM (x = 2.3)	100 (FA) & 50 (tributyrin)	234
	Rice bran FAs	14 : 1 MeOH : FA, 65 °C, 3 h, 41 mg mL^{-1} POM	2 (x = 3)–92 (x = 1)	245
	Eruca sativa Gars. oil	5.3 : 1 MeOH : oil, 20 °C, 1 h, 20 μmol POM (x = 2.5)	40	235
		5.3 : 1 MeOH : oil, 55 °C, 0.75 h, 541 : 1 oil : POM (x = 2.5)	99	
	Yellow horn oil	12 : 1 MeOH : oil, 60 °C, 0.2 h, 1 wt% POM (x = 2.5)	96% yield	246
	Soybean oil	30 : 1 MeOH : oil, 140 °C, 8 h, 3 wt% POM (x = 2)	86	236
$Cs_2H_2[SiW_{12}O_{40}]$	Soybean oil	30 : 1 MeOH : oil, 140 °C, 8 h, 3 wt% POM	72	236
$Cs_xH_{6-x}[PV_3MoW_8O_{40}]$	Soybean oil	30 : 1 MeOH : oil, 140 °C, 8 h, 3 wt% POM	25 (x = 5)–93 (x = 1)	236
	Free FAs (20% oleic acid)	30 : 1 MeOH : oil, 140 °C, 4 h, 3 wt% POM	95	236
$Zn_{1.2}H_{0.6}[PW_{12}O_{40}]$	Palmitic acid	5 : 1 MeOH : FA, 65 °C, 4 h, 0.06 mmol POM	96	247
	Waste cooking oil	28 : 1 MeOH : FA, 65 °C, 12 h, 2.5 wt% POM	>97	247
$Sn_{1.2}H_{0.6}[PW_{12}O_{40}]$	Macauba oil	12 : 1 EtOH : oil, 90 °C, 8 h, 2 mol% POM	100% yield	237
$[H\text{-pyrazine–}SO_3H]_{1.5}[PW_{12}O_{40}]$	Oleic acid	1 : 1 MeOH : FA, 25 °C, 24 h, 200 mg POM	83	248
$[MIM\text{-}PSH]_2H[PW_{12}O_{40}]$	Palmitic acid	13 : 1 EtOH : FA, 80 °C, 5 h, 7 wt% POM	92% yield	249
$TBA_6[P_2W_{17}\text{-}SO_3H]$	Oleic acid	10 : 1 MeOH : FA, 70 °C, 0.3 h, 10 wt% POM	99% yield	201

MIM-PSH = 3-(1-methylimidazolium-3-yl)propane-1-sulfonate.

acidity of HPAs makes them promising catalysts for the production of biodiesel.

It has also been shown that the catalytic activity of HPAs in biodiesel production can be tuned by exchanging some of the protons for different counter-cations, as described for the hydrolysis of polysaccharides. For instance, the catalytic activity of $H_3[PW_{12}O_{40}]$ towards the esterification of palmitic acid could be varied by using glycine (Gly) counterions. $[GlyH]_1H_2[PW_{12}O_{40}]$ was found to be ideal for this purpose since the Gly counter ion enabled better mass transport while leaving two available Brønsted acid protons.[229] This is in agreement with the ideal exchange ratio reported for polysaccharide hydrolysis in Section 2.3.1. Moreover, this homogeneous POM catalyst was reported to be highly water-tolerant, stable, and non-toxic.[229] The POM also self-separated since the product formed an organic layer in which the POM was immiscible, allowing for the POM catalyst to be recycled and reused for several cycles.[229] Similarly, micellar catalysts for the esterification of fatty acids were obtained by exchanging one of the protons in $H_5[BW_{12}O_{40}]$ or $H_5[TiPW_{11}O_{40}]$ with the surfactant CTA.[239,244] These micellar catalysts could be easily recycled without significant loss of activity or loss of the catalyst and exhibited higher catalytic activity than the HPAs alone (Table 5). This was proposed to be due to the fatty acid and alcohol substrates being concentrated around the catalyst within micelles.[239,244] The catalytic activity was also found to increase with increasing chain length of the surfactant counter-cation up to around C_{16}, which corresponds to the chain length of CTA and palmitic acid. Therefore, in accordance with the studies on biomass conversion (Section 2.3.1), the catalytic activity of

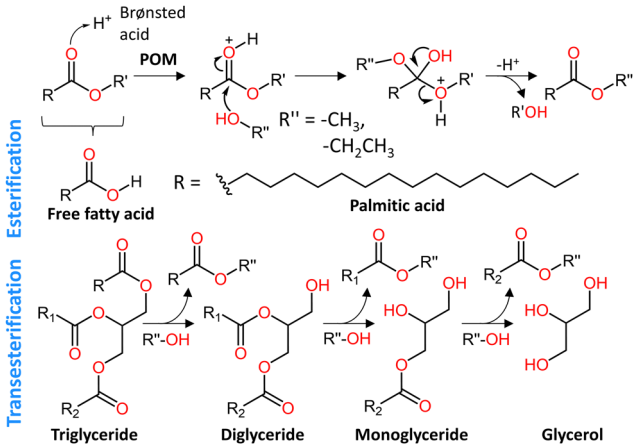

Fig. 17 General mechanism for the (trans)esterification of free fatty acids (*e.g.*, palmitic acid) and triglycerides (*via* di- and monoglycerides) catalyzed by Brønsted acidic HPA catalysts.

HPAs towards biodiesel production can be enhanced by varying the counter-cation.

Cation exchange can also facilitate the separation of the POM after the reaction by forming insoluble salts that can act as heterogeneous catalysts.[189] For instance, a fully heterogeneous catalyst towards the esterification of palmitic acid was obtained by exchanging the protons in $H_3[PW_{12}O_{40}]$ by NH_4, and partial exchange was shown to result in higher activity than the fully exchanged ammonium salt ($(NH_4)_3[PW_{12}O_{40}]$).[250] Similarly, exchanging the protons with Cs^+ was used to form insoluble salts of $H_3[PW_{12}O_{40}]$ that could catalyze the esterification of palmitic acid and the transesterification of tributyrin, a triglyceride, with methanol (both separately and simultaneously).[234] Furthermore, $Cs_xH_{3-x}[PW_{12}O_{40}]$ with x = 2.0–2.3 gave higher conversion due to having more accessible surface acid sites (Table 5).[234] Moreover, $Cs_{2.5}H_{0.5}[PW_{12}O_{40}]$ has been shown to display higher catalytic activity towards the transesterification of vegetable oil into biodiesel than H_2SO_4, while being tolerant towards water content and the presence of free fatty acids as well as being easily recyclable.[235,246,251] However, $Cs_1H_2[PW_{12}O_{40}]$ was shown to be more active than salts with a higher content of Cs^+ in the esterification of rice bran fatty acids with methanol (Table 5), which was proposed to be due to the higher Brønsted acidity of $Cs_1H_2[PW_{12}O_{40}]$.[245] Similarly, the catalytic activity of Cs salts of a mixed metal Keggin HPA ($[PV_3MoW_8O_{40}]^{6-}$), prepared by cation exchange, was recently reported to decrease with increasing amounts of Cs^+ (Table 5) due to a drop in the Brønsted acidity. However, since $Cs_1H_5[PV_3MoW_8O_{40}]$ was partially soluble, $Cs_2H_4[PV_3MoW_8O_{40}]$ was determined to be the best heterogeneous catalyst.[236] In addition, $Cs_2H_4[PV_3MoW_8O_{40}]$ was shown to be an effective and recyclable heterogeneous catalyst in the simultaneous transesterification of soybean oil and esterification of free fatty acids with superior conversion to $Cs_2H_2[SiW_{12}O_{40}]$ and $Cs_2H[PW_{12}O_{40}]$ (Table 5).[236] Mixed ammonium and Cs salts ($(NH_4)_xCs_{2.5-x}H_{0.5}[PW_{12}O_{40}]$; x = 0.5, 1, 1.5, 2) were also investigated and $(NH_4)_2Cs_{0.5}H_{0.5}[PW_{12}O_{40}]$ gave the highest turnover frequency for the esterification of oleic acid with ethanol, which was determined to be due to it having a higher surface area, pore size, and number of mesopores.[252] Consequently, exchanging the counter-cation to form insoluble salts can produce highly effective heterogeneous catalysts for biodiesel production with their catalytic activity depending on the structure and acid strength of the solid catalyst imparted by the cation exchange.

HPAs with several other organic and inorganic counter-cations have also been explored as heterogeneous catalysts for biodiesel production. For example, Sn^{2+} and Zr^{4+} HPA salts have been reported to form heterogeneous catalysts that benefit from the synergistic combination of the Lewis acidic cations with the Brønsted acidic HPAs.[237,247] Moreover, crystals of $[PW_{12}O_{40}]^{3-}$ with sulfonic acid functionalized pyrazinium ($[H\text{-pyrazine-}SO_3H]^{2+}$) displayed exceptional activity towards the esterification of free fatty acids using only equimolar amounts of methanol at room temperature, in contrast to typically reported conditions involving excess methanol and elevated temperatures (Table 5).[248] Such combinations of $[PW_{12}O_{40}]^{3-}$ with IL cations also allow for facile recyclability of the catalyst.[248,249] Due to the advantages of heterogeneous catalysis, particularly regarding the ease of recovery and reuse of the catalyst, research focus has shifted in recent years towards the heterogenization of HPAs.

The TBA salt of a Wells–Dawson POM covalently functionalized with sulfonic acid groups, $TBA_6[P_2W_{17}\text{-}SO_3H]$, which was discussed in Section 2.3.2, was also reported to act as a phase transfer catalyst for the esterification of free fatty acids that displayed higher activity than $H_3[PW_{12}O_{40}]$, the monolacunary Wells–Dawson POM ($[P_2W_{17}O_{61}]^{10-}$), and H_2SO_4 (Table 5).[201] This higher catalytic activity was proposed to be due to the formation of a catalytically active emulsion, as a result of the use of TBA as the counter-cation, because it allowed for better interactions between the substrates and the POM active sites.[201] As the reaction progressed, a phase separation took place and the POM catalyst precipitated out of solution, allowing easy recovery of both the catalyst and products.[201] As for biomass conversion, this is also the only example of the use of a covalently functionalized hybrid POM for the production of biodiesel and suggests that such hybrid systems should be investigated further.

In contrast to the extensive research on the use of POMs for biodiesel production due to the Brønsted acidity of HPAs, the redox activity of POMs towards lipids has been scarcely explored. However, different salts of $M_{3/n}[PMo_{12}O_{40}]$ (M^{n+} = H^+, K^+, Zn^{2+}, Cu^{2+}, Cr^{3+}, Fe^{3+}, and Al^{3+}) have been explored as catalysts for the oxidation of glycerol, the major by-product of biodiesel production, into added-value platform chemicals such as lactic acid.[253] The oxidation of glycerol into lactic acid takes place in the presence of O_2 *via* a radical chain mechanism involving the formation of dihydroxyacetone and glyceraldehyde, which are interconvertible isomers (Fig. 18).[253] Then, the dehydration of glyceraldehyde produces pyruvaldehyde, which reacts with water to form lactic acid. The activity and selectivity for these different reaction products were found to depend on

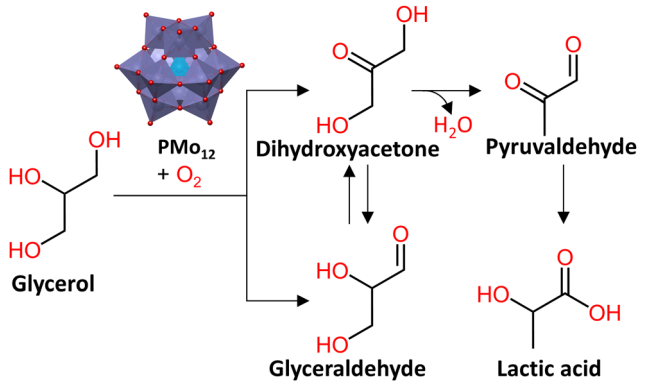

Fig. 18 Oxidation of glycerol by $[PMo_{12}O_{40}]^{3-}$ (PMo_{12}) under an O_2 atmosphere to form dihydroxyacetone or glyceraldehyde, which interconvert, leading to the dehydration of dihydroxyacetone into pyruvaldehyde that is then converted into lactic acid.

the counter-cation. The counter-cation with the highest charge (Al^{3+}) resulted in the highest conversion and selectivity for lactic acid, while Cu^{2+} completely inhibited the reaction.[253] This was proposed to be due to the influence of the counter-cation on the generation of radicals, and the role of Al^{3+} in catalyzing the dehydration reaction. Yet, oxidation of fatty acids or other lipids has not been significantly explored. Nevertheless, a recent report has shown that $(NH_4)_6[Mo_7O_{24}]$ can induce the peroxidation of phospholipids in the cell membranes of glioblastoma cells, which may be linked to its anti-cancer activity.[254] Therefore, the redox activity of POMs towards lipids should be explored further.

3. Reactivity of MOC-based materials

In the previous sections, the focus was predominantly on MOCs acting as homogeneous catalysts in biomolecular transformations. Although this facilitates the study of their reactivity, it presents several disadvantages for practical applications, especially in the separation and reuse of the catalyst. In contrast, heterogeneous catalysts allow for easy separation and reuse of the catalyst since the catalytically active sites and the substrates are in separate phases, thereby providing an efficient solution for reliable catalyst durability and product isolation.[255] As a result, inherently insoluble MOCs and insoluble hybrid materials containing MOCs have been developed as alternatives that can catalyze biomolecular reactions heterogeneously.

The most notable and well-studied examples of these types of materials are MOC-based MOFs, which can function as heterogeneous catalysts for a diverse array of biologically relevant reactions, owing to their three-dimensional network of MOCs interconnected by organic linker molecules. Moreover, the composition, morphology, and architecture of MOFs can be tailored to specific reactions, making them highly versatile catalysts that offer high potential for designing efficient catalytic processes.[256] In addition, MOFs and MOF-based hybrid materials (*e.g.*, POM@MOF) can outperform traditional porous materials like zeolites in terms of their ability to control porosity, backbone functionalization, guest immobilization, and active site modification. The porosity of MOFs can be fine-tuned by selecting appropriate organic linkers or by adjusting synthesis parameters to induce missing-linker or missing-cluster defects to further facilitate the diffusion of substrate molecules and favor the accessibility of active sites. Additionally, MOFs can serve as supports or hosts for the uniform immobilization or encapsulation of a large number of reactive species, preventing them from leaching, agglomerating, or deactivating during reactions. Hence, MOFs are highly versatile materials that provide many avenues to create highly promising efficient catalysts.[45,50–52,257–259] Moreover, MOFs have been shown to catalyze a wide range of biomolecular transformations as has been recently described in detail in a recent review.[59] Therefore, this section will only focus on the reactivity towards biomolecules of MOFs based on MOCs, especially to draw comparisons with the studies on discrete clusters. Other hybrid materials based on MOCs will also be discussed where relevant to highlight where the limits of MOFs lie and where improvements are still needed.

3.1. Amino acids, peptides and proteins

3.1.1. Hydrolysis of peptides. Inspired by the hydrolytic activity of Zr–POMs towards peptides and proteins, the catalytic activity of MOFs based on hexanuclear Zr^{4+} clusters, $\{Zr_6O_8\}$, was also investigated by our group. The hydrolysis of simple peptide bond model systems, such as Gly-Gly and other Gly–X dipeptides, with MOFs was first investigated by Ly *et al.*[260] This study employed MOF-808, which consists of $\{Zr_6O_8\}$ nodes connected by six benzene-1,3,5-tricarboxylate (BTC) linkers to form a framework with a pore size of 18.4 Å (Fig. 19(a)).[260] MOF-808 was shown to hydrolyze Gly-Gly to form Gly and cGly-Gly as a byproduct. It reduced the activation energy by approximately 22 kJ mol^{-1} and enhanced the rate of hydrolysis by almost 3 orders of magnitude compared to Zr–POMs under the same reaction conditions to give nearly 100% conversion after just 3 h (Table 6), while the Zr–POMs required several days to reach 100% conversion.[80,83] The hydrolysis of Gly-Gly under the same conditions was also attempted with Zr_6-based clusters capped with benzoate ($Zr_6(OH)_4O_4(C_6H_5CO_2)_{12}$) or methacrylate ($Zr_6(OH)_4O_4(CH_2{=}C(CH_3)CO_2)_{12}$) ligands (Fig. 1(f)). However, the discrete MOCs produced no hydrolytic products after 5 h, which was attributed to all Zr^{4+} centers being coordinatively saturated.[260] Consequently, Zr-based MOFs present distinct advantages over Zr–POMs and even discrete Zr_6 clusters.

The mechanism of MOF-808 reactivity towards peptide bonds was proposed to be similar to that observed for M–POMs. The reaction was catalyzed *via* coordination of the dipeptide to the redox inactive and Lewis acidic Zr^{4+} centers, which occurs either through exchange with formate ligands (often present in MOFs from the use of formic acid during their synthesis) or directly at defect sites with missing BTC linkers. Coordination likely takes place at two adjacent Zr^{4+} centers *via* an N-terminal N atom and a peptide carbonyl O atom of Gly-Gly, thereby activating the carbonyl group of the peptide bond towards a nucleophilic attack, as suggested by computational

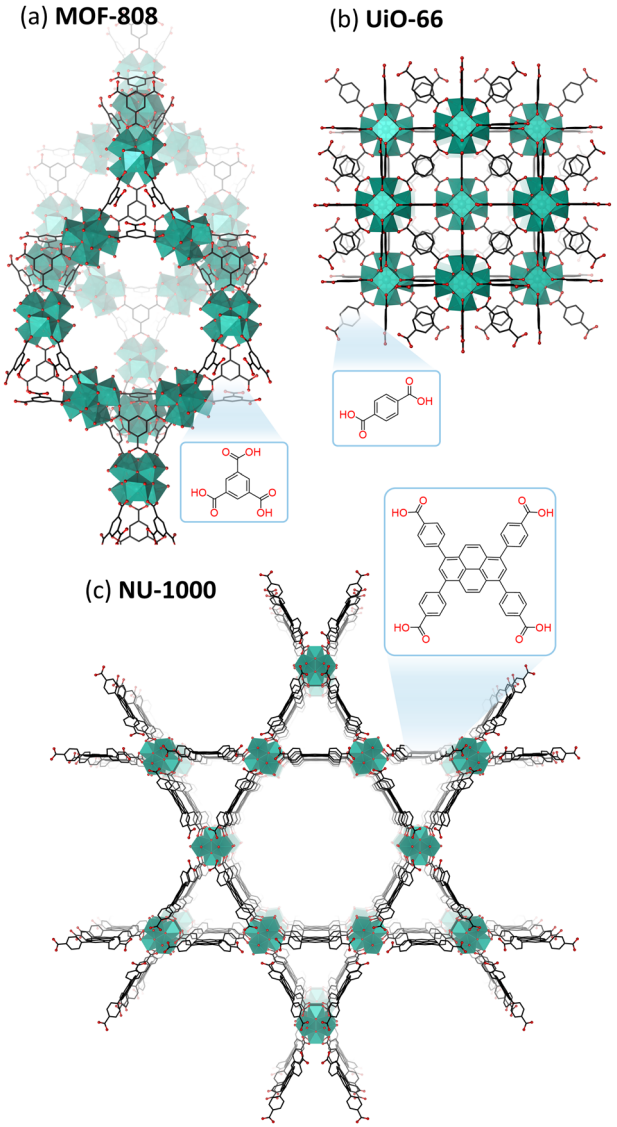

Fig. 19 Structures of $\{M_6O_8\}$-based MOFs: (a) MOF-808, (b) UiO-66, and (c) NU-1000.

modeling. Therefore, more missing linker defects result in an acceleration of the reaction rate, which motivates the use of MOFs with a higher number of missing linker defects, provided that MOF stability is not adversely affected. Overall, this shows that MOF-808 is an effective heterogeneous catalyst for the hydrolysis of peptide bonds due to the Lewis acidity of Zr^{4+} centers in available active sites.

The reaction rate of hydrolysis catalyzed by MOF-808 was found to depend on the nature of the dipeptide's structure in a similar way to what was observed for M–POMs. It was found that the C-terminal carboxylate group is important in the hydrolytic reaction since modifying it resulted in a slower reaction.[260] Gly-Gly hydrolysis in the presence of non-reactive multidentate carboxylic acids also caused a decrease in the reaction rate due to their ability to competitively coordinate to Zr^{4+} centers instead of Gly-Gly. The greatest decrease was observed upon the addition of acids with short aliphatic chains since their interaction with the MOF is not sterically hindered. Similarly, conversion of Gly–X dipeptides decreased with increasing side chain bulkiness (Gly-Gly > Gly-Ala > Gly-Asp > Gly-Asn > Gly-Lys ≈ Gly-Arg) due to steric hindrance.[260] On the other hand, Gly-Met and Gly-Phe displayed higher reaction rates, which was proposed to be due to their thiol and aromatic functionalities that facilitated interactions with the linker molecules, while Gly–X dipeptides with hydrophobic residues exhibited lower conversion rates due to the lack of favorable interactions with both the linkers and the $\{Zr_6O_8\}$ cluster core.[260] Hence, the hydrolytic activity of MOF-808 depends on the composition of the peptide because of the role of terminal carboxylate groups in the hydrolysis reaction and the interactions of side chains with the linker molecules.

While Ly *et al.* briefly investigated the binding mode of Gly-Gly to the $\{Zr_6O_8\}$ cluster core using DFT calculations,[260] Conic *et al.* went a step further by elucidating the full reaction mechanism of Gly-Gly hydrolysis after binding to the $\{Zr_6O_8\}$ cluster.[267] More specifically, DFT calculations were used to gain a deeper understanding of the composition and arrangement of the dangling ligands surrounding the $\{Zr_6O_8\}$ cluster under the hydrolysis reaction conditions and to elucidate the mechanism underlying efficient hydrolysis of Gly-Gly catalyzed by MOF-808. Under the conditions used for hydrolysis reactions, it was determined that the active sites of MOF-808 likely consist of protonated $\{Zr_6O_8H_4\}$ clusters with negatively charged ligands (*i.e.*, bridging BTC and formate ligands) to reach charge-neutrality. Some of the formate ligands were found to be exchangeable with water and hydroxide, resulting in $Zr_6O_4(OH)_4(BTC)_2(HCOO)_6$ and $Zr_6O_4(OH)_4(BTC)_2(HCOO)_5(OH)(H_2O)$ being predicted to be the most favorable structures. Binding of Gly-Gly was proposed to occur through the replacement of one of the formate ligands and it was found that: (i) formation of a neutral complex is preferred, (ii) binding to Zr^{4+} is strongest in the order carboxylate > carbonyl > amine, and (iii) complex stability is influenced by the relative coordination geometry of the dipeptide on the $\{Zr_6O_8\}$ cluster core, especially with respect to the μ_3-OH groups due to potentially stabilizing hydrogen bonding.[267] However, while binding of the carboxylate group in bidentate bridging mode is slightly more favorable, only bridging coordination to the amide carbonyl oxygen and N-terminal nitrogen results in activation towards hydrolysis (Fig. 20). In addition, hydrolysis was proposed to involve nucleophilic attack by a free external water molecule (Fig. 20), as the attack by core oxygens, coordinated OH^-, or coordinated H_2O is not viable due to their position on the cluster with respect to coordinated Gly-Gly. This external H_2O molecule can be activated towards nucleophilic attack by the neighboring carboxylate group, in a similar mechanism to that established for a Zr–POM,[83] which is followed by multiple proton shuffling steps and conformational changes (Fig. 20). The preferred reaction pathway involves two main transition states: nucleophilic attack on the amide carbon and breaking of the C–N bond with either one serving as the rate-determining step. However, the proton shuffling and conformational changes

Table 6 Conditions and rate constants (k_{obs}) for selected reports on MOF-catalyzed peptide hydrolysis

MOF	Substrate	Reaction conditions	Conversion/%	$k_{obs}/\times10^{-6}$ s^{-1}	Ref.
MOF-808(Zr)	Gly-Gly	pD 7.4, 60 °C, 4 h, 1 eq. MOF	92	269	260
	Gly-Gly-NH_2	pD 7.4, 60 °C, 1 eq. MOF	—	55	260
	Gly-Gly-Ala	pD 7.4, 60 °C, 1 eq. MOF	—	206	260
MOF-808(Zr) (35–850 nm)	Gly-Gly	pD 7.6, 60 °C, 20 h, 1 eq. MOF	71 (850 nm)–94 (35 nm)	17.3 (850 nm)–38.7 (35 nm)	261
UiO-66(Zr)	Gly-Gly	pD 7.8, 60 °C, 360 h, 1 eq. MOF	64	0.8	262
UiO-66(Zr)-NO_2	Gly-Gly	pD 7.8, 60 °C, 1 eq. MOF	—	8.4	262
UiO-66(Zr)-NH_2	Gly-Gly	pD 7.8, 60 °C, 1 eq. MOF	—	9.0	262
UiO-66(Zr)-TFA	Gly-Gly	pD 7.8, 60 °C, 1 eq. MOF	—	8.0	262
UiO-66(Zr/Ce)	Gly-Gly	pD 7.4, 60 °C, 1 eq. MOF	—	0.6–1.35 (depending on %Ce)	263
NU-1000(Zr)	Gly-Gly	pD 7.4, 60 °C, 72 h, 1 eq. MOF	53	1.6	264
NU-1000(Hf)	Gly-Gly	pD 7.4, 60 °C, 24 h, 1 eq. MOF	7	0.8	265
MIP-201	Gly-Gly	pD 7.4, 60 °C, 24 h, 1 eq. MOF	80	18.5	266

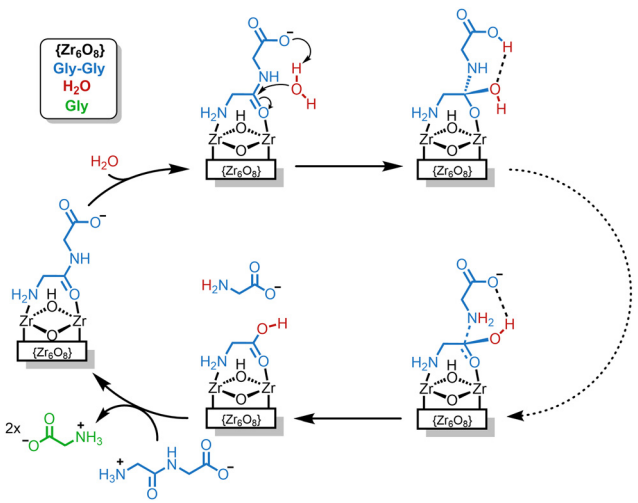

Fig. 20 Proposed mechanism of Gly-Gly hydrolysis by a $\{Zr_6O_8\}$-based MOF. Adapted from ref. 267.

after the nucleophilic attack were not investigated in detail as they were assumed to have low energy barriers and the implicit solvent model used is too inaccurate for these low-energy calculations.[267] Therefore, additional computational and experimental studies are required to confirm these findings.

Following these mechanistic studies, the structure–activity relationships of MOFs were investigated further to optimize them as catalysts for protein hydrolysis. This was achieved by studying the impact of varying the linker functionality and the MOF framework on the hydrolysis of dipeptides. In this context, the catalytic activity of $\{Zr_6O_8\}$-based UiO-66 MOFs (Fig. 19(b)) with different linkers – the typical 1,4-benzenedicarboxylate (BDC) linker and BDC derivatives with electron-withdrawing (NO_2) or electron-donating (NH_2) groups – were investigated, all of which bind to the cluster at twelve sites.[262] The modified UiO-66(Zr)-NO_2 and UiO-66(Zr)-NH_2 variants were both observed to provide a 10-fold increase in catalytic activity with respect to standard UiO-66(Zr) (Table 6). The high reactivity of UiO-66(Zr)-NH_2 is surprising since the amino group's electron-donating ability should reduce the Lewis acidity of $\{Zr_6O_8\}$, thus reducing its ability to activate peptide bonds towards nucleophilic attack by water. However, since the particle size of all three UiO-66 variants was practically identical, it was suggested that the reason for the higher activity was the greater porosity and larger number of missing linkers in UiO-66(Zr)-NH_2, which makes the internal catalytic sites more accessible to the dipeptide.[262] This was confirmed by inducing missing linker defects using trifluoroacetic acid (TFA) to form a UiO-66 structure with higher porosity (UiO-66(Zr)-TFA) that hydrolyzed Gly-Gly with a similar reaction rate to UiO-66(Zr)-NO_2 and UiO-66(Zr)-NH_2 (Table 6). Furthermore, the different UiO-66 variants displayed distinct selectivities in the hydrolysis of Gly–X dipeptides, with UiO-66(Zr)-TFA showing preference for dipeptides with nucleophilic groups susceptible to intramolecular *N*,*O*-rearrangement (Gly-Ser and Gly-Asp). This was suggested to result from a greater contribution of Brønsted acid sites that aid the hydrolysis of the formed ester intermediate. In contrast, UiO-66(Zr)-NO_2 showed a greater contribution of Lewis acid sites, likely linked to the electron-withdrawing effect of the $-NO_2$ group, since it did not show increased reactivity toward any dipeptide in particular.[262] Therefore, this study demonstrates that the reactivity and selectivity of MOFs can be controlled through the number and functionality of the linkers.

The structure of MOFs also plays a key role in the hydrolysis reaction partly because of how it affects the adsorption of dipeptides onto the MOF. Therefore, Loosen *et al.* investigated the factors that influence peptide adsorption onto different MOF structures: MOF-808, UiO-66, and NU-1000 where MOF NU-1000 is composed of $\{M_6O_8\}$ clusters with eight 1,3,6,8-(*p*-benzoate)pyrene linkers per cluster (Fig. 19(c)).[268] Adsorption of Gly ($^-OOCCH_2\mathbf{NH_3}^+$) and Gly-Gly ($^-OOCCH_2NHOCCH_2\mathbf{NH_3}^+$) was observed to be significantly affected by the repulsion between the ammonium ($-NH_3^+$) group and the positively charged surface of the MOFs. Gly is generally adsorbed less by all MOFs than Gly-Gly since the $-NH_3^+$ group in Gly-Gly is further away from the cluster when Gly-Gly is coordinated *via* its carboxylate group (**Zr**-$OOCCH_2\mathbf{NH_3}^+$ *vs.* **Zr**-$OOCCH_2$-$NHOCCH_2\mathbf{NH_3}^+$). Furthermore, the absorption of Gly-Gly was found to increase for all MOFs with increasing pH (pH 3 and pH 7), which was attributed to the MOF surface charge becoming less positive, resulting in a decrease in repulsion between

the cluster and the $-NH_3^+$ group of the peptide. Moreover, MOF-808 displayed greater adsorption of Gly-Gly compared to UiO-66 and NU-1000 under all investigated reaction conditions, which was proposed to be due to the presence of more available Zr^{4+} sites, since MOF-808 has six linkers per cluster while UiO-66 and NU-1000 have a higher linker connectivity.[268] Interestingly, N- and C-terminal protected peptides displayed distinct adsorption behavior for the different MOF architectures. From this, it was suggested that adsorption of peptides by hydrophilic MOFs, such as MOF-808 and UiO-66, is primarily driven by C-terminal carboxylate coordination to $\{Zr_6O_8\}$ clusters. In contrast, peptide adsorption to the hydrophobic NU-1000 was mainly influenced by repulsive electrostatic interactions of the N-terminal $-NH_3^+$ group of the dipeptide and hydrophobic interactions of the side chain of the dipeptide with the large aromatic linker of the MOF.[268] Because of these interactions, Gly–X dipeptides with more hydrophilic side chains were adsorbed more favorably by MOF-808 while NU-1000 highly favored the adsorption of dipeptides with hydrophobic/aromatic side chains, and the extent of adsorption increased with increasing hydrophobicity of the dipeptide. However, dipeptides with functional groups that allowed for coordination to the $\{Zr_6O_8\}$ cluster – such as carboxylate, amide, and hydroxide groups – also resulted in more favorable adsorption on NU-1000. On the other hand, despite these systematic studies, a clear trend could not be established for the adsorption of Gly–X dipeptides to UiO-66. Nevertheless, the adsorption did not seem to depend on differences in particle size or pore size between the MOFs. Smaller particle size and higher external surface area did, however, favor adsorption of Gly-Gly by MOF-808, which suggests that hydrolysis most likely occurs on the external surface of the MOF, even though its pore size is sufficiently large to allow for permeation of dipeptides and other small oligopeptides.[261] In addition to particle size, porosity, and connectivity, the three-dimensional features of the MOF architecture can influence reactivity as well since the entropic contribution to the Gibbs free energy of hydrolysis is relatively large, as observed when comparing Zr-based NU-1000 and MOF-808.[264] Thus, while more detailed analysis remains necessary, the intricate MOF network allows for tunability of both the reactivity and selectivity.

Another factor that can impact reactivity, is the nature of the metal atom in the $\{M_6O_8\}$ cluster. This was investigated by comparing NU-1000 MOFs (Fig. 19(c)) based on either Zr^{4+} or Hf^{4+}, both of which gave similar results for the hydrolysis of Gly-Gly (Table 6).[265] However, similar reaction rates were observed for the hydrolysis of Gly-Gly, Gly-Ala, Gly-Asp, and Gly-Ile catalyzed by NU-1000(Hf) despite the size differences of the dipeptides, which is distinctly different from the results of NU-1000(Zr) and indicates that NU-1000(Hf) is relatively less sensitive to steric hindrance of the peptide substrate.[265] Furthermore, while reaction rates for dipeptide and protein hydrolysis were similar, NU-1000(Zr) consistently performed better. This cannot result from differences in the intrinsic Brønsted acidity of Zr^{4+} and Hf^{4+}, since both MOFs perform best at pH 7–8, nor can it result from differences in enthalpy and entropy contributions, since the same $\Delta G^{\ddagger}$ was observed for the reaction with both MOFs. The differences in the reactivity most likely arise as a result of small structural variations as opposed to differences in the intrinsic reactivity of both metals.[265] Hence, even though Zr^{4+} and Hf^{4+} are similar, they can influence the MOF structure, and thus the reactivity, differently.

To enhance the reactivity and structural diversity of the MOFs used for peptide bond hydrolysis, different methods have been employed. While linker substitution and substitution of Zr^{4+} by Hf^{4+} both improved hydrolysis in different ways, no additional functionality was introduced.[262,265] For this purpose, a series of bimetallic UiO-66 MOFs with different Ce/Zr ratios were synthesized and employed for peptide bond hydrolysis.[263] Due to the superior reactivity of Ce^{4+} compared to Zr^{4+}, UiO-66(Ce) has shown a higher catalytic activity compared to UiO-66(Zr). However, the stability of UiO-66(Ce) under the conditions typically used for hydrolysis is lower compared to UiO-66(Zr) due to the facile reduction of Ce^{4+} to Ce^{3+}, which is less Lewis acidic. To circumvent the low stability of pure Ce^{4+}-based MOFs and still benefit from the increased reactivity of Ce^{4+}, bimetallic UiO-66(Ce/Zr) MOFs were synthesized containing different ratios of $CeZr_5$ and Ce_6 clusters based on the overall Ce/Zr ratio (28, 43, 61, and 87 mol% Ce). The reactivity towards the hydrolysis of Gly-Gly was similar for all variants (Table 6) and their stability was confirmed to be similar to that of UiO-66(Zr). Only a slight increase in the reactivity was observed upon increasing the number of Ce_6 clusters, while increasing the content of $CeZr_5$ clusters caused a slight decrease in the reactivity, which was attributed to the dipeptide's coordination to two different metal centers (Ce and Zr) being less favorable.[263] While the introduction of Ce^{4+} into MOFs did not significantly increase reactivity in peptide bond hydrolysis, the scope of reactions could be expanded. Ce^{4+} can function as a one-electron oxidizing agent, which endows UiO-66(Zr/Ce) MOFs with redox activity that could be leveraged to catalyze oxidation as well as hydrolytic reactions. As a result, the oxidation of cysteine to cystine was successfully catalyzed by a UiO-66(Zr/Ce) MOF. Moreover, the combined oxidation and hydrolysis of tripeptide glutathione was investigated, and a preference for oxidation was observed even though it was substantially slower than cysteine oxidation owing to steric hindrance or unfavorable coordination.[263] These studies show that the reaction scope can be successfully expanded by incorporating metals with different properties into the same MOF structure. Therefore, the effect of other metals should be investigated further, as it could enable one-pot reactions combining multiple reaction steps.

3.1.2. Hydrolysis of proteins. The hydrolytic activity of MOC-based MOFs towards peptides indicates that MOFs are potentially promising heterogeneous catalysts for the hydrolysis of proteins. Indeed, several MOC-based MOFs have been shown to catalyze protein hydrolysis.

The first example of protein hydrolysis catalyzed by MOC-based MOFs was the hydrolysis of HEWL by MOF-808(Zr) with 55% hydrolysis after 25 h at 60 °C.[260] Only four fragments of *ca.*

Table 7 Conditions and number of peptide fragments of selected reports based on SDS-PAGE for the MOF-catalyzed hydrolysis of various proteins

MOF	Protein[a]	Reaction conditions	No. of fragments	Proposed cleavage sites	Ref.
MOF-808(Zr)	HEWL	Phosphate buffer, pH 7.4, 60 °C, 3.1 mg mL^{-1} MOF	4	Asp18–Asn19, Asp52–Tyr53, Asp119–Val120	260,264
	HHM	H_2O, pH 7.4, 60 °C, 2 μmol MOF	4	Asp20–Ile21, Asp44–Lys45, Asp126–Ala127[b]	270
		+ SDS	7	Asp44–Lys45[b], Asp60–Leu61[b], Asp109–Ala110, Asp122–Phe123, Asp126–Ala127[b]	
		+ CHAPS	4	Asp20–Ile21, Asp44–Lys45, Asp126–Ala127[b]	
		+ Zw3–12	2	Asp126–Ala127[b]	
		+ TX-100	4	Asp60–Leu61, Asp126–Ala127[b]	
MOF-808(Zr) (35–850 nm)	HEWL	H_2O, pH 7.2, 60 °C, 2 μmol MOF	5	Asp18–Asn19[b], Asp52–Tyr53, Asp66–Gly67, Asp101–Gly102, Asp119–Val120	261
NU-1000(Zr)	HEWL	H_2O, pH 7.0, 60 °C, 2 μmol MOF	3	Asp18–Asn19[b], Asp52–Tyr53, Asp119–Val120	264
NU-1000(Hf)	HEWL	H_2O, pH 7.0, 60 °C, 2 μmol MOF	3	Asp18–Asn19[b], Asp52–Tyr53, Asp119–Val120	265
MIP-201	HHM	HEPES/H_2O, pH 7.4, 60 °C, 2.8 mg mL^{-1} MOF	6	Asp20–Ile21[b], Asp60–Leu61[b], Asp109–Ala110, Asp122–Phe123[b], Asp126–Asp127[b]	266

[a] HEWL = Hen Egg White Lysozyme; HHM = Horse Heart Myoglobin. [b] More than one peptide fragment may be assigned to this cleavage site.

12.2, 10.7, 8.2, and 6.4 kDa were observed using SDS-PAGE (Table 7), indicating selective peptide bond cleavage. This is much faster than what was described for various Zr–POMs under similar reaction conditions,[70,88] which can be attributed to a higher density of Zr^{4+} ions that function as the active sites for hydrolysis. In regard to the hydrolysis mechanism, and the interaction mode between MOF-808 and HEWL, the following hypotheses have been suggested: (i) partial unfolding of HEWL at 60 °C could enable the protein to diffuse into the MOF's pores to access internal $\{Zr_6O_8\}$ active sites,[269] or (ii) initial hydrolysis of HEWL occurs most likely in the half-spherical pockets on the surface of MOF-808 that are similar in size to the protein, thereby facilitating diffusion of hydrolytic fragments into the pores for further cleavage. Although no unambiguous evidence could be obtained for either scenario, considering the limited number of $\{Zr_6O_8\}$ active sites (~1%) on the MOF's external surface area, hydrolysis of initially formed fragments within the MOF is plausible, especially given the high efficiency of the hydrolytic reaction.[260]

Even though MOF-808 showed promising hydrolytic activity, it was synthesized in a highly explosive and dangerous mixture of dimethylformamide (DMF) and formic acid at an elevated temperature, like many other MOFs.[260] Therefore, adjusting this synthesis procedure to ensure its safety and a lower environmental impact would be an important step in their development as nanozymes. Dai *et al.* accomplished this by synthesizing the $\{Zr_6O_8\}$ clusters first in isopropanol and water and then using them to form the MOF-808 structure in a safer mixture of water and formic acid.[261] In addition to a greener synthesis, more monodisperse MOF-808 nanocrystals were obtained with a tunable size, thereby ensuring that the reactivity is identical throughout the whole synthetic batch. This is important because the hydrolytic activity of MOFs towards proteins is mainly affected by the MOF's macro characteristics, such as the particle size and external/internal surface areas, instead of the linker identity, which is much less important considering the vast size of the substrate.[264] Hence, varying the particle size and, therefore, the MOF's external surface allowed tuning of the number and concentration of peptide fragments, as observed for the hydrolysis of HEWL by a series of MOF-808 with different sizes (Table 7).[261] Moreover, reproducibility, scalability, and low variability are essential for the implementation of MOFs in industrial applications and can be achieved through safer synthetic strategies, such as the one reported by Dai *et al.*

Hydrolysis of HEWL using NU-1000(Zr) and NU-1000(Hf) was also investigated, which allows for the influence of the nature of the metal center to be examined (Table 7). Both MOFs produced fragments of *ca.* 12.5, 10.3, and 8.5 kDa, which indicates that both Zr- and Hf-based NU-1000 cleave the protein with the same selectivity,[264,265] and that the selectivity is not affected by the MOF structure since similar fragments were also observed with MOF-808.[260] This also shows that the MOF structure likely has a direct impact on the number of peptide fragments produced, since more fragments were observed for MOF-808.[260] However, visualization of the hydrolytic fragments produced by NU-1000 using SDS-PAGE was very difficult, which was attributed to strong adsorption at the liquid–solid interface. In order to recover the peptide fragments from the MOF, various elution protocols were attempted by incubation with established protein eluents. While this was unsuccessful for glycine-HCl and guanidine-HCl eluents, the intact protein band could be visualized after incubation in 1% aqueous ammonia at ambient temperature, which also destroyed the MOF due to the low stability of NU-1000 under highly basic conditions.[264] Nevertheless, the observed hydrolytic activity of MOF-808 and NU-1000 shows that MOFs can selectively cleave proteins to produce peptide fragments suitable for middle-down proteomics. The cleavage was postulated to occur at Asp–X and X–Asp peptide bonds, similarly to Zr–POMs. Although the reactivity is still governed by the Lewis acidic metal centers, the MOF structure clearly plays a role, most likely by influencing the interactions between the MOF and the protein and/or the peptide fragments.

While several examples have indicated the hydrolytic potential of Zr- and Hf-based MOFs,[260,264–266] the detailed elucidation of the interaction mechanism remains an issue owing to the heterogeneous nature of these materials.

Furthermore, the adsorption of proteins and their hydrolytic fragments onto MOFs makes studying the reaction particularly challenging. Therefore, to increase the applicability of MOFs for protein hydrolysis, issues related to strong substrate adsorption need to be addressed, which starts by finding a suitable elution protocol that is not detrimental to the MOF's structure. Alternatively, more stable MOF structures can be used to withstand elution conditions. For instance, MIP-201, consisting of $\{Zr_6O_8\}$ building units coordinated to six 3,3,5,5′-tetracarboxydiphenylmethane (H_4mdip) linkers (Fig. 21(a)), was used for the cleavage of myoglobin and was successfully recycled and regenerated for several hydrolysis reaction cycles (Table 7).[266] This was possible because of the very high stability of this MOF, as it remained stable, even after prolonged incubation in boiling water under highly acidic conditions or under basic conditions (pH 10), which would allow for elution of protein fragments using basic media without destruction of the MOF.[266] Hence, finding better elution protocols or using more stable MOFs would enable more detailed studies of their reactivity and would make the implementation of MOFs in bio-technological applications more feasible.

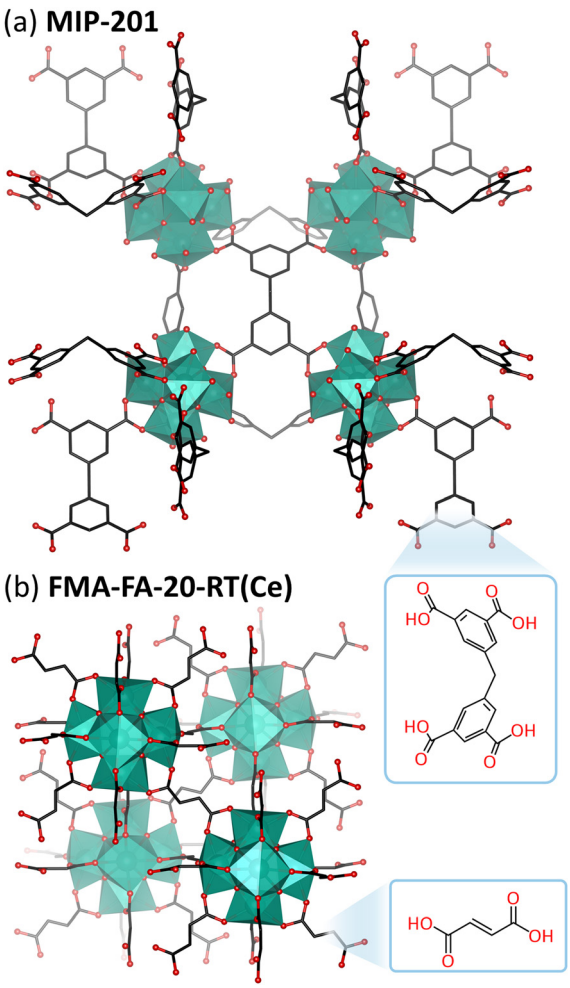

Fig. 21 Structures of (a) MIP-201, consisting of $\{Zr_6O_8\}$ clusters, and (b) FMA-FA-20-RT(Ce), consisting of $\{Ce_6O_8\}$ clusters.

MOF-808(Zr) has also been shown to remain active towards the hydrolysis of myoglobin in the presence of surfactants, making it an interesting catalyst for proteomics applications alongside M–POMs, especially for studying water-insoluble proteins that must be solubilized with surfactants. MOF-808(Zr) cleaved myoglobin producing fragments of *ca.* 4.6, 13.7, 12.2, and 11.1 kDa (Table 7), with a hydrolysis efficiency of around 63% after 8 days in the absence of any surfactant.[270] However, addition of surfactants affects both the protein structure and the MOF-protein interactions in a rather complex manner and, therefore, the structure of the surfactant used was determined to play an important role in the reaction outcome. The anionic surfactant SDS promoted protein hydrolysis by causing larger protein unfolding (±65% hydrolysis efficiency after 8 days) whereas zwitterionic CHAPS and neutral TX-100 surfactants inhibited hydrolysis by interacting with the MOF's active sites or forming micelles on its surface: around 39% and 31% hydrolysis efficiency after 8 days, respectively. Interestingly, while hydrolysis of myoglobin in the presence of CHAPS merely reduced the hydrolysis efficiency, hydrolysis in the presence of TX-100 caused a different cleavage selectivity.[270] Therefore, the addition of specific types of surfactants can influence both the efficiency and selectivity of protein hydrolysis by MOFs. This is extremely valuable for the development of MOFs as catalysts for protein hydrolysis as it shows that the reactivity of MOFs can be tuned through using additives, such as surfactants, and that the MOF catalyst does not completely lose its activity in the presence of surfactants, unlike natural proteases.

Besides Zr^{4+} and Hf^{4+}, other metal centers have also been described for protein hydrolysis. For instance, an FMA(Ce) MOF, which is homologous to UiO-66 with fumaric acid (FMA) ligands instead of BDC linkers (Fig. 21(b)), was used for the hydrolysis of bovine serum albumin (BSA) in a study on MOF-catalyzed hydrolysis of amide, phosphoester, phosphoanhydride, and glycosidic bonds.[44] The study showed that the hydrolytic activity could be increased by increasing the Lewis acidity of the incorporated metals, either by choosing a different metal or tuning the Lewis acidity by linker exchange, and by improving the active site density. The latter can easily be accomplished by selecting short linkers such as FMA. However, this also decreases pore size/volume, thus direct improvement using this strategy is less straightforward. Multiple MOF architectures were synthesized using acetic (AA), formic (FA), and TFA as modulators that can affect the morphology, size, yield, degree of crystallinity, and number of defects.[271,272] Out of all the tested MOFs, FMA-FA-20-RT(Ce) (synthesized at 25 °C using a molar ratio of 20 : 1 FA : FMA to introduce missing linker defects) was shown to be most catalytically active in initial model reactions, and was further investigated for the hydrolysis of BSA.[44] The reaction was followed by gel permeation chromatography (GPC), which indicated 100% BSA hydrolysis after 36 h at 60 °C, or after 7 days at 37 °C. While the efficiency of FMA-FA-20-RT(Ce) is 7 times lower in comparison to the commonly employed protease trypsin, this MOF is also 10 000 times more economical than trypsin. Moreover, FMA-FA-20-RT(Ce)

produces hydrolytic fragments of similar length compared to trypsin, even though it has considerable preference towards cleavage of bonds involving Arg, Lys, and Asp residues while trypsin only cleaves at Arg and Lys amino acids. Furthermore, MOF-808(Zr) was also investigated toward BSA hydrolysis, but performed considerably slower, with only 50% BSA hydrolysis after 24 h at 60 °C. Since the surface area of MOF-808 is much larger compared to FMA-FA-20-RT(Ce), this highlights the superior performance of Ce^{4+} compared to Zr^{4+} active sites.

In summary, several MOFs have shown great potential for the hydrolysis of proteins. However, while the mechanism for peptide bond hydrolysis and oxidative cleavage of proteins catalyzed by various MOCs has been elucidated in great detail,[70,80,87,130,273] the studies with MOFs are still to be developed further. Although initial reports yielded some insights,[260,264,266,267] the exact mechanism of MOF-catalyzed peptide bond hydrolysis in larger protein substrates, and especially in insoluble protein substrates, needs to be studied more extensively.

3.1.3. Peptide bond formation. As previously discussed for POMs, it is important to note that peptide bond hydrolysis is a reversible process, and the reverse reaction (peptide bond formation) can be achieved in the absence of water. While there have been a few reports of amide bond formation in model systems using MOC-based MOF catalysts,[274,275] peptide bond formation between amino acids has only been reported once to the best of our knowledge. In this report, de Azambuja *et al.* assessed the reactivity of Zr-based MOF-808, NU-1000, and UiO-66 towards dipeptide cyclization and intermolecular peptide formation between amino acids in organic solvents as model reactions for amide bond formation.[276] UiO-66 was found to be the most suitable MOF catalyst since the recovery of the products was easier and, unlike with MOF-808, hydrolysis products were not detected. Furthermore, these MOFs were shown to be highly water-tolerant and could catalyze the reaction under ambient conditions without the need for additives, unlike other catalysts commonly used for peptide bond formation. Therefore, the use of MOC-based MOFs for this type of reactivity could potentially be exploited for the formation of synthetic peptides and bio-inspired molecules that may be of interest for biotechnological or pharmaceutical applications.

3.2. Nucleic acids and nucleotides

3.2.1. Hydrolysis of nucleic acids and their model systems. For the hydrolytic or oxidative cleavage of phosphoester bonds in various substrates, mainly gold and metal-oxide nanoparticles have been employed as (photo)catalysts.[277] Contrastingly, the cleavage of phosphoester bonds using cluster-based materials has been underreported, with the cleavage of DNA by MOFs having been described only recently.[278] To understand both what has been accomplished and what still needs to be addressed, this section will cover examples of phosphoester bond cleavage using cluster-based materials and discuss the hydrolysis mechanism for relevant substrates.

In 2012, Han *et al.* reported on the use of a phosphotungstate POM embedded into several Zn- and lanthanide-based MOFs, for hydrolysis of DNA model substrate BNPP.[279] While the heterogeneous catalysis of phosphoester bond cleavage was successful due to the reactivity of the well-dispersed POMs and the insolubility of the larger framework, the reaction rate was only moderate ($t_{1/2}$ = 161.7–286.1 h) and the mechanism was not fully elucidated. A more comprehensive investigation was later carried out using MOC-based MOFs, in which the activation process, active site, and reaction mechanism were explored using Zr-based UiO-66, UiO-67, PCN-700, PCN-701, and PCN-703 frameworks (Fig. 22 and Table 8).[280] Out of all these MOFs, UiO-66 displayed the highest reactivity ($K_M = 1.55 \times 10^{-4}$ M), which was comparable to that of alkaline phosphatase. Furthermore, the lower activity of UiO-67 with respect to UiO-66 (Table 8) was proposed to be due to UiO-66 having inherently more linker vacancies. This was confirmed by following the reactivity of PCN-type MOFs, which increased in the order of PCN-703 < PCN-701 < PCN-700 corresponding to their increasing number of coordinatively unsaturated sites (CUS): 1, 2, and 4, respectively (Fig. 22 and Table 8). This demonstrates the importance of CUS for catalyzing phosphoester bond hydrolysis.

The catalytic activity was significantly boosted if the MOF was activated under strong acidic (pH 2–3) or basic (pH 8) conditions because monocarboxylate ligands bound to the $\{Zr_6O_8\}$ clusters can be more easily exchanged at more extreme pH values.[280] As a result, more catalytically effective defects are introduced. In addition, the influence of pH on the hydrolysis of NPP catalyzed by UiO-66 was investigated and the best

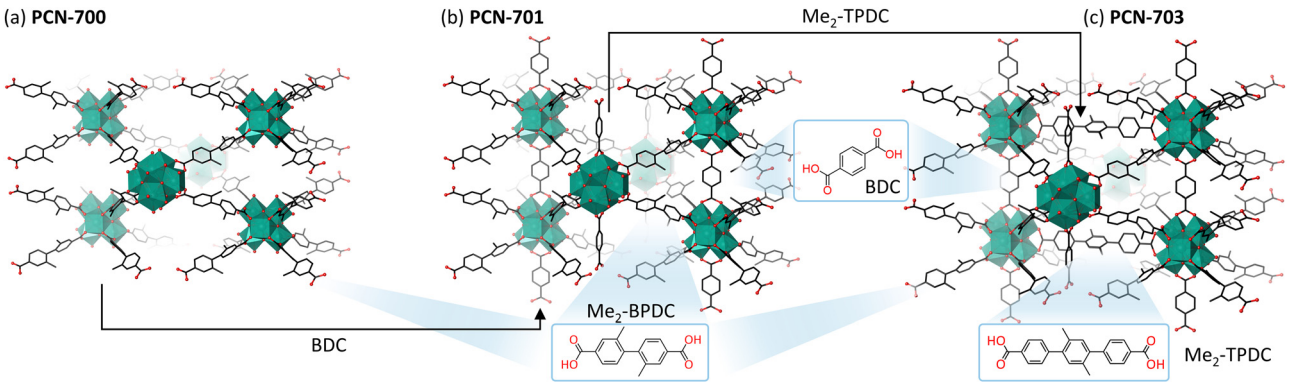

Fig. 22 Structures of MOFs (a) PCN-700, (b) PCN-701, and (c) PCN-703, which differ in terms of the linkers connecting the $\{Zr_6O_8\}$ clusters.

Table 8 Selected conditions and percentage conversion/rate constants reported for MOF-catalyzed phosphoester/phosphoanhydride bond hydrolysis

MOF	Substrate	MOF connectivity	Reaction conditions	Conversion & rate constant	Ref.
UiO-66(Zr)	NPP	12 (many missing linker defects)	100 mM HEPES, pH 8.0, 37 °C, 0.08 mg mL^{-1} MOF	108 μM h^{-1}	280
UiO-67(Zr)	NPP	12 (limited number of missing linker defects)	100 mM HEPES, pH 8.0, 37 °C, 0.08 mg mL^{-1} MOF	60 μM h^{-1}	280
PCN-700(Zr)	NPP	8	100 mM HEPES, pH 8.0, 37 °C, 1.5 mg mL^{-1} MOF	73.2 μM h^{-1}	280
PCN-701(Zr)	NPP	10	100 mM HEPES, pH 8.0, 37 °C, 1.5 mg mL^{-1} MOF	57.6 μM h^{-1}	280
PCN-703(Zr)	NPP	12	100 mM HEPES, pH 8.0, 37 °C, 1.5 mg mL^{-1} MOF	25.8 μM h^{-1}	280
MOF(Hf/Ni)	NPP	12	50 mM HEPES, pH 7.4, r.t., 0.2 eq. MOF	194 μM h^{-1}	281
	BNPP	12	50 mM HEPES, pH 7.4, r.t., 0.2 eq. MOF	18.9 μM h^{-1}	281
	NPA	12	50 mM HEPES, pH 7.4, r.t., 0.2 eq. MOF	5.8 μM h^{-1}	281
	NPS	12	50 mM HEPES, pH 7.4, r.t., 0.2 eq. MOF	1.5 μM h^{-1}	281
HMUiO-66(Ce)	ssDNA	12 (assembled with macroporous template)	20 mM HEPES, pH 7.4, 60 °C, 6 h, 0.35 mg mL^{-1} MOF	100% conversion	278
	Plasmid pBR322	12 (assembled with macroporous template)	20 mM HEPES, pH 7.4, 60 °C, 24 h, 0.35 mg mL^{-1} MOF	74% conversion	278
FMA-FA-20-RT(Ce)	NPP	12	pH 9.0, 37 °C, 0.5 mg mL^{-1} MOF	$t_{1/2} \leq 2$ min	44
	ATP	12	pH 10.0, 37 °C, 12 h, 0.5 mg mL^{-1} MOF	21.5% conversion	44
	ADP	12	pH 10.0, 37 °C, 12 h, 0.5 mg mL^{-1} MOF	18.5% conversion	44
	AMP	12	pH 7.0, 37 °C, 12 h, 0.5 mg mL^{-1} MOF	5.0% conversion	44
PCN(Fe)	NPP	8	20 mM HEPES, pH 7.2, 65 °C, 0.75 mg mL^{-1} MOF	186 μM h^{-1}	282
UiO-66(Ce)	ATP	12	20 mM HEPES, pH 7.4, 37 °C, 1 h, 4.2 mg mL^{-1} MOF	58.2% conversion	283

hydrolysis rate was observed at pH 8.[280] This was explained by the effect that pH has on Zr-bound water molecules and hydroxyl ions, which results in different reaction pathways depending on their protonation state. Based on DFT calculations and Diffuse Reflectance Infrared Fourier Transform Spectroscopy (DRIFTS), the most likely pathway at pH 8 was proposed to involve: (i) indirect coordination of NPP through H-bonding with a Zr-bound hydroxide; (ii) stabilization by a water molecule that is hydrogen bonded to both the substrate and a Zr-bound hydroxide; (iii) nucleophilic attack by the H-bonded water; and finally (iv) dissociation of the formed *p*-nitrophenoxide ion to yield $H_2PO_4^-$ (Fig. 23(a)).[280] Furthermore, higher pH favored the reaction since this gave a lower $\Delta G^{\ddagger}$ for the conformation of $\{Zr_6O_8\}$. However, above pH 8, the reaction rate was observed to decrease again, which was postulated to occur because of electrostatic repulsion between NPP and the $\{Zr_6O_8\}$ cluster due to changes in the protonation state at high pH values. Therefore, although the $\Delta G^{\ddagger}$ of $\{Zr_6O_8\}$ at pH 8 was not optimal, the reaction rate was the highest due to lower repulsion.

Dong *et al.* further expanded this research by using Hf/Ni mixed-metal MOFs to hydrolyze NPP with near-complete position-selectivity, where phosphomonoesters were preferably hydrolyzed over other phosphoesters, and type-selectivity, where P–O rather than C–O or S–O bonds were cleaved.[281] They were assembled using isonicotinic and 3-aminoisonicotinic acid ligands, to form MOF(Hf/Ni) and MOF(Hf/Ni)–NH_2 (Fig. 23(b)), respectively, with micropores of approximately 7.4 Å, and a large BET surface (1040 m^2 g^{-1}). These MOFs were shown to display a high thermostability and solution stability towards leaching of Hf^{4+} and Ni^{2+} in HEPES buffer due to the high connectivity and elevated charge density exhibited by the Hf_6 cluster.[281] Furthermore, phosphatase-like hydrolysis of NPP was observed for both MOF(Hf/Ni) and MOF(Hf/Ni)-NH_2 (Table 8). Both MOFs significantly outperformed UiO-66(Hf), which suggests that the presence of Ni^{2+} ions notably improved the catalytic activity. This probably results from the impact of Ni^{2+} on the polarizability of the phosphoryl group and modification of transition state structures. In addition, MOF(Hf/Ni)-NH_2 displayed a higher reaction rate than MOF(Hf/Ni), which likely stems from the role of the amino functionalities as either base- or proton-transfer agents. The positive impact of both Ni^{2+} and –NH_2 groups was confirmed by the drastically reduced catalytic activity of other MOFs without Ni and/or without the –NH_2 group (MOF(Hf/Cu), MOF(Hf/Cu)-NH_2, MOF(Zr/Ni), MOF(Zr/Ni)-NH_2, MOF(Zr/Cu), MOF(Zr/Cu)-NH_2). However, while MOF(Hf/Ni) displayed excellent hydrolytic activity towards NPP, its activity in the hydrolysis of BNPP, 4-nitrophenyl acetate (NPA), and 4-nitrophenyl sulfate (NPS) was significantly lower or non-existent (Fig. 23(c) and (d)). This was rationalized based on the structure of the other substrates: steric hindrance of BNPP impedes diffusion through MOF

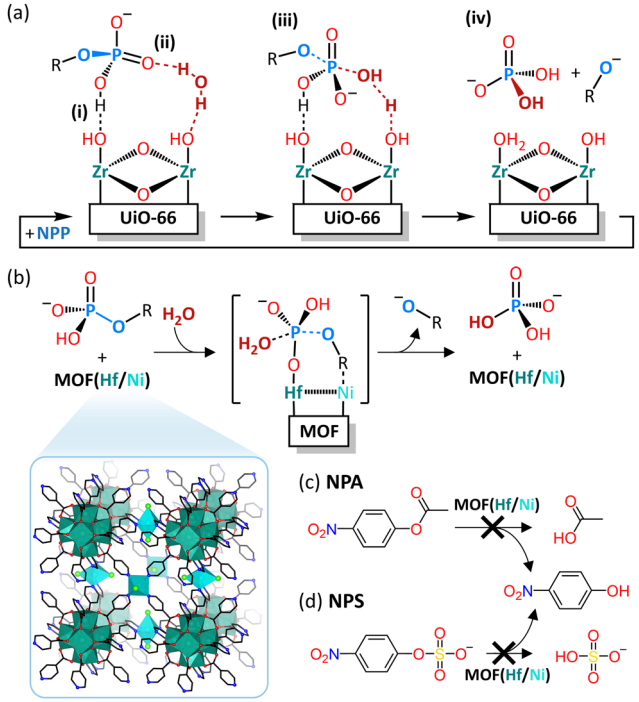

Fig. 23 Proposed mechanism of phosphoester bond hydrolysis of model systems (a) catalyzed by UiO-66(Zr) or (b) catalyzed by MOF(Hf/Ni), with the structure of MOF(Hf/Ni) shown in the inset (hafnium in teal, oxygen in red, carbon in black, nickel in light blue, nitrogen in blue, chlorine in light green). The unsuccessful hydrolysis of (c) 4-nitrophenyl acetate (NPA) and (d) 4-nitrophenyl sulfate (NPS) demonstrates the selectivity of MOF(Hf/Ni) towards hydrolysing P–O bonds over C–O and S–O bonds.

pores, the different geometry of NPA causes the formation of an unstable complex, and hydrolysis of NPS requires an expansive transition state with a much smaller solvent effect that is sterically unfavorable. Based on DFT calculations, complex stability with the four different substrates decreases in accordance with the experimental results: NPP ≫ BNPP > NPA > NPS (Table 8). DFT calculations were also used to define the hydrolysis mechanism for NPP, which proceeds *via* (i) coordination of the nitryl group of the substrate to Ni^{2+}, followed by (ii) stabilization of the complex through π–π stacking between the MOF's linker and the substrate's nitrophenol group, and (iii) P═O···Hf coordination between the substrate's phosphate group and the $\{Hf_6O_8\}$ cluster (stabilized by hydrogen bonding), thereby enabling hydrolysis by nucleophilic attack of water (Fig. 23(b)). Finally, the cytotoxicity and biocompatibility of the MOFs were explored for future biomedical applications, which revealed that all investigated MOFs have very low cytotoxicity and that MOF(Hf/Ni) was the least cytotoxic, most probably due to its high stability.[281] Therefore, MOF(Hf/Ni) is a promising candidate for biomedical applications.

While successful hydrolysis of nucleic acid model systems, including the hydrolysis of structurally similar chemical warfare agents, has often been reported,[48,284–289] examples of phosphoester bond cleavage in larger substrates, such as DNA and RNA, remain very scarce. Li *et al.* hydrolyzed phosphoester bonds in NPP and BNPP using FMA-FA-20-RT(Ce) (Fig. 21(b) and Table 8), which was also used for peptide bond hydrolysis, but DNA hydrolysis was not successful.[44] This is probably the result of the larger size of DNA prohibiting it from entering the MOF pores. In contrast, Yang *et al.* reported the hydrolysis of single-stranded DNA (ssDNA) using a hierarchically macro-microporous UiO-66(Ce) framework with a maximum pore size of 110 nm (HMUiO-66(Ce)), which completely hydrolyzed an 88-mer ssDNA within 6 h under physiological conditions (37 °C, pH 7.4).[278] HMUiO-66(Ce) was synthesized using a microemulsion-guided assembly, which allowed for large macropores that facilitate diffusion of large substrates, such as DNA, and thin microporous walls with a lot of solvent-exposed $\{Ce_6O_8\}$ clusters for easy substrate access. Furthermore, HMUiO-66(Ce) structure is an excellent artificial nuclease due to the presence of Ce^{4+} and its abundance of highly accessible Ce^{4+}–OH sites (Table 8). Moreover, the ssDNA hydrolysis yield could be increased by raising the temperature (40–80 °C) and decreasing/increasing the pH (pH 3–9) because HMUiO-66(Ce) has excellent thermal and chemical stability, which is sorely lacking in natural enzymes. The efficiency of the catalyst was further confirmed by successfully cleaving double-stranded DNA in the form of a supercoiled plasmid. Finally, comparative analysis between the ^{31}P NMR signal of free DNA (−1.21 ppm) and DNA in HMUiO-66(Ce) (−7.55 ppm) revealed the monodentate coordination of P–OH to Ce^{4+}–OH, making the phosphoester bond more susceptible to nucleophilic attack of water.[278]

The reported ability of certain MOFs to catalyze the cleavage of phosphoester bonds in DNA has potential implications for many biomedical applications, such as genetic engineering as well as biological imaging and sensing.[46,290,291] For example, Wang *et al.* reported the double role of PCN-8908, composed of $\{Zr_6O_8\}$ clusters and methane-tetrakis(*p*-terphenyl carboxylate) linkers, as a delivery vehicle for Cpf1-encoding plasmids and as a catalyst for phosphoester bond cleavage.[290] While hydrolysis of DNA was not directly observed (hydrolytic activity was only demonstrated with diethyl phosphate), the MOF did increase the efficacy of the developed protocol, where DNA was cleaved using Cpf1/crRNA, with the editing efficiency of two genes increasing by 5-fold or more. Additionally, PCN-224(Zr), which is constructed from $\{Zr_6O_8\}$ clusters that are each linked by 10 tetrakis(4-carboxyphenyl)porphyrin ligands, was reported to cause quenching of fluorescently labeled DNA *via* fluorescence resonance energy transfer (FRET), likely through the formation of Zr–O–P bonds between the ssDNA and the MOF. Since the formation of Zr–O–P bonds can be carefully tuned by occupying Zr^{4+} with free phosphate, the fluorescence behavior can be made to respond to various stimuli. This has been explored further in the creation of molecular sensing and logic systems capable of detecting multiple molecules.[291] Hence, the hydrolytic activity of MOFs towards phosphoester bonds has promising biotechnological applications and should be explored further.

3.2.2. Hydrolysis of ATP. Hydrolysis of phosphoester and phosphoanhydride bonds, found in molecules such as ATP, require specialized hydrolases optimized for one specific cleavage reaction (Fig. 24(a)). However, some of the phosphatase-mimicking MOFs discussed above possess sufficient Lewis

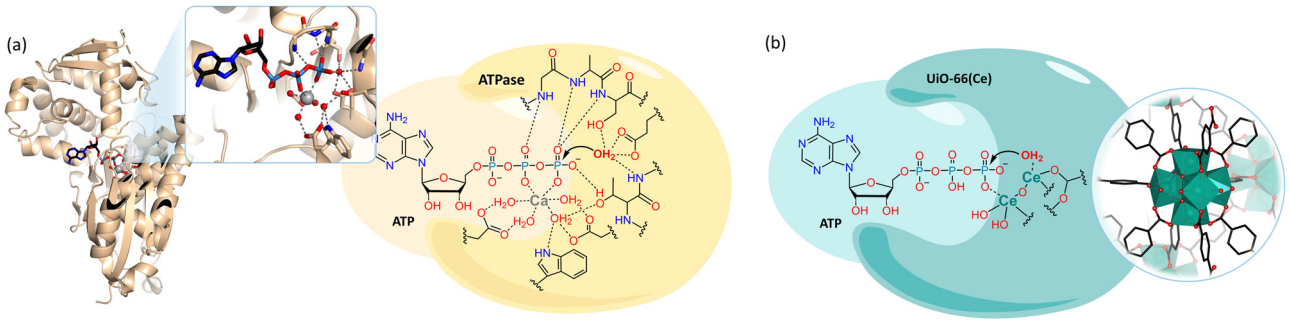

Fig. 24 Schematic representation of (a) the activation of ATP towards hydrolysis by an ATPase, based on a crystal structure of the protein (left; PDB code 3CJA), compared with (b) the proposed mechanism of activation by UiO-66(Ce). Adapted from ref. 283.

acidity for the activation of both bonds. This was established by Li *et al.*, who employed FMA-FA-20-RT(Ce) (Fig. 21(b)) to hydrolyze phosphoester bonds in model substrates, NPP and BNPP, as well as phosphoanhydride bonds in ATP and ADP.[44] In addition, it was found that both ATP and ADP were hydrolyzed by FMA-FA-20-RT(Ce) at similar rates, while AMP was hydrolyzed significantly slower. For all substrates, the observed mechanism aligned with cleavage of the P–O bond through Lewis acid activation by Ce^{4+} and nucleophilic addition of Ce^{3+}–OH, leading to a pentacoordinated intermediate that subsequently decomposes to the respective reaction products. The catalytic activity provided by the synergistic combination of different functionalities was also reported for another MOF consisting of $\{Zr_6O_8\}$ clusters and iron porphyrin linkers (PCN(Fe)), which has the same crystal structure as the well-established PCN-222.[282] PCN(Fe) was shown to be active towards an array of reactions, owing to its oxidase-, peroxidase-, and phosphatase-like activity, including the dephosphorylation of ATP with $\{Zr_6O_8\}$ clusters acting as the active site.[282] However, while ATP dephosphorylation was indeed observed, this study did not yield information on the mechanism or the kinetics of the reaction.[282]

A more detailed mechanistic study into the reactivity of MOFs towards nucleotides was presented in the first example of phosphoanhydride bond cleavage by a MOF reported in 2020 by Yang *et al.*, which involved the hydrolysis of ATP to ADP/AMP by UiO-66(Ce) (Table 8).[283] The mechanism of dephosphorylation for UiO-66(Ce) was found to be similar to that of the natural ATPase enzyme apyrase (Fig. 24), with coordination of the metal cation (Ce^{4+} in the case of the MOF and Ca^{2+} for apyrase) to one or two phosphate groups of the substrate followed by nucleophilic attack of water (coordinated to Ce^{3+} in the MOF or bound to the side chains of protein residues in the ATPase). While the mechanism itself is almost identical to that reported by Li *et al.*,[44] the enzyme-mimetic character of the proposed mechanism and the significance of both Ce^{3+} and Ce^{4+} were elaborated on in more detail.[283] Furthermore, while FMA-FA-20-RT(Ce) hydrolyzed ATP, ADP, and AMP, UiO-66(Ce) did not hydrolyze the phosphoester bond in AMP, which is an interesting demonstration of the selectivity of UiO-66(Ce) towards phosphoanhydride bonds. Furthermore, UiO-66(Ce) exhibited lower apparent K_M values for ATP and ADP substrates compared to apyrase, with the sequential ADP hydrolysis being remarkably slower. This indicates that UiO-66(Ce) has higher substrate affinity due to its greater active site density, even though the hydrolysis mechanism is nearly identical to that of apyrase.[283] This bio-inspired approach where MOFs are compared to natural enzymes can provide valuable insights into how MOFs catalyze certain reactions, but also about the function of enzymes that catalyze the same reactions. However, despite these recent advances, further experimental and computational research is required to make MOFs, and other cluster-based hybrid systems, ready for potential applications.

3.3. Carbohydrates

3.3.1. Hydrolysis of polysaccharides. To convert biomass waste into biofuels or platform chemicals, the large polysaccharide structures must be hydrolyzed into monomeric units first. This bioconversion process requires the extraction of cellulose and hemicellulose components, followed by depolymerization of the carbohydrate polymers through hydrolysis of glycosidic bonds to produce free sugar monomers. As previously discussed in Section 2.3.1, the breakdown of lignocellulosic biomass into sugar monomers is typically performed *via* acid hydrolysis or enzymatic hydrolysis, both of which have several drawbacks.[292–295] Therefore, other catalytic routes are being explored, including the use of MOCs (Section 2.3.1) and MOC-based materials, especially as alternative heterogeneous catalysts for biomass valorization into platform chemicals that can be upgraded into various chemical compounds using an array of reaction mechanisms,[180,296] which will be discussed in the next section.

The previously described FMA-FA-20-RT(Ce) framework (Fig. 21(b)), which was studied for its hydrolytic activity toward an extensive array of biologically relevant bonds, was also investigated toward hydrolysis of glycosidic bonds.[44] Initial studies on the hydrolysis of 2-nitrophenyl β-D-galactopyranoside and 4-nitrophenyl *N*-acetyl-β-D-glucosaminide were both successful, with the latter being cleaved more efficiently. However, the sugar dimers maltose, which contains an α-1,4-glycosidic bond, and lactose, which contains the same β-1,4-glycosidic bond that is found in cellulose, could not be hydrolyzed into sugar monomers. This indicates that the nitrophenyl leaving groups assist in the hydrolysis. Therefore, carboxymethyl chitosan was chosen as a

model polymer instead of cellulose because the carboxymethyl group can favorably interact with the MOF's Ce clusters, thus assisting the hydrolysis reaction. Indeed, through the use of GPC, it was found that FMA-FA-20-RT(Ce) can successfully cleave carboxymethyl chitosan at 37 or 60 °C and pH 8 with limited recyclability.[44] Consequently, it was concluded that FMA-FA-20-RT(Ce) requires substrates with specific functional groups to lower the sorption energy for successful glycosidic bond hydrolysis, which means it cannot be used for biomass valorization as such, and further optimization is needed.

More recently, Han *et al.* reported cellulose hydrolysis using a hybrid catalyst (PW_{12}@MIL-101-X) based on MOF MIL-101(Fe) that acts both as carrier for the hydrolytically active $H_3[PW_{12}O_{40}]$ and as a means to activate cellulose for hydrolysis by modifying its BDC linkers with electron-withdrawing groups (X = –Br, $–NH_2$, –Cl, $–NO_2$).[297] The addition of electron-withdrawing moieties on the MOF caused it to selectively adsorb cellulose by forming hydrogen bonds *via* its hydroxyl groups, which further weakens the existing hydrogen bonds within cellulose and thereby makes hydrolysis more efficient. Hence, the greatest glucose yield (16.2%) was obtained for PW_{12}@MIL-101-NO_2 at 180 °C after 11 h due to the strong electron-withdrawing character of $–NO_2$ (Table 9).[297] However, the recyclability was sub-optimal with a loss of 4.3% in glucose yield after 3 cycles due to the weak interaction between POM and MOF, which led to a reduced catalyst loading within MIL-101-X for X = Br, Cl, NO_2. PW_{12}@MIL-101-NH_2, on the other hand, did not experience a significant loss in glucose yield after repeated cycles owing to stabilization of the POM through electrostatic interactions with $–NH_3^+$, formed by protonation of the $–NH_2$ groups.[297] This highlights the importance of creating catalyst materials that are both reactive and stable, which can be achieved through careful design of the structure. Moreover, this shows the promising potential of combining POMs and MOFs, which has been recently explored for a wide range of reactions in organic chemistry and should be explored further with biomolecules.[47]

Overall, few examples of cellulose hydrolysis using MOC-based MOFs have been reported. However, this reaction could benefit greatly from MOF-related advantages, such as their heterogeneous nature facilitating catalyst separation after the reaction, since the current processes (*i.e.*, acid hydrolysis) are not environmentally conscious and, therefore, further research should be stimulated. Along with designing MOFs as a new class of catalysts for biomass conversion, MOFs have also been used to improve existing enzymatic catalysis. By using MOFs as protective coatings, biomolecules are effectively sheltered from harsh reaction conditions in which their performance is negatively impacted or in which they degrade entirely.[302] Various MOF structures have already been used to encapsulate and stabilize β-glucosidase for hydrolysis of cellulose in conditions that would otherwise be detrimental to the protein structure (*e.g.*, high temperature), with the benefit of enzyme heterogenization.[49,303,304] However, to the best of our

Table 9 Selected conditions and product yields reported for the conversion of sugars catalyzed by MOFs

MOF	Substrates	Reactivity	Reaction conditions	Product yield	Ref.
PW_{12}@MIL-101(Fe)-NO_2	Cellulose	Hydrolysis	H_2O, 180 °C, 3–11 h, 12 mg mL^{-1} MOF	16.2% glucose	297
PW_{12}@MIL-101(Fe)-NH_2	Cellulose	Hydrolysis	H_2O, 180 °C, 3–11 h, 12 mg mL^{-1} MOF	12.9% glucose	297
UiO-66(Zr)-SO_3H	Fructose	Dehydration	DMSO, 120 °C, 1 h, 60 mg mL^{-1} MOF	85% HMF	298
UiO-66(Zr)	Glucose	Isomerization Epimerization	H_2O, 100 °C, 24 h, 25 mg mL^{-1} MOF	5.0% fructose 6.3% mannose	299
UiO-66(Zr)-NH_2	Glucose	Isomerization Epimerization Dehydration	H_2O, 100 °C, 24 h, 25 mg mL^{-1} MOF	4.0% fructose 3.3% mannose 1.0% HMF	299
NU-1000(Zr)	Glucose	Isomerization Dehydration	H_2O, 140 °C, 5 h, 10 mg mL^{-1} MOF	19% fructose 2.3% HMF	300
NU-1000(Zr)-PO_4	Glucose	Isomerization Dehydration	H_2O/THF, 140 °C, 5 h, 10 mg mL^{-1} MOF	5.0% fructose 25% HMF	300
UiO-66(Zr)	Glucose	Hydrolysis Isomerization Dehydration	H_2O, 140 °C, 3 h, 0.03 eq. MOF	1.6% fructose 0.5% mannose 3.5% HMF	301
Nano UiO-66(Zr)	Glucose	Hydrolysis Isomerization Dehydration	H_2O, 140 °C, 3 h, 0.03 eq. MOF	4.2% fructose 5.3% mannose 4.0% HMF	301
Ultra-nano UiO-66(Zr)	Glucose	Hydrolysis Isomerization Dehydration	H_2O, 140 °C, 3 h, 0.03 eq. MOF	5.0% fructose 6.1% mannose 4.4% HMF	301
MSBDC(50)-UiO-66(Zr)	Glucose	Hydrolysis Isomerization Dehydration	H_2O, 140 °C, 3 h, 0.03 eq. MOF	8.1% fructose 7.3% mannose 6.5% HMF	301
Nano MSBDC(50)-UiO-66(Zr)	Glucose	Hydrolysis Isomerization Dehydration	H_2O, 140 °C, 3 h, 0.03 eq. MOF	6.4% fructose 6.8% mannose 7.7% HMF	301
Naphtha(100)-UiO-66	Glucose	Hydrolysis Isomerization Dehydration	H_2O, 140 °C, 3 h, 0.03 eq. MOF	6.6% fructose 1.2% mannose 3.7% HMF	301

MSBDC = 2-monosulfo-benzene-1,4-dicarboxylate.

knowledge, MOC-based MOFs have not been reported for this purpose. Nevertheless, Zr- and Hf-based MOCs could be interesting for these applications as the synergy between the reactivity of the MOCs and that of the encapsulated enzyme may produce particularly effective catalysts.

3.3.2. Dehydration of sugars into platform chemicals. After depolymerization, glucose can be processed into other useful reagents, such as HMF, which are obtained from glucose through isomerization into fructose and subsequent dehydration, as discussed in Section 2.3.2. HMF can then undergo further reactions to produce an array of useful platform chemicals. For example, it can be oxidized into 2,5-furandicarboxylic acid, which can replace terephthalic acid in polyethylene terephthalate (PET) production. Hence, the dehydration of glucose to HMF has been catalyzed with various MOF architectures.

In 2014, Chen *et al.* reported the dehydration of fructose with >90% HMF yield in DMSO catalyzed by MIL-101(Cr)-SO_3H consisting of trimeric Cr^{3+} units, which are composed of $\{CrO_6\}$ octahedra linked by a central μ_3-O ligand and are interconnected by Brønsted acidic 2-sulfoterephthalate linkers (Fig. 25).[298] The addition of sulfonic acid creates the Brønsted acidity needed for dehydration, while the Lewis acidity of Cr^{3+} can promote the isomerization of glucose to fructose. However, the Cr metal used in this MOF is known to be toxic and harmful to the environment,[31] and the substitution of Cr in MIL-101 with other trivalent cations has been found to render the material unstable.[305] Consequently, alternative MOF architectures have been investigated as a means to gradually eliminate reliance on Cr. With this purpose, Luo *et al.* studied the isomerization of glucose using UiO-66(Zr) and compared it to MIL-101(Cr).[299] MIL-101(Cr) promoted glucose isomerization in both water and methanol at 100 °C and favored glucose epimerization to mannose (Fig. 25) at higher temperatures. In contrast, UiO-66(Zr) displayed simultaneous glucose isomerization and epimerization in aqueous media (Fig. 25), with the latter occurring through an intramolecular carbon skeleton rearrangement facilitated by UiO-66(Zr) that was not observed for MIL-101(Cr). This difference in behavior can be attributed to the larger ionic radius and increased polarizability of the Zr^{4+} sites, leading to the formation of an eight-coordinate mononuclear complex that could promote carbon skeleton rearrangement (Fig. 25). On the other hand, MIL-101(Cr) with two Cr^{3+} sites formed a hexa-coordinate binuclear complex due to the lower polarizability and steric hindrance of the trimeric units, resulting in glucose isomerization without carbon skeleton rearrangement (Fig. 25).[299] This contrasting behavior between MIL-101(Cr) and UiO-66(Zr) confirms the importance of both the structure and metal choice within MOFs. Furthermore, these studies show that the reactivity and selectivity are influenced by the nature of the active sites and their local environment within the framework, which must be considered when designing a MOF for a particular application.

Various Zr-based MOFs have been employed for the conversion of glucose, such as NU-1000(Zr) with $\{Zr_6O_8\}$ cluster nodes that possess phosphate capping ligands in addition to the formate capping ligands to tune their Lewis acidity and avoid unwanted side reactions (Table 9).[300] Additionally, UiO-66(Zr)

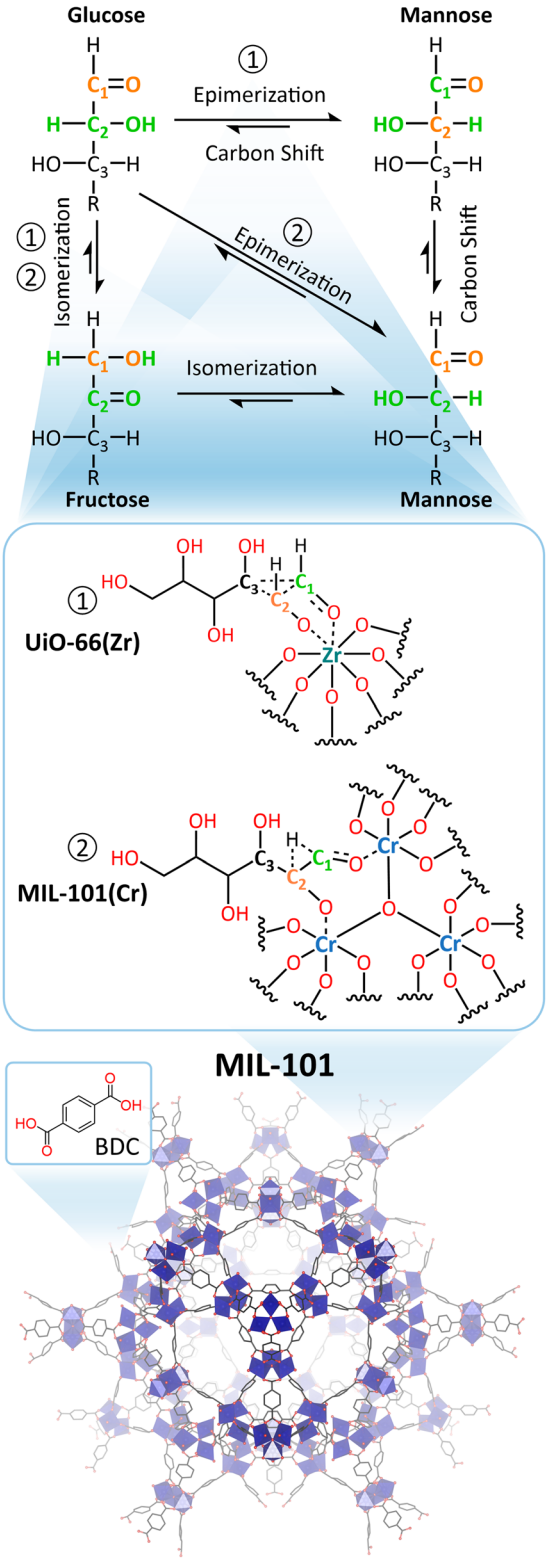

Fig. 25 Interconversion between glucose, fructose, and mannose depending on the MOF used, either UiO-66(Zr) or MIL-101, with the structure of MIL-101 with BDC linkers shown at the bottom. Adapted from ref. 299.

modified with sulfonate-containing linkers was shown to catalyze the isomerization of glucose to fructose and dehydration to HMF in alcohol media because of its inherent defect-induced Lewis acidity (Table 9).[306] Furthermore, Oozeerally *et al.* showed that nano and ultra-nano UiO-66(Zr) MOFs, produced by slightly modifying the synthesis conditions, displayed increased catalytic performance (Table 9).[301] This can be attributed to two aspects of the reaction: (i) reduced particle size is accomplished by the introduction of more defects, which increases the number of accessible Zr^{4+} sites and the Lewis acidity, and (ii) the reaction can only occur on the external surface area because glucose is unable to enter the UiO-66 pores, which makes smaller particles with a larger surface-to-volume ratio more suitable. Secondly, partial substitution of the linkers in UiO-66(Zr) with 2-sulfoterephthalate resulted in much better catalytic performance owing to their electron-withdrawing effect, which enhances Lewis acidity of nearby defective Zr^{4+} sites. Thirdly, the hydrophobicity of UiO-66 was increased by functionalization with naphthalene, resulting in drastically enhanced selectivity towards fructose isomerization, and subsequent dehydration to HMF, instead of mannose epimerization. Finally, the introduction of free carboxylate groups increased HMF yield due to their mild Brønsted acidity, while leaving glucose conversion unaffected (Table 9). Because of these insights, the work by Oozeerally *et al.* serves as a roadmap for the future design of Zr-based MOFs for the conversion of glucose and as inspiration for other catalytic processes.[301]

HMF can further undergo a very wide range of different reactions, including condensation,[307,308] hydrogenation,[308–312] reduction,[308] oxidation,[307,313] esterification,[314,315] and etherification,[316] to functionalize it for specific downstream applications. These reactions are often suitable for both cascade and tandem one-pot reactions and while the scope should be expanded by further investigating these multi-step reactions, various examples are already known.[187,256,307] Moreover, MOFs are often regarded as greener alternatives compared to current practices that require large amounts of solvent or water, highly acidic/basic conditions, or precious metal catalysts, which further stimulates their development within this field. However, since these subsequent reactions are more relevant for industrial processes and because they have been discussed in great detail before,[187,256,259] they will not be discussed further here.

3.4. Lipids

Similarly to POMs, MOFs and other heterogeneous MOC-based hybrid materials have been explored as catalysts for the production of biofuels from lipids. To achieve this, increasing the Lewis and Brønsted acidity is a priority because they are necessary to increase the reactivity toward the esterification of fatty acids and transesterification of triglycerides during this process. However, while research on lipid (trans)esterification with POMs has been more extensively explored, using MOC-based materials and MOFs has not been studied to the same extent yet, especially with respect to the reaction mechanism. In this regard, the group of W. Yang has recently made progress using MOFs for biodiesel production from microalgal lipids, which are especially interesting substrates since microalgae have a fast growth rate, high photosynthetic efficiency, and very high lipid content, making them the most abundant natural source for biodiesel.[317,318] Two distinct paths were chosen to increase the reactivity and solve problems related to other porous catalysts for these types of reactions. Enhanced access to active sites was postulated by opting for a two-dimensional MOF structure and enhanced Brønsted acidity was achieved by immobilizing an ionic liquid cation on a MOF.

In the first approach, the two-dimensional MOF TATAB(Zr), consisting of $\{Zr_6O_8\}$ clusters connected by 4,4′,4″-*s*-triazin-1,3,5-triyltri-*p*-aminobenzoic acid (TATAB) linkers (Fig. 26(a)), was employed for the esterification of free fatty acids and transesterification of triglycerides in a microalgal lipid mixture (*i.e.*, palmitic, palmitoleic, stearic, oleic, and linoleic acid) to synthesize the main component of biodiesel: fatty acid methyl esters (FAMEs).[317] The microalgal lipid mixture was converted to FAME using TATAB(Zr) with an efficiency of 98.2% in methanol after 2 h at 195 °C (Table 10). This is not only the most effective catalyst based on MOCs reported for this reaction, but it also benefits from an easy synthesis procedure and economical catalyst use. Three possible reaction mechanisms were postulated (Fig. 26(a)): (i) methanol coordinated to Zr^{4+} releases a proton that causes the formation of water from a Zr-bound hydroxide (Zr–OH), after which nucleophilic attack of the formed Zr-OCH_3 on a triglyceride produces an intermediate that further decomposes to form FAME; (ii) the carbonyl oxygen of the triglyceride coordinates to Zr^{4+} and a nucleophilic attack by free methanol causes the formation of an intermediate that further decomposes to form FAME; or (iii) both the triglyceride and methanol are coordinated to the same $\{Zr_6O_8\}$ cluster, thus both carbocations can directly react to form FAME.[317] These reaction pathways are also possible for the methanolic (trans)-esterification of monoglycerides, diglycerides, and free fatty acids. Furthermore, when compared with three-dimensional MOF-808(Zr), TATAB(Zr) performed significantly better. This is

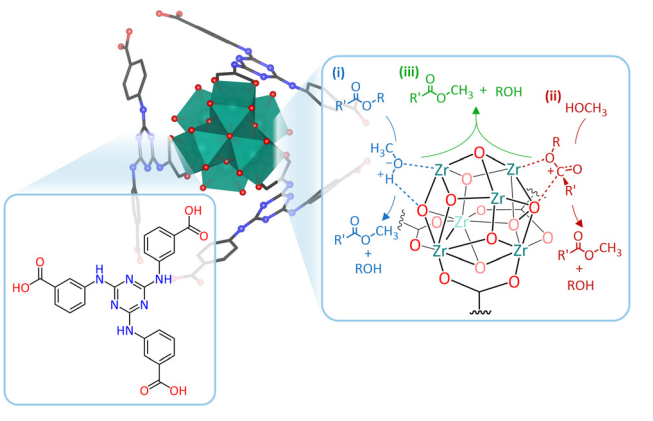

Fig. 26 Structural representation of the Zr_6 cluster in TATAB(Zr) and TATAB linker along with a scheme for the three proposed reaction pathways for the transesterification of triglyceride. Adapted from ref. 317.

Table 10 Selected conditions and percentage conversion reported for MOF-catalyzed (trans)esterification of free fatty acids (FA) and oil mixtures

Heterogeneous hybrid catalyst	Substrates	Reactivity	Reaction conditions	Conversion/%	Ref.
$H_3[PMo_{12}O_{40}]$/BTC(Fe)	Oleic acid	Esterification	16 : 1 MeOH : FA, 160 °C, 3 h, 10 wt% MOF	72	319
$Sn_{1.5}[PW_{12}O_{40}]$/BTC(Cu)	Oleic acid	Esterification	20 : 1 MeOH : FA, 160 °C, 4 h, 0.2 g MOF	88	320
TATAB(Zr)	Microalgal lipids	Transesterification	20 : 1 MeOH : oil, 195 °C, 2 h, 2 wt% MOF	98	317
IL/$H_3[PMo_{12}O_{40}]$/MIL-101(Fe)	Soybean oil	Transesterification	30 : 1 MeOH : oil, 120 °C, 8 h, 9 wt% MOF	93	321
IL/POM/UiO-66(Zr)-2COOH	Soybean oil	Transesterification	35 : 1 MeOH : oil, 110 °C, 6 h, 10 wt% MOF	92–96	322
IL/$H_3[PMo_{12}O_{40}]$/$CoFe_2O_4$/MIL-88B(Fe)-NH_2	Soybean oil	Transesterification	30 : 1 MeOH : oil, 140 °C, 8 h, 8 wt% MOF	96	323
$Arg_2H_3[PW_{12}O_{40}]$/ZIF-8	Insect lipids	Transesterification	9 : 1 MeOH : oil, 60 °C, 4 h, 3 wt% MOF	94	324

mainly attributed to the inaccessibility of the internal active Zr^{4+} sites of MOF-808, but it can also be correlated to the higher degree of unsaturation and stronger overall acidity of TATAB(Zr).[317] Consequently, two-dimensional MOFs should be explored further, not only for this reaction but for all the other reactions discussed in this review.

The second approach for increasing reactivity in the (trans)esterification of microalgal lipid mixtures to FAME, was explored using the isoreticular metal–organic framework-3 (IRMOF-3), consisting of tetranuclear Zn^{2+} units connected by six 2-amino-1,4-benzenedicarboxylic acid (NH_2-BDC) linkers, combined with the Brønsted acidic IL 1-butylsulfonate-3-methylimidazolium bisulfate ([BSO_3HMIm][HSO_4]).[318] Therefore, the catalyst has both Lewis (Zn^{2+}) and Brønsted acid (HSO_4^-) sites that can be exploited, resulting in similar FAME conversion as for TATAB(Zr) (Table 10).[318] The reaction mechanism was proposed to also be similar to that of TATAB(Zr), but in this case, the Lewis basic sites (uncoordinated –NH_2 and imidazole) are primarily responsible for the transesterification of triglycerides.[318] Similar systems, where the Lewis acidity of various MOFs was combined with the Brønsted acidity of ILs, have also been described for the esterification of oleic acids.[325–327] Furthermore, MOF systems that incorporate both ILs and POMs, which add to the Brønsted acidity, have been utilized for (trans)esterification of single fatty acids and other oil mixtures, such as vegetable oil and soybean oil (Table 10).[319–323] However, these have a lower conversion efficiency compared to both the TATAB(Zr) and IRMOF-3/IL systems because the accessibility to the active sites or the overall acidity is not optimized to the same extent. Therefore, there is still significant potential for exploring this second route for achieving better catalytic activity in biodiesel production using MOC-based materials.

Compared to completely MOF-based catalysts for lipid (trans)esterification, more examples of POM-based hybrids have been explored. Initially, the focus of research was driven by the heterogenization of POMs due to the benefits associated with heterogeneous catalysis. In that regard, POMs have been immobilized on various supports ranging from solid zirconia and zirconium phosphate to mesoporous materials (*i.e.*, zeolites and MOFs) and nanoparticles.[243,324,328–332] However, recent developments with MOFs have provided valuable insights about the reaction mechanism and clarified that the reaction is not significantly influenced by specific MOF parameters, but rather that it depends on the active site accessibility and the acidity/basicity of the catalyst.

4. Conclusions and outlook

MOCs and MOC-based materials have been established to be a powerful family of catalysts for biomolecular transformations with potential applications in many fields, such as medicine, biotechnology, and biofuel production. MOCs, as discrete clusters or as part of MOFs and other materials, have been shown to effectively catalyze a wide range of reactions (*e.g.*, hydrolysis, amidation, oxidation, isomerization, dehydration, (trans)esterification, *etc.*) of an even wider range of biomolecules: amino acids, peptides, (glyco)proteins, nucleic acids, nucleotides, sugars, fatty acids, triglycerides, *etc*. Furthermore, the diversity of this family of clusters in terms of metal composition and structure means that they can be tuned to optimize the reactivity for the desired application. However, this requires an in-depth understanding of structure–activity relationships, which can be gained from the multiple mechanistic studies presented in this review. These studies show that the reactivity of MOCs is generally linked to their Lewis acidity, Brønsted acidity, and/or redox activity. For instance, highly Lewis acidic metal centers are needed for peptide, phosphoester, and phosphoanhydride bond hydrolysis as well as for peptide bond formation since coordination to C═O or P═O bonds activates them towards nucleophilic attack. On the other hand, Brønsted acidity is needed to promote the hydrolysis of glycosidic bonds as well as the (trans)esterification of fatty acids and triglycerides. In addition, by combining Lewis and Brønsted acidity the direct conversion of biomass to HMF can be achieved *via* isomerization and dehydration reactions. Similarly, through a combination of Lewis acidity and redox activity, the hydrolysis of peptide bonds can be tuned. However, the redox properties of MOCs and MOC-based materials have not been as extensively investigated for biomolecular transformations, despite having been explored in many organic reactions.[29] Therefore, there is still immense untapped potential for the design of MOCs as highly active and selective catalysts in biochemical reactions, and investigating their mechanism of action is the first step in this direction.

Many mechanistic insights have been obtained from investigating the reactivity of discrete MOCs, particularly POMs. Their relatively simple atomically precise structures and their solubility in different solvents make them more amenable to spectroscopic and computational studies compared to MOC-based heterogeneous catalysts. However, POMs can have complex speciation in solution, which makes it difficult to determine the catalytically active species. As a result, less labile

polyoxotungstate M–POMs have been most extensively investigated. While the solubility of certain discrete MOCs as homogeneous catalysts is advantageous for studying their reactivity, it makes catalyst recycling challenging. Therefore, several strategies for the heterogenization of POMs have been explored, especially for HPAs that could be used in biofuel production. One way of achieving this for POMs is through ion exchange with surfactants, ionic liquid cations, or large monovalent ions (*e.g.*, NH_4^+, Cs^+, *etc.*) to form insoluble salts. This also allows for the structural and catalytic properties of the counter-cation to be exploited to enhance the reactivity. Alternatively, MOCs can be heterogenized by incorporation into solid structures, such as MOFs. In this respect, MOFs have been shown to be particularly suitable due to their porosity and high surface area. Furthermore, the reactivity of MOFs can be tuned through careful choice of their structure, the number of defects, the nature of the MOC, and the functionality of the organic linker. Therefore, the reactivity of multiple MOC-based MOFs towards biomolecules has been increasingly explored in recent years.

When transitioning towards heterogeneous catalysis, the knowledge gained from the reactivity of discrete MOCs can be translated to MOC-based materials. This can be most clearly seen from the studies on the reactivity of MOCs towards peptide bonds in the context of proteomics analysis, as Zr/Hf-based soluble POMs, neutral MOCs, and MOC-based MOFs catalyzed the hydrolysis reaction in similar ways with differences in their reactivity likely linked to their structure. For instance, $\{Zr_6O_8\}$-based MOF-808 gave rise to a faster reaction rate for the hydrolysis of the dipeptide Gly-Gly than Zr–POMs and discrete Zr_6 clusters, but a similar selectivity was likely achieved as for Zr–POMs.[260] However, the study of the reactivity of discrete MOCs towards biomolecules has been mainly limited to POMs even though there are several other classes of MOCs that have potential as catalysts, such as the Zr^{4+}, Hf^{4+}, and Ce^{4+} clusters that have been used extensively as building blocks for MOFs. Moreover, Zr^{4+}, Hf^{4+}, and Ce^{4+} have been shown to be particularly interesting due to their high Lewis acidity, high coordination number, and oxophilicity. Furthermore, the redox activity of Ce^{4+} makes it promising for oxidation reactions, either through direct oxidation of biomolecules or indirectly *via* the formation of ROS. Therefore, further studies on the reactivity of these discrete MOCs towards biomolecules could open new avenues of research and help direct the development of new related heterogeneous materials, such as 2D MOFs, which have not been as extensively explored so far.

Further research into the reactivity of metal–oxo clusters and cluster-based materials should ideally build upon the insights obtained until now from simple model systems to tackle more complex biomolecules, such as DNA or membrane proteins, while bearing in mind the limitations of such model systems for predicting the reactivity towards large biomolecules. In addition, the cytotoxicity and pharmacokinetics of MOCs need to be considered for their use in biomedical applications.[57,333–336] Therefore, additional studies on the impact of MOCs on living organisms and on their stability in biological systems are needed to develop them for these applications.[337,338] These studies could benefit from the molecular-level insights discussed in this review by establishing a link between reactivity and cytotoxicity, which has been scarcely investigated in detail. Additionally, the study of the cytotoxicity of POMs and the development of biocompatible POMs with low off-target toxicity is of primordial importance for their implementation in biomedical applications since clinical trials of POM-based inorganic drugs have been largely hampered by their cytotoxicity.[57] Moreover, while this review covers the reactivity of MOCs towards the main types of biomolecules present in organisms, the lessons learned from these studies can be applied to other biomolecules, such as terpenes and their derivatives,[234,339–342] as well as in synthetic chemistry, especially in the production of pharmaceuticals.[343]

Author contributions

The manuscript was written through contributions of all authors. All authors have given approval to the final version of the manuscript.

Conflicts of interest

There are no conflicts to declare.

Acknowledgements

We thank KU Leuven and the Research Foundation Flanders (FWO) for funding. D. E. S. M. (1183021N), N. D. S. (1267623N), and S. A. M. A. (1115319N), thank the FWO for fellowships. Some of the figures were created using **https://Biorender.com** or PyMOL.

References

1 J. Bolleddula and S. K. Chowdhury, Carbon–carbon bond cleavage and formation reactions in drug metabolism and the role of metabolic enzymes, *Drug Metab. Rev.*, 2015, **47**, 534–557.
2 J. Sukumaran and U. Hanefeld, Enantioselective C–C bond synthesis catalysed by enzymes, *Chem. Soc. Rev.*, 2005, **34**, 530–542.
3 L. Chen, Z. Deng and C. Zhao, Nitrogen–Nitrogen Bond Formation Reactions Involved in Natural Product Biosynthesis, *ACS Chem. Biol.*, 2021, **16**, 559–570.
4 R. Fasan, Tuning P450 Enzymes as Oxidation Catalysts, *ACS Catal.*, 2012, **2**, 647–666.
5 P. Gamba and N. Zenkin, Transcription fidelity and its roles in the cell, *Curr. Opin. Microbiol.*, 2018, **42**, 13–18.
6 A. Sallmyr, I. Rashid, S. K. Bhandari, T. Naila and A. E. Tomkinson, Human DNA ligases in replication and repair, *DNA Repair*, 2020, **93**, 102908.
7 J. C. Bowman, A. S. Petrov, M. Frenkel-Pinter, P. I. Penev and L. D. Williams, Root of the Tree: The Significance, Evolution, and Origins of the Ribosome, *Chem. Rev.*, 2020, **120**, 4848–4878.

8 M. Simonović and T. A. Steitz, A structural view on the mechanism of the ribosome-catalyzed peptide bond formation, *Biochim. Biophys. Acta, Gene Regul. Mech.*, 2009, **1789**, 612–623.
9 T. S. Raju, *Co- and Post-Translational Modifications of Therapeutic Antibodies and Proteins*, John Wiley & Sons, Inc., Hoboken, NJ, USA, 2019, pp. 183–202.
10 H. An, A. Ordureau, M. Körner, J. A. Paulo and J. W. Harper, Systematic quantitative analysis of ribosome inventory during nutrient stress, *Nature*, 2020, **583**, 303–309.
11 S. C. L. Kamerlin and A. Warshel, On the Energetics of ATP Hydrolysis in Solution, *J. Phys. Chem. B*, 2009, **113**, 15692–15698.
12 J. C. Fontecilla-Camps, The Complex Roles of Adenosine Triphosphate in Bioenergetics, *ChemBioChem*, 2022, **23**, e202200064.
13 B.-T. Wang, S. Hu, X.-Y. Yu, L. Jin, Y.-J. Zhu and F.-J. Jin, Studies of Cellulose and Starch Utilization and the Regulatory Mechanisms of Related Enzymes in Fungi, *Polymers*, 2020, **12**, 530.
14 A. Lovegrove, C. H. Edwards, I. De Noni, H. Patel, S. N. El, T. Grassby, C. Zielke, M. Ulmius, L. Nilsson, P. J. Butterworth, P. R. Ellis and P. R. Shewry, Role of polysaccharides in food, digestion, and health, *Crit. Rev. Food Sci. Nutr.*, 2017, **57**, 237–253.
15 R. Zechner, P. C. Kienesberger, G. Haemmerle, R. Zimmermann and A. Lass, Adipose triglyceride lipase and the lipolytic catabolism of cellular fat stores, *J. Lipid Res.*, 2009, **50**, 3–21.
16 H. Sun, W. Ou, L. Sun, B. Wang and C. Su, Recent advances in nature-inspired nanocatalytic reduction of organic molecules with water, *Nano Res.*, 2022, **15**, 10292–10315.
17 J. H. Schrittwieser, S. Velikogne, M. Hall and W. Kroutil, Artificial Biocatalytic Linear Cascades for Preparation of Organic Molecules, *Chem. Rev.*, 2018, **118**, 270–348.
18 A. J. J. Straathof, S. Panke and A. Schmid, The production of fine chemicals by biotransformations, *Curr. Opin. Biotechnol*, 2002, **13**, 548–556.
19 S. Maroa and F. Inambao, A review of sustainable biodiesel production using biomass derived heterogeneous catalysts, *Eng. Life Sci.*, 2021, **21**, 790–824.
20 L. Marchetti and M. Levine, Biomimetic Catalysis, *ACS Catal.*, 2011, **1**, 1090–1118.
21 J. Liu and G. Wulff, Functional Mimicry of Carboxypeptidase A by a Combination of Transition State Stabilization and a Defined Orientation of Catalytic Moieties in Molecularly Imprinted Polymers, *J. Am. Chem. Soc.*, 2008, **130**, 8044–8054.
22 E. E. Kim and H. W. Wyckoff, Reaction mechanism of alkaline phosphatase based on crystal structures, *J. Mol. Biol.*, 1991, **218**, 449–464.
23 J. Zabret, S. Bohn, S. K. Schuller, O. Arnolds, M. Möller, J. Meier-Credo, P. Liauw, A. Chan, E. Tajkhorshid, J. D. Langer, R. Stoll, A. Krieger-Liszkay, B. D. Engel, T. Rudack, J. M. Schuller and M. M. Nowaczyk, Structural insights into photosystem II assembly, *Nat Plants*, 2021, **7**, 524–538.
24 F. de Azambuja, J. Moons and T. N. Parac-Vogt, The Dawn of Metal–oxo Clusters as Artificial Proteases: From Discovery to the Present and Beyond, *Acc. Chem. Res.*, 2021, **54**, 1673–1684.
25 Y. Zhang, F. de Azambuja and T. N. Parac-Vogt, The forgotten chemistry of group(IV) metals: A survey on the synthesis, structure, and properties of discrete Zr(IV), Hf(IV), and Ti(IV) oxo clusters, *Coord. Chem. Rev.*, 2021, **438**, 213886.
26 A. A. Fertig, W. W. Brennessel, J. R. McKone and E. M. Matson, Concerted Multiproton–Multielectron Transfer for the Reduction of O_2 to H_2O with a Polyoxovanadate Cluster, *J. Am. Chem. Soc.*, 2021, **143**, 15756–15768.
27 D. Van den Eynden, R. Pokratath, J. P. Mathew, E. Goossens, K. De Buysser and J. De Roo, Fatty acid capped, metal oxo clusters as the smallest conceivable nanocrystal prototypes, *Chem. Sci.*, 2023, **14**, 573–585.
28 N. Li, J. Liu, B. Dong and Y. Lan, Polyoxometalate-Based Compounds for Photo- and Electrocatalytic Applications, *Angew. Chem., Int. Ed.*, 2020, **59**, 20779–20793.
29 S.-S. Wang and G.-Y. Yang, Recent Advances in Polyoxometalate-Catalyzed Reactions, *Chem. Rev.*, 2015, **115**, 4893–4962.
30 D. Van den Eynden, R. Pokratath and J. De Roo, Nonaqueous Chemistry of Group 4 Oxo Clusters and Colloidal Metal Oxide Nanocrystals, *Chem. Rev.*, 2022, **122**, 10538–10572.
31 A. D. Dayan and A. J. Paine, Mechanisms of chromium toxicity, carcinogenicity and allergenicity: Review of the literature from 1985 to 2000, *Hum. Exp. Toxicol.*, 2001, **20**, 439–451.
32 P. Yang and U. Kortz, Discovery and Evolution of Polyoxopalladates, *Acc. Chem. Res.*, 2018, **51**, 1599–1608.
33 S. Bhattacharya, A. Barba-Bon, T. A. Zewdie, A. B. Müller, T. Nisar, A. Chmielnicka, I. A. Rutkowska, C. J. Schürmann, V. Wagner, N. Kuhnert, P. J. Kulesza, W. M. Nau and U. Kortz, Discrete, Cationic Palladium(II)-Oxo Clusters via f-Metal Ion Incorporation and their Macrocyclic Host-Guest Interactions with Sulfonatocalixarenes, *Angew. Chem., Int. Ed.*, 2022, **61**, e202203114.
34 W. Huang, Q. Liu, W. Chen, M. Feng and Z. Zheng, Recent Advances in the Catalytic Applications of Lanthanide-Oxo Clusters, *Magnetochemistry*, 2021, **7**, 161.
35 C. J. Reed and T. Agapie, A Terminal Fe^{III}–Oxo in a Tetranuclear Cluster: Effects of Distal Metal Centers on Structure and Reactivity, *J. Am. Chem. Soc.*, 2019, **141**, 9479–9484.
36 W. Wang, L. B. Fullmer, N. A. G. Bandeira, S. Goberna-Ferrón, L. N. Zakharov, C. Bo, D. A. Keszler and M. Nyman, Crystallizing Elusive Chromium Polycations, *Chem*, 2016, **1**, 887–901.
37 G. Kickelbick and U. Schubert, Oxozirconium Methacrylate Clusters: $Zr_6(OH)_4O_4(OMc)_{12}$ and $Zr_4O_2(OMc)_{12}$ (OMc = Methacrylate), *Chem. Ber.*, 1997, **130**, 473–478.
38 S. Øien-Ødegaard, C. Bazioti, E. A. Redekop, Ø. Prytz, K. P. Lillerud and U. Olsbye, A Toroidal Zr_{70} Oxysulfate Cluster and Its Diverse Packing Structures, *Angew. Chem., Int. Ed.*, 2020, **59**, 21397–21402.

39 Y. Bai, Y. Dou, L.-H. Xie, W. Rutledge, J.-R. Li and H.-C. Zhou, Zr-based metal–organic frameworks: design, synthesis, structure, and applications, *Chem. Soc. Rev.*, 2016, **45**, 2327–2367.
40 Z. Hu, Y. Wang and D. Zhao, The chemistry and applications of hafnium and cerium(IV) metal–organic frameworks, *Chem. Soc. Rev.*, 2021, **50**, 4629–4683.
41 H. Assi, G. Mouchaham, N. Steunou, T. Devic and C. Serre, Titanium coordination compounds: from discrete metal complexes to metal–organic frameworks, *Chem. Soc. Rev.*, 2017, **46**, 3431–3452.
42 U. Schubert, Clusters with a Zr_6O_8 core, *Coord. Chem. Rev.*, 2022, **469**, 214686.
43 F. Luo, X. Liang, W. Chen, S. Wang, X. Gao, Z. Zhang and Y. Fang, High-efficient and scalable solar-driven MOF-based water collection unit: From module design to concrete implementation, *Chem. Eng. J.*, 2023, **465**, 142891.
44 S. Li, Z. Zhou, Z. Tie, B. Wang, M. Ye, L. Du, R. Cui, W. Liu, C. Wan, Q. Liu, S. Zhao, Q. Wang, Y. Zhang, S. Zhang, H. Zhang, Y. Du and H. Wei, Data-informed discovery of hydrolytic nanozymes, *Nat. Commun.*, 2022, **13**, 827.
45 X. Huang, S. Zhang, Y. Tang, X. Zhang, Y. Bai and H. Pang, Advances in metal–organic framework-based nanozymes and their applications, *Coord. Chem. Rev.*, 2021, **449**, 214216.
46 H.-S. Wang, Metal–organic frameworks for biosensing and bioimaging applications, *Coord. Chem. Rev.*, 2017, **349**, 139–155.
47 P. Mialane, C. Mellot-Draznieks, P. Gairola, M. Duguet, Y. Benseghir, O. Oms and A. Dolbecq, Heterogenisation of polyoxometalates and other metal-based complexes in metal-organic frameworks: From synthesis to characterisation and applications in catalysis, *Chem. Soc. Rev.*, 2021, **50**, 6152–6220.
48 F.-J. Ma, S.-X. Liu, C.-Y. Sun, D.-D. Liang, G.-J. Ren, F. Wei, Y.-G. Chen and Z.-M. Su, A Sodalite-Type Porous Metal–Organic Framework with Polyoxometalate Templates: Adsorption and Decomposition of Dimethyl Methylphosphonate, *J. Am. Chem. Soc.*, 2011, **133**, 4178–4181.
49 L. Wang, W. Zhi, J. Wan, J. Han, C. Li and Y. Wang, Recyclable β-Glucosidase by One-Pot Encapsulation with Cu-MOFs for Enhanced Hydrolysis of Cellulose to Glucose, *ACS Sustainable Chem. Eng.*, 2019, **7**, 3339–3348.
50 A. Bavykina, N. Kolobov, I. S. Khan, J. A. Bau, A. Ramirez and J. Gascon, Metal–Organic Frameworks in Heterogeneous Catalysis: Recent Progress, New Trends, and Future Perspectives, *Chem. Rev.*, 2020, **120**, 8468–8535.
51 A. Dhakshinamoorthy, Z. Li and H. Garcia, Catalysis and photocatalysis by metal organic frameworks, *Chem. Soc. Rev.*, 2018, **47**, 8134–8172.
52 L. Jiao, Y. Wang, H.-L. Jiang and Q. Xu, Metal-Organic Frameworks as Platforms for Catalytic Applications, *Adv. Mater.*, 2018, **30**, 1703663.
53 M. Aureliano, N. I. Gumerova, G. Sciortino, E. Garribba, A. Rompel and D. C. Crans, Polyoxovanadates with emerging biomedical activities, *Coord. Chem. Rev.*, 2021, **447**, 214143.
54 G. Awasthi, S. Shivgotra, S. Nikhar, S. Sundarrajan, S. Ramakrishna and P. Kumar, Progressive Trends on the Biomedical Applications of Metal Organic Frameworks, *Polymers*, 2022, **14**, 4710.
55 H.-S. Wang, Y.-H. Wang and Y. Ding, Development of biological metal–organic frameworks designed for biomedical applications: from bio-sensing/bio-imaging to disease treatment, *Nanoscale Adv.*, 2020, **2**, 3788–3797.
56 A. Bijelic, M. Aureliano and A. Rompel, The antibacterial activity of polyoxometalates: structures, antibiotic effects and future perspectives, *Chem. Commun.*, 2018, **54**, 1153–1169.
57 A. Bijelic, M. Aureliano and A. Rompel, Polyoxometalates as Potential Next-Generation Metallodrugs in the Combat Against Cancer, *Angew. Chem., Int. Ed.*, 2019, **58**, 2980–2999.
58 D. E. Salazar Marcano, N. D. Savić, S. A. M. Abdelhameed, F. de Azambuja and T. N. Parac-Vogt, Exploring the Reactivity of Polyoxometalates toward Proteins: From Interactions to Mechanistic Insights, *JACS Au*, 2023, **3**, 978–990.
59 C. Simms, A. Mullaliu, S. Swinnen, F. de Azambuja and T. N. Parac-Vogt, MOF catalysis meets biochemistry: molecular insights from the hydrolytic activity of MOFs towards biomolecules, *Mol. Syst. Des. Eng.*, 2023, **8**, 270–288.
60 A. Radzicka and R. Wolfenden, Rates of Uncatalyzed Peptide Bond Hydrolysis in Neutral Solution and the Transition State Affinities of Proteases, *J. Am. Chem. Soc.*, 1996, **118**, 6105–6109.
61 H. Molina, D. M. Horn, N. Tang, S. Mathivanan and A. Pandey, Global proteomic profiling of phosphopeptides using electron transfer dissociation tandem mass spectrometry, *Proc. Natl. Acad. Sci. U. S. A.*, 2007, **104**, 2199–2204.
62 B. Meyer, D. G. Papasotiriou and M. Karas, 100% protein sequence coverage: a modern form of surrealism in proteomics, *Amino Acids*, 2011, **41**, 291–310.
63 D. L. Swaney, C. D. Wenger and J. J. Coon, Value of using multiple proteases for large-scale mass spectrometry-based proteomics, *J. Proteome Res.*, 2010, **9**, 1323–1329.
64 J. J. Hlavaty, J. S. Benner, L. J. Hornstra and I. Schildkraut, Identification of the metal-binding sites of restriction endonucleases by Fe2+-mediated oxidative cleavage, *Biochemistry*, 2000, **39**, 3097–3105.
65 N. B. Grodsky, S. Soundar and R. F. Colman, Evaluation by site-directed mutagenesis of aspartic acid residues in the metal site of pig heart NADP-dependent isocitrate dehydrogenase, *Biochemistry*, 2000, **39**, 2193–2200.
66 X. Cheng, S. Shaltiel and S. S. Taylor, Mapping Substrate-Induced Conformational Changes in cAMP-Dependent Protein Kinase by Protein Footprinting, *Biochemistry*, 1998, **37**, 14005–14013.
67 J. Suh and W. S. Chei, Metal complexes as artificial proteases: toward catalytic drugs, *Curr. Opin. Chem. Biol.*, 2008, **12**, 207–213.
68 M. R. Ermácora, J. M. Delfino, B. Cuenoud, A. Schepartz and R. O. Fox, Conformation-dependent cleavage of staphylococcal nuclease with a disulfide-linked iron chelate, *Proc. Natl. Acad. Sci. U. S. A.*, 1992, **89**, 6383–6387.

69 P. Giansanti, L. Tsiatsiani, T. Y. Low and A. J. R. Heck, Six alternative proteases for mass spectrometry-based proteomics beyond trypsin, *Nat. Protoc.*, 2016, **11**, 993–1006.
70 H. G. T. Ly, G. Absillis, R. Janssens, P. Proost and T. N. Parac-Vogt, Highly Amino Acid Selective Hydrolysis of Myoglobin at Aspartate Residues as Promoted by Zirconium(IV)-Substituted Polyoxometalates, *Angew. Chem., Int. Ed.*, 2015, **54**, 7391–7394.
71 N. E. Wezynfeld, T. Frączyk and W. Bal, Metal assisted peptide bond hydrolysis: Chemistry, biotechnology and toxicological implications, *Coord. Chem. Rev.*, 2016, **327–328**, 166–187.
72 T. N. Parac and N. M. Kostić, Regioselective Cleavage by a Palladium(II) Aqua Complex of a Polypeptide in Different Overall Conformations, *Inorg. Chem.*, 1998, **37**, 2141–2144.
73 T. N. Parac, G. M. Ullmann and N. M. Kostić, New Regioselectivity in the Cleavage of Histidine-Containing Peptides by Palladium(II) Complexes Studied by Kinetic Experiments and Molecular Dynamics Simulations, *J. Am. Chem. Soc.*, 1999, **121**, 3127–3135.
74 R. Gao, L. Xu, M. Sun, M. Xu, C. Hao, X. Guo, F. M. Colombari, X. Zheng, P. Král, A. F. de Moura, C. Xu, J. Yang, N. A. Kotov and H. Kuang, Site-selective proteolytic cleavage of plant viruses by photoactive chiral nanoparticles, *Nat. Catal.*, 2022, **5**, 694–707.
75 P. H. Ho, K. Stroobants and T. N. Parac-Vogt, Hydrolysis of serine-containing peptides at neutral pH promoted by $[MoO_4]^{2-}$ oxyanion, *Inorg. Chem.*, 2011, **50**, 12025–12033.
76 P. H. Ho, T. Mihaylov, K. Pierloot and T. N. Parac-Vogt, Hydrolytic activity of vanadate toward serine-containing peptides studied by kinetic experiments and DFT theory, *Inorg. Chem.*, 2012, **51**, 8848–8859.
77 N. I. Gumerova and A. Rompel, Polyoxometalates in solution: speciation under spotlight, *Chem. Soc. Rev.*, 2020, **49**, 7568–7601.
78 K. Stroobants, P. H. Ho, E. Moelants, P. Proost and T. N. Parac-Vogt, Selective hydrolysis of hen egg white lysozyme at Asp-X peptide bonds promoted by oxomolybdate, *J. Inorg. Biochem.*, 2014, **136**, 73–80.
79 S. Vanhaecht, G. Absillis and T. N. Parac-Vogt, Amino acid side chain induced selectivity in the hydrolysis of peptides catalyzed by a Zr(IV)-substituted Wells–Dawson type polyoxometalate, *Dalton Trans.*, 2013, **42**, 15437–15446.
80 G. Absillis and T. N. Parac-Vogt, Peptide Bond Hydrolysis Catalyzed by the Wells–Dawson $Zr(\alpha_2\text{-}P_2W_{17}O_{61})_2$ Polyoxometalate, *Inorg. Chem.*, 2012, **51**, 9902–9910.
81 H. G. T. Ly, T. Mihaylov, G. Absillis, K. Pierloot and T. N. Parac-Vogt, Reactivity of Dimeric Tetrazirconium(IV) Wells–Dawson Polyoxometalate toward Dipeptide Hydrolysis Studied by a Combined Experimental and Density Functional Theory Approach, *Inorg. Chem.*, 2015, **54**, 11477–11492.
82 H. G. T. Ly, G. Absillis and T. N. Parac-Vogt, Comparative study of the reactivity of zirconium(IV)-substituted polyoxometalates towards the hydrolysis of oligopeptides, *Eur. J. Inorg. Chem.*, 2015, 2206–2215.
83 H. G. T. Ly, G. Absillis and T. N. Parac-Vogt, Amide bond hydrolysis in peptides and cyclic peptides catalyzed by a dimeric Zr(IV)-substituted Keggin type polyoxometalate, *Dalton Trans.*, 2013, **42**, 10929–10938.
84 H. G. T. Ly, G. Absillis and T. N. Parac-Vogt, Influence of the amino acid side chain on peptide bond hydrolysis catalyzed by a dimeric Zr(IV)-substituted Keggin type polyoxometalate, *New J. Chem.*, 2016, **40**, 976–984.
85 K. Stroobants, E. Moelants, H. G. T. Ly, P. Proost, K. Bartik and T. N. Parac-Vogt, Polyoxometalates as a novel class of artificial proteases: Selective hydrolysis of lysozyme under physiological pH and temperature promoted by a cerium(IV) Keggin-type polyoxometalate, *Chem. – Eur. J.*, 2013, **19**, 2848–2858.
86 H. G. T. Ly, G. Absillis, S. R. Bajpe, J. A. Martens and T. N. Parac-Vogt, Hydrolysis of dipeptides catalyzed by a zirconium(IV)-substituted Lindqvist type polyoxometalate, *Eur. J. Inorg. Chem.*, 2013, 4601–4611.
87 T. T. Mihaylov, H. G. T. Ly, K. Pierloot and T. N. Parac-Vogt, Molecular insight from DFT computations and kinetic measurements into the steric factors influencing peptide bond hydrolysis catalyzed by a dimeric Zr(IV)-substituted Keggin type polyoxometalate, *Inorg. Chem.*, 2016, **55**, 9316–9328.
88 K. Stroobants, G. Absillis, E. Moelants, P. Proost and T. N. Parac-Vogt, Regioselective hydrolysis of human serum albumin by Zr^{IV}-substituted polyoxotungstates at the interface of positively charged protein surface patches and negatively charged amino acid residues, *Chem. – Eur. J.*, 2014, **20**, 3894–3897.
89 K. Stroobants, G. Absillis, P. S. Shestakova, R. Willem and T. N. Parac-Vogt, Hydrolysis of Tetraglycine by a Zr(IV)-Substituted Wells–Dawson Polyoxotungstate Studied by Diffusion Ordered NMR Spectroscopy, *J. Cluster Sci.*, 2014, **25**, 855–866.
90 A. Sap, G. Absillis and T. N. Parac-Vogt, Selective hydrolysis of oxidized insulin chain B by a Zr(IV)-substituted Wells–Dawson polyoxometalate, *Dalton Trans.*, 2015, **44**, 1539–1548.
91 P. J. Boersema, A. Kahraman and P. Picotti, Proteomics beyond large-scale protein expression analysis, *Curr. Opin. Biotechnol*, 2015, **34**, 162–170.
92 K. Chandramouli and P.-Y. Qian, Proteomics: Challenges, Techniques and Possibilities to Overcome Biological Sample Complexity, *Hum. Genomics Proteomics*, 2009, **2009**, 239204.
93 S. A. M. Abdelhameed, H. G. T. Ly, J. Moons, F. de Azambuja, P. Proost and T. N. Parac-Vogt, Expanding the reactivity of inorganic clusters towards proteins: The interplay between the redox and hydrolytic activity of Ce(IV)-substituted polyoxometalates as artificial proteases, *Chem. Sci.*, 2021, **12**, 10655–10663.
94 J. Moons, L. S. Van Rompuy, A. Rodriguez, S. A. M. Abdelhameed, W. Simons and T. N. Parac-Vogt, Hydrolysis of transferrin promoted by a cerium(IV)-Keggin polyoxometalate, *Polyhedron*, 2019, **170**, 570–575.
95 A. Sap, L. Van Tichelen, A. Mortier, P. Proost and T. N. Parac-Vogt, Tuning the selectivity and reactivity of metal-substituted polyoxometalates as artificial proteases

by varying the nature of the embedded Lewis acid metal ion, *Eur. J. Inorg. Chem.*, 2016, 5098–5105.

96 L. Vandebroek, E. De Zitter, H. G. T. Ly, D. Conić, T. Mihaylov, A. Sap, P. Proost, K. Pierloot, L. Van Meervelt and T. N. Parac-Vogt, Protein-assisted formation and stabilization of catalytically active polyoxometalate species, *Chem. – Eur. J.*, 2018, **24**, 10099–10108.

97 H. G. T. Ly, T. T. Mihaylov, P. Proost, K. Pierloot, J. N. Harvey and T. N. Parac-Vogt, Chemical mimics of aspartate-directed proteases: predictive and strictly specific hydrolysis of a globular protein at asp-*x* sequence promoted by polyoxometalate complexes rationalized by a combined experimental and theoretical approach, *Chem. – Eur. J.*, 2019, **25**, 14370–14381.

98 A. V. Anyushin, A. Sap, T. Quanten, P. Proost and T. N. Parac-Vogt, Selective Hydrolysis of Ovalbumin Promoted by Hf(IV)-Substituted Wells–Dawson-Type Polyoxometalate, *Front. Chem.*, 2018, **6**, 614.

99 L. S. Van Rompuy, N. D. Savić, A. Rodriguez and T. N. Parac-Vogt, Selective Hydrolysis of Transferrin Promoted by Zr-Substituted Polyoxometalates, *Molecules*, 2020, **25**, 3472.

100 A. Cristobal, F. Marino, H. Post, H. W. P. Van Den Toorn, S. Mohammed and A. J. R. Heck, Toward an Optimized Workflow for Middle-Down Proteomics, *Anal. Chem.*, 2017, **89**, 3318–3325.

101 L. Tsiatsiani and A. J. R. Heck, Proteomics beyond trypsin, *FEBS J.*, 2015, **282**, 2612–2626.

102 A. Sap, E. Dezitter, L. Vanmeervelt and T. N. Parac-Vogt, Structural Characterization of the Complex between Hen Egg-White Lysozyme and Zr^{IV}-Substituted Keggin Polyoxometalate as Artificial Protease, *Chem. – Eur. J.*, 2015, **21**, 11692–11695.

103 L. Vandebroek, Y. Mampaey, S. Antonyuk, L. Van Meervelt and T. N. Parac-Vogt, Noncovalent Complexes Formed between Metal-Substituted Polyoxometalates and Hen Egg White Lysozyme, *Eur. J. Inorg. Chem.*, 2019, 506–511.

104 V. Goovaerts, K. Stroobants, G. Absillis and T. N. Parac-Vogt, Molecular interactions between serum albumin proteins and Keggin type polyoxometalates studied using luminescence spectroscopy, *Phys. Chem. Chem. Phys.*, 2013, **15**, 18378–18387.

105 H. G. T. Ly and T. N. Parac-Vogt, Spectroscopic Study of the Interaction between Horse Heart Myoglobin and Zirconium(IV)-Substituted Polyoxometalates as Artificial Proteases, *ChemPhysChem*, 2017, **18**, 2451–2458.

106 K. Stroobants, V. Goovaerts, G. Absillis, G. Bruylants, E. Moelants, P. Proost and T. N. Parac-Vogt, Molecular origin of the hydrolytic activity and fixed regioselectivity of a Zr^{IV}-substituted polyoxotungstate as artificial protease, *Chem. – Eur. J.*, 2014, **20**, 9567–9577.

107 V. Goovaerts, K. Stroobants, G. Absillis and T. N. Parac-Vogt, Eu(III) luminescence and tryptophan fluorescence spectroscopy as a tool for understanding interactions between hen egg white lysozyme and metal-substituted Keggin type polyoxometalates, *J. Inorg. Biochem.*, 2015, **150**, 72–80.

108 V. Goovaerts, K. Stroobants, G. Absillis and T. N. Parac-Vogt, Understanding the regioselective hydrolysis of human serum albumin by Zr(IV)-substituted polyoxotungstates using tryptophan fluorescence spectroscopy, *Inorganics*, 2015, **3**, 230–245.

109 K. Stroobants, D. Saadallah, G. Bruylants and T. N. Parac-Vogt, Thermodynamic study of the interaction between hen egg white lysozyme and Ce(IV)-Keggin polyoxotungstate as artificial protease, *Phys. Chem. Chem. Phys.*, 2014, **16**, 21778–21787.

110 M. Aureliano, N. I. Gumerova, G. Sciortino, E. Garribba, C. C. McLauchlan, A. Rompel and D. C. Crans, Polyoxidovanadates' interactions with proteins: An overview, *Coord. Chem. Rev.*, 2022, **454**, 214344.

111 S. Lentink, D. E. Salazar Marcano, M. A. Moussawi and T. N. Parac-Vogt, Exploiting Interactions between Polyoxometalates and Proteins for Applications in (Bio)chemistry and Medicine, *Angew. Chem., Int. Ed.*, 2023, e202303817.

112 L. Vandebroek, L. Van Meervelt and T. N. Parac-Vogt, Direct observation of the Zr^{IV} interaction with the carboxamide bond in a noncovalent complex between Hen Egg White Lysozyme and a Zr-substituted Keggin polyoxometalate, *Acta Crystallogr., Sect. C: Struct. Chem.*, 2018, **74**, 1348–1354.

113 S. Lentink, D. E. Salazar Marcano, M. A. Moussawi, L. Vandebroek, L. Van Meervelt and T. N. Parac-Vogt, Fine-tuning non-covalent interactions between hybrid metal–oxo clusters and proteins, *Faraday Discuss.*, 2023, **244**, 21–38.

114 A. Sap, L. Vandebroek, V. Goovaerts, E. Martens, P. Proost and T. N. Parac-Vogt, Highly Selective and Tunable Protein Hydrolysis by a Polyoxometalate Complex in Surfactant Solutions: A Step toward the Development of Artificial Metalloproteases for Membrane Proteins, *ACS Omega*, 2017, **2**, 2026–2033.

115 N. D. Savić, D. E. Salazar Marcano, T. Quanten and T. N. Parac-Vogt, Broadening the Scope of Polyoxometalates as Artificial Proteases in Surfactant Solutions: Hydrolysis of Ovalbumin by Zr(IV)-Substituted Keggin Complex, *Inorganics*, 2021, **9**, 22.

116 T. Quanten, T. De Mayaer, P. Shestakova and T. N. Parac-Vogt, Selectivity and Reactivity of Zr^{IV} and Ce^{IV} Substituted Keggin Type Polyoxometalates Toward Cytochrome *c* in Surfactant Solutions, *Front. Chem.*, 2018, **6**, 372.

117 N. D. Savić, D. E. Salazar Marcano, S. Swinnen, A. Mullaliu and T. N. Parac-Vogt, Self-Assembled Protein-Surfactant Nanoaggregates for Tunable Peptide Bond Hydrolysis by Polyoxometalate Nanoclusters, *ACS Appl. Nano Mater.*, 2022, **5**, 17159–17172.

118 J. Moons, F. de Azambuja, J. Mihailovic, K. Kozma, K. Smiljanic, M. Amiri, T. Cirkovic Velickovic, M. Nyman and T. N. Parac-Vogt, Discrete Hf18 Metal–oxo Cluster as a Heterogeneous Nanozyme for Site-Specific Proteolysis, *Angew. Chem., Int. Ed.*, 2020, 59, 9094–9101.

119 D. L. Collins-Wildman, M. Kim, K. P. Sullivan, A. M. Plonka, A. I. Frenkel, D. G. Musaev and C. L. Hill, Buffer-Induced

Acceleration and Inhibition in Polyoxometalate-Catalyzed Organophosphorus Ester Hydrolysis, *ACS Catal.*, 2018, **8**, 7068–7076.

120 T. Quanten, N. D. Savić and T. N. Parac-Vogt, Hydrolysis of Peptide Bonds in Protein Micelles Promoted by a Zirconium(IV)-Substituted Polyoxometalate as an Artificial Protease, *Chem. – Eur. J.*, 2020, **26**, 11170–11179.

121 T. Quanten, P. Shestakova, D. Van Den Bulck, C. Kirschhock and T. N. Parac-Vogt, Interaction Study and Reactivity of Zr^{IV}-Substituted Wells–Dawson Polyoxometalate towards Hydrolysis of Peptide Bonds in Surfactant Solutions, *Chem. – Eur. J.*, 2016, **22**, 3775–3784.

122 N. D. Savić, D. E. Salazar Marcano and T. N. Parac-Vogt, Expanding the Scope of Polyoxometalates as Artificial Proteases towards Hydrolysis of Insoluble Proteins, *Chem. – Eur. J.*, 2022, **28**, e202104224.

123 T. Quanten, P. Shestakova, A. Kondinski and T. N. Parac-Vogt, Effect of $[Zr(\alpha\text{-}PW_{11}O_{39})_2]^{10-}$ polyoxometalate on the self-assembly of surfactant molecules in water studied by fluorescence and DOSY NMR spectroscopy, *Inorganics*, 2018, **6**, 112.

124 V. R. Pattabiraman and J. W. Bode, Rethinking amide bond synthesis, *Nature*, 2011, 480, 471–479.

125 M. T. Sabatini, L. T. Boulton, H. F. Sneddon and T. D. Sheppard, A green chemistry perspective on catalytic amide bond formation, *Nat. Catal.*, 2019, **2**, 10–17.

126 F. de Azambuja and T. N. Parac-Vogt, Water-Tolerant and Atom Economical Amide Bond Formation by Metal-Substituted Polyoxometalate Catalysts, *ACS Catal.*, 2019, **9**, 10245–10252.

127 Y. Zhang, F. de Azambuja and T. N. Parac-Vogt, Zirconium oxo clusters as discrete molecular catalysts for the direct amide bond formation, *Catal. Sci. Technol.*, 2022, **12**, 3190–3201.

128 Y. Zhang, I. Y. Kokculer, F. de Azambuja and T. N. Parac-Vogt, Dynamic environment at the Zr6 oxo cluster surface is key for the catalytic formation of amide bonds, *Catal. Sci. Technol.*, 2022, **13**, 100–110.

129 F. de Azambuja, J. Lenie and T. N. Parac-Vogt, Homogeneous Metal Catalysts with Inorganic Ligands: Probing Ligand Effects in Lewis Acid Catalyzed Direct Amide Bond Formation, *ACS Catal.*, 2021, **11**, 271–277.

130 S. A. M. Abdelhameed, F. de Azambuja, T. Vasović, N. D. Savić, T. Ćirković Veličković and T. N. Parac-Vogt, Regioselective protein oxidative cleavage enabled by enzyme-like recognition of an inorganic metal oxo cluster ligand, *Nat. Commun.*, 2023, **14**, 486.

131 D. Pramanik, C. Ghosh and S. G. Dey, Heme–Cu bound Aβ peptides: spectroscopic characterization, reactivity, and relevance to Alzheimer's Disease, *J. Am. Chem. Soc.*, 2011, **133**, 15545–15552.

132 V. Sosa, T. Moliné, R. Somoza, R. Paciucci, H. Kondoh and M. E. LLeonart, Oxidative stress and cancer: an overview, *Ageing Res. Rev.*, 2013, **12**, 376–390.

133 S. Reuter, S. C. Gupta, M. M. Chaturvedi and B. B. Aggarwal, Oxidative stress, inflammation, and cancer: How are they linked?, *Free Radical Biol. Med.*, 2010, **49**, 1603–1616.

134 S. Ramos, R. O. Duarte, J. J. G. Moura and M. Aureliano, Decavanadate interactions with actin: Cysteine oxidation and vanadyl formation, *Dalton Trans.*, 2009, 7985–7994.

135 G. Fraqueza, L. A. E. Batista de Carvalho, M. P. M. Marques, L. Maia, C. A. Ohlin, W. H. Casey and M. Aureliano, Decavanadate, decaniobate, tungstate and molybdate interactions with sarcoplasmic reticulum Ca^{2+}-ATPase: quercetin prevents cysteine oxidation by vanadate but does not reverse ATPase inhibition, *Dalton Trans.*, 2012, **41**, 12749–12758.

136 S. Ramos, M. Manuel, T. Tiago, R. Duarte, J. Martins, C. Gutiérrez-Merino, J. J. G. Moura and M. Aureliano, Decavanadate interactions with actin: Inhibition of G-actin polymerization and stabilization of decameric vanadate, *J. Inorg. Biochem.*, 2006, **100**, 1734–1743.

137 S. A. M. Abdelhameed, L. Vandebroek, F. de Azambuja and T. N. Parac-Vogt, Redox Activity of Ce(IV)-Substituted Polyoxometalates toward Amino Acids and Peptides, *Inorg. Chem.*, 2020, **59**, 10569–10577.

138 S. Hua, G. Inesi and C. Toyoshima, Distinct Topologies of Mono- and Decavanadate Binding and Photo-oxidative Cleavage in the Sarcoplasmic Reticulum ATPase, *J. Biol. Chem.*, 2000, **275**, 30546–30550.

139 D. A. Butterfield and M. Perluigi, Redox Proteomics: A Key Tool for New Insights into Protein Modification with Relevance to Disease, *Antioxid. Redox Signaling*, 2017, **26**, 277–279.

140 A. Radzicka and R. Wolfenden, A Proficient Enzyme, *Science*, 1995, **267**, 90–93.

141 W. W. Cleland and A. C. Hengge, Enzymatic Mechanisms of Phosphate and Sulfate Transfer, *Chem. Rev.*, 2006, **106**, 3252–3278.

142 M. M. Aboelnga and S. D. Wetmore, Unveiling a Single-Metal-Mediated Phosphodiester Bond Cleavage Mechanism for Nucleic Acids: A Multiscale Computational Investigation of a Human DNA Repair Enzyme, *J. Am. Chem. Soc.*, 2019, **141**, 8646–8656.

143 T. K. N. Luong, G. Absillis, P. Shestakova and T. N. Parac-Vogt, Solution Speciation of the Dinuclear Zr^{IV}-substituted Keggin Polyoxometalate $[\{\alpha\text{-}PW_{11}O_{39}Zr(\mu\text{-}OH)(H_2O)\}_2]^{8-}$ and Its Reactivity towards DNA-Model Phosphodiester Hydrolysis, *Eur. J. Inorg. Chem.*, 2014, 5276–5284.

144 T. K. N. Luong, P. Shestakova, G. Absillis and T. N. Parac-Vogt, Detailed Mechanism of Phosphoanhydride Bond Hydrolysis Promoted by a Binuclear Zr^{IV}-Substituted Keggin Polyoxometalate Elucidated by a Combination of ^{31}P, ^{31}P DOSY, and ^{31}P EXSY NMR Spectroscopy, *Inorg. Chem.*, 2016, **55**, 4864–4873.

145 Z. Yu and J. Cowan, Metal complexes promoting catalytic cleavage of nucleic acids—biochemical tools and therapeutics, *Curr. Opin. Chem. Biol.*, 2018, **43**, 37–42.

146 T. Yamase, Anti-tumor, -viral, and -bacterial activities of polyoxometalates for realizing an inorganic drug, *J. Mater. Chem.*, 2005, **15**, 4773–4782.

147 M. Cindrić, T. K. Novak, S. Kraljević, M. Kralj and B. Kamenar, Structural and antitumor activity study of

γ-octamolybdates containing aminoacids and peptides, *Inorg. Chim. Acta*, 2006, **359**, 1673–1680.

148 B. Hasenknopf, Polyoxometalates: introduction to a class of inorganic compounds and their biomedical applications, *Front. Biosci., Landmark Ed.*, 2005, **10**, 275–287.

149 J. T. Rhule, C. L. Hill, D. A. Judd and R. F. Schinazi, Polyoxometalates in Medicine, *Chem. Rev.*, 1998, **98**, 327–358.

150 A. Ogata, S. Mitsui, H. Yanagie, H. Kasano, T. Hisa, T. Yamase and M. Eriguchi, A novel anti-tumor agent, polyoxomolybdate induces apoptotic cell death in AsPC-1 human pancreatic cancer cells, *Biomed. Pharmacother.*, 2005, **59**, 240–244.

151 G. Absillis, E. Cartuyvels, R. Van Deun and T. N. Parac-Vogt, Hydrolytic Cleavage of an RNA-Model Phosphodiester Catalyzed by a Highly Negatively Charged Polyoxomolybdate $[Mo_7O_{24}]_6^-$ Cluster, *J. Am. Chem. Soc.*, 2008, **130**, 17400–17408.

152 L. Van Lokeren, E. Cartuyvels, G. Absillis, R. Willem and T. N. Parac-Vogt, Phosphoesterase activity of polyoxomolybdates: Diffusion ordered NMR spectroscopy as a tool for obtaining insights into the reactivity of polyoxometalate clusters, *Chem. Commun.*, 2008, 2774–2776.

153 G. Absillis, R. Van Deun and T. N. Parac-Vogt, Polyoxomolybdate Promoted Hydrolysis of a DNA-Model Phosphoester Studied by NMR and EXAFS Spectroscopy, *Inorg. Chem.*, 2011, **50**, 11552–11560.

154 A. Ogata, H. Yanagie, E. Ishikawa, Y. Morishita, S. Mitsui, A. Yamashita, K. Hasumi, S. Takamoto, T. Yamase and M. Eriguchi, Antitumour effect of polyoxomolybdates: Induction of apoptotic cell death and autophagy in in vitro and in vivo models, *Br. J. Cancer*, 2008, **98**, 399–409.

155 A. Kolesarova, M. Capcarova, A. V. Sirotkin, M. Medvedova, A. Kalafova, T. Filipejova and J. Kovacik, In vitro assessment of molybdenum-induced secretory activity, proliferation and apoptosis of porcine ovarian granulosa cells, *J. Environ. Sci. Health, Part A: Toxic/Hazard. Subst. Environ. Eng.*, 2011, **46**, 170–175.

156 H. Yanagie, A. Ogata, S. Mitsui, T. Hisa, T. Yamase and M. Eriguchi, *Biomed. Pharmacother.*, 2006, **60**, 349–352.

157 E. Cartuyvels, G. Absillis and T. N. Parac-Vogt, Questioning the paradigm of metal complex promoted phosphodiester hydrolysis: $[Mo_7O_{24}]^{6-}$ polyoxometalate cluster as an unlikely catalyst for the hydrolysis of a DNA model substrate, *Chem. Commun.*, 2008, 85–87.

158 F. F. Martins, Á. Sánchez-González, J. Lanuza, H. N. Miras, X. Lopez, N. A. Bandeira and A. Gil, Probing the Catalytically Active Species in POM-Catalysed DNA-Model Hydrolysis, *Chem. – Eur. J.*, 2021, **27**, 8977–8984.

159 N. Steens, A. M. Ramadan and T. N. Parac-Vogt, When structural and electronic analogy leads to reactivity: the unprecedented phosphodiesterase activity of vanadates, *Chem. Commun.*, 2009, 965–967.

160 N. Steens, A. M. Ramadan, G. Absillis and T. N. Parac-Vogt, Hydrolytic cleavage of DNA-model substrates promoted by polyoxovanadates, *Dalton Trans.*, 2010, **39**, 585–592.

161 S. Vanhaecht, G. Absillis and T. N. Parac-Vogt, Hydrolysis of DNA model substrates catalyzed by metal-substituted Wells–Dawson polyoxometalates, *Dalton Trans.*, 2012, **41**, 10028–10034.

162 E. Ishikawa and T. Yamase, ^{31}P NMR and isothermal titration calorimetry studies on polyoxomolybdates-catalyzed hydrolysis of ATP, *J. Inorg. Biochem.*, 2006, **100**, 344–350.

163 E. Cartuyvels, K. Van Hecke, L. Van Meervelt, C. Görller-Walrand and T. N. Parac-Vogt, Structural characterization and reactivity of γ-octamolybdate functionalized by proline, *J. Inorg. Biochem.*, 2008, **102**, 1589–1598.

164 E. Ishikawa and T. Yamase, Catalytic Hydrolysis of Adenosine Triphosphate (ATP) by Antitumoral ε-Keggin Core Compound, $[H_2Mo^V_{12}O_{28}(OH)_{12}(Mo^{VI}O_3)_4]^{6-}$, at pH 5 and 7.5, *Eur. J. Inorg. Chem.*, 2013, 1917–1925.

165 F. de Azambuja, N. Steens and T. N. Parac-Vogt, Kinetic and Interaction Studies of Adenosine-5′-Triphosphate (ATP) Hydrolysis with Polyoxovanadates, *Metals*, 2021, **11**, 1678.

166 T. K. N. Luong, P. Shestakova and T. N. Parac-Vogt, Kinetic studies of phosphoester hydrolysis promoted by a dimeric tetrazirconium(IV) Wells–Dawson polyoxometalate, *Dalton Trans.*, 2016, **45**, 12174–12180.

167 B. Kandasamy, S. Vanhaecht, F. M. Nkala, T. Beelen, B. S. Bassil, T. N. Parac-Vogt and U. Kortz, Gallium(III)-Containing, Sandwich-Type Heteropolytungstates: Synthesis, Solution Characterization, and Hydrolytic Studies toward Phosphoester and Phosphoanhydride Bond Cleavage, *Inorg. Chem.*, 2016, **55**, 9204–9211.

168 T. K. N. Luong, G. Absillis, P. Shestakova and T. N. Parac-Vogt, Hydrolysis of the RNA model substrate catalyzed by a binuclear Zr^{IV}-substituted Keggin polyoxometalate, *Dalton Trans.*, 2015, **44**, 15690–15696.

169 T. K. N. Luong, T. T. Mihaylov, G. Absillis, P. Shestakova, K. Pierloot and T. N. Parac-Vogt, Phosphate Ester Bond Hydrolysis Promoted by Lanthanide-Substituted Keggin-type Polyoxometalates Studied by a Combined Experimental and Density Functional Theory Approach, *Inorg. Chem.*, 2016, **55**, 9898–9911.

170 T. K. N. Luong, I. Govaerts, J. Robben, P. Shestakova and T. N. Parac-Vogt, Polyoxometalates as artificial nucleases: hydrolytic cleavage of DNA promoted by a highly negatively charged Zr^{IV}-substituted Keggin polyanion, *Chem. Commun.*, 2017, **53**, 617–620.

171 X. Wang, J. Liu, J. Li, Y. Yang, J. Liu, B. Li and M. T. Pope, Synthesis and antitumor activity of cyclopentadienyltitanium substituted polyoxotungstate $[CoW_{11}O_{39}(CpTi)]^{7-}$ ($Cp=\eta_5$-C_5H_5), *J. Inorg. Biochem.*, 2003, **94**, 279–284.

172 T. Enomoto, S. Tanuma and M. A. Yamada, ATP requirement for the processes of DNA replication in isolated HeLa cell nuclei, *J. Biochem.*, 1981, **89**, 801–807.

173 X. Lu, J. Errington, V. J. Chen, N. J. Curtin, A. V. Boddy and D. R. Newell, Cellular ATP depletion by LY309887 as a predictor of growth inhibition in human tumor cell lines, *Clin. Cancer Res.*, 2000, **6**, 271–277.

174 Y. Zhu, M. Delbianco and P. H. Seeberger, Automated Assembly of Starch and Glycogen Polysaccharides, *J. Am. Chem. Soc.*, 2021, **143**, 9758–9768.
175 J. Tian, J. Wang, S. Zhao, C. Jiang, X. Zhang and X. Wang, Hydrolysis of cellulose by the heteropoly acid $H_3PW_{12}O_{40}$, *Cellulose*, 2010, **17**, 587–594.
176 Y. Sakamoto, K. Imamura and A. Onda, Hydrolysis of Oligosaccharides and Polysaccharides on Sulfonated Solid Acid Catalysts: Relations between Adsorption Properties and Catalytic Activities, *ACS Omega*, 2020, **5**, 24964–24972.
177 C. O. Tuck, E. Pérez, I. T. Horváth, R. A. Sheldon and M. Poliakoff, Valorization of Biomass: Deriving More Value from Waste, *Science*, 2012, **337**, 695–699.
178 Z. Sun, B. Fridrich, A. de Santi, S. Elangovan and K. Barta, Bright Side of Lignin Depolymerization: Toward New Platform Chemicals, *Chem. Rev.*, 2018, **118**, 614–678.
179 K. V. Solomon, C. H. Haitjema, J. K. Henske, S. P. Gilmore, D. Borges-Rivera, A. Lipzen, H. M. Brewer, S. O. Purvine, A. T. Wright, M. K. Theodorou, I. V. Grigoriev, A. Regev, D. A. Thompson and M. A. O'Malley, Early-branching gut fungi possess a large, comprehensive array of biomass-degrading enzymes, *Science*, 2016, **351**, 1192–1195.
180 X. Liu, X. Duan, W. Wei, S. Wang and B. J. Ni, Photocatalytic conversion of lignocellulosic biomass to valuable products, *Green Chem.*, 2019, **21**, 4266–4289.
181 A. T. Martínez, How to break down crystalline cellulose, *Science*, 2016, **352**, 1050–1051.
182 R. W. Torget, J. S. Kim and Y. Y. Lee, Fundamental Aspects of Dilute Acid Hydrolysis/Fractionation Kinetics of Hardwood Carbohydrates. 1. Cellulose Hydrolysis, *Ind. Eng. Chem. Res.*, 2000, **39**, 2817–2825.
183 C. Li and Z. K. Zhao, Efficient Acid-Catalyzed Hydrolysis of Cellulose in Ionic Liquid, *Adv. Synth. Catal.*, 2007, **349**, 1847–1850.
184 G. Brodeur, E. Yau, K. Badal, J. Collier, K. B. Ramachandran and S. Ramakrishnan, Chemical and Physicochemical Pretreatment of Lignocellulosic Biomass: A Review, *Enzyme Res.*, 2011, **2011**, 787532.
185 K. Shimizu, H. Furukawa, N. Kobayashi, Y. Itaya and A. Satsuma, Effects of Brønsted and Lewis acidities on activity and selectivity of heteropolyacid-based catalysts for hydrolysis of cellobiose and cellulose, *Green Chem.*, 2009, **11**, 1627–1632.
186 T. Peng, Z. Wooke and N. L. B. Pohl, Scope and limitations of carbohydrate hydrolysis for de novo glycan sequencing using a hydrogen peroxide/metallopeptide-based glycosidase mimetic, *Carbohydr. Res.*, 2018, **458–459**, 85–88.
187 J. Zhong, J. Pérez-Ramírez and N. Yan, Biomass valorisation over polyoxometalate-based catalysts, *Green Chem.*, 2021, **23**, 18–36.
188 I. V. Kozhevnikov, Catalysis by Heteropoly Acids and Multicomponent Polyoxometalates in Liquid-Phase Reactions, *Chem. Rev.*, 1998, **98**, 171–198.
189 N. Mizuno and M. Misono, Heterogeneous Catalysis, *Chem. Rev.*, 1998, **98**, 199–218.
190 M. Nakamura, M. S. Islam, M. A. Rahman, R. N. Nahar, M. Fukuda, Y. Sekine, J. N. Beltramini, Y. Kim and S. Hayami, Microwave aided conversion of cellulose to glucose using polyoxometalate as catalyst, *RSC Adv.*, 2021, **11**, 34558–34563.
191 M. S. Islam, M. Nakamura, N. N. Rabin, M. A. Rahman, M. Fukuda, Y. Sekine, J. N. Beltramini, Y. Kim and S. Hayami, Microwave-assisted catalytic conversion of chitin to 5-hydroxymethylfurfural using polyoxometalate as catalyst, *RSC Adv.*, 2021, **12**, 406–412.
192 J. Tian, C. Fang, M. Cheng and X. Wang, Hydrolysis of Cellulose over $Cs_xH_{3-x}PW_{12}O_{40}$ (X = 1-3) Heteropoly Acid Catalysts, *Chem. Eng. Technol.*, 2011, **34**, 482–486.
193 M. Cheng, T. Shi, S. Wang, H. Guan, C. Fan and X. Wang, Fabrication of micellar heteropolyacid catalysts for clean production of monosaccharides from polysaccharides, *Catal. Commun.*, 2011, **12**, 1483–1487.
194 S. Zhao, M. Cheng, J. Li, J. Tian and X. Wang, One pot production of 5-hydroxymethylfurfural with high yield from cellulose by a Brønsted–Lewis-surfactant-combined heteropolyacid catalyst, *Chem. Commun.*, 2011, **47**, 2176–2178.
195 J. Hao, X. Song, S. Jia, W. Mao, Y. Yan and J. Zhou, Catalytic Conversion of Starch to 5-Hydroxymethylfurfural by Tin Phosphotungstate, *Front. Energy Res.*, 2021, **9**, 1–10.
196 H. Zheng, Z. Sun, X. Yi, S. Wang, J. Li, X. Wang and Z. Jiang, A water-tolerant $C_{16}H_3PW_{11}CrO_{39}$ catalyst for the efficient conversion of monosaccharides into 5-hydroxymethylfurfural in a micellar system, *RSC Adv.*, 2013, **3**, 23051–23056.
197 K. Shimizu, R. Uozumi and A. Satsuma, Enhanced production of hydroxymethylfurfural from fructose with solid acid catalysts by simple water removal methods, *Catal. Commun.*, 2009, **10**, 1849–1853.
198 Q. Zhao, L. Wang, S. Zhao, X. Wang and S. Wang, High selective production of 5-hydroymethylfurfural from fructose by a solid heteropolyacid catalyst, *Fuel*, 2011, **90**, 2289–2293.
199 C. Fan, H. Guan, H. Zhang, J. Wang, S. Wang and X. Wang, Conversion of fructose and glucose into 5-hydroxymethylfurfural catalyzed by a solid heteropolyacid salt, *Biomass Bioenergy*, 2011, **35**, 2659–2665.
200 P. Zhao, Y. Zhang, Y. Wang, H. Cui, F. Song, X. Sun and L. Zhang, Conversion of glucose into 5-hydroxymethylfurfural catalyzed by acid-base bifunctional heteropolyacid-based ionic hybrids, *Green Chem.*, 2018, **20**, 1551–1559.
201 L. Lian, X. Chen, X. Yi, Y. Liu, W. Chen, A. Zheng, H. N. Miras and Y. Song, Modulation of Self-Separating Molecular Catalysts for Highly Efficient Biomass Transformations, *Chem. – Eur. J.*, 2020, **26**, 11900–11908.
202 J. Chen, G. Zhao and L. Chen, Efficient production of 5-hydroxymethylfurfural and alkyl levulinate from biomass carbohydrate using ionic liquid-based polyoxometalate salts, *RSC Adv.*, 2014, **4**, 4194–4202.
203 C. Larabi, W. Al Maksoud, K. C. Szeto, A. Roubaud, P. Castelli, C. C. Santini and J. J. Walter, Thermal

decomposition of lignocellulosic biomass in the presence of acid catalysts, *Bioresour. Technol.*, 2013, **148**, 255–260.

204 T. Okuhara, Water-tolerant solid acid catalysts, *Chem. Rev.*, 2002, **102**, 3641–3666.

205 R.-J. van Putten, J. C. van der Waal, E. de Jong, C. B. Rasrendra, H. J. Heeres and J. G. de Vries, Hydroxymethylfurfural, A Versatile Platform Chemical Made from Renewable Resources, *Chem. Rev.*, 2013, **113**, 1499–1597.

206 H. Li, X. He, Q. Zhang, F. Chang, W. Xue, Y. Zhang and S. Yang, Polymeric Ionic Hybrid as Solid Acid Catalyst for the Selective Conversion of Fructose and Glucose to 5-Hydroxymethylfurfural, *Energy Technol.*, 2013, **1**, 151–156.

207 Y. Qu, C. Huang, J. Zhang and B. Chen, Efficient dehydration of fructose to 5-hydroxymethylfurfural catalyzed by a recyclable sulfonated organic heteropolyacid salt, *Bioresour. Technol.*, 2012, **106**, 170–172.

208 K. Li, L. Bai, P. N. Amaniampong, X. Jia, J.-M. Lee and Y. Yang, One-Pot Transformation of Cellobiose to Formic Acid and Levulinic Acid over Ionic-Liquid-based Polyoxometalate Hybrids, *ChemSusChem*, 2014, **7**, 2670–2677.

209 Z. Sun, M. Cheng, H. Li, T. Shi, M. Yuan, X. Wang and Z. Jiang, One-pot depolymerization of cellulose into glucose and levulinic acid by heteropolyacid ionic liquid catalysis, *RSC Adv.*, 2012, **2**, 9058.

210 H. Nie, Y. Li and X.-L. Sun, Recent advances in sialic acid-focused glycomics, *J. Proteomics*, 2012, **75**, 3098–3112.

211 C. Büll, M. H. den Brok and G. J. Adema, Sweet escape: Sialic acids in tumor immune evasion, *Biochim. Biophys. Acta, Rev. Cancer*, 2014, **1846**, 238–246.

212 G. Walsh, Biopharmaceutical benchmarks 2014, *Nat. Biotechnol.*, 2014, **32**, 992–1000.

213 F. N. Lamari and N. K. Karamanos, Separation methods for sialic acids and critical evaluation of their biologic relevance, *J. Chromatogr. B: Anal. Technol. Biomed. Life Sci.*, 2002, **781**, 3–19.

214 L. S. Van Rompuy and T. N. Parac-Vogt, Polyoxometalates as sialidase mimics: selective and non-destructive removal of sialic acid from a glycoprotein promoted by phosphotungstic acid, *Chem. Commun.*, 2017, **53**, 10600–10603.

215 L. S. Van Rompuy, J. Moons, J. Aelbers, T. Struyf, W. Van den Ende and T. N. Parac-Vogt, Selective Hydrolysis of Terminal Glycosidic Bond in α-1-Acid Glycoprotein Promoted by Keggin and Wells–Dawson Type Heteropolyacids, *Chem. – Eur. J.*, 2020, **26**, 16463–16471.

216 D. Voß, S. Ponce, S. Wesinger, B. J. M. Etzold and J. Albert, Combining autoclave and LCWM reactor studies to shed light on the kinetics of glucose oxidation catalyzed by doped molybdenum-based heteropoly acids, *RSC Adv.*, 2019, **9**, 29347–29356.

217 B. B. Sarma and R. Neumann, Polyoxometalate-mediated electron transfer–oxygen transfer oxidation of cellulose and hemicellulose to synthesis gas, *Nat. Commun.*, 2014, **5**, 4621.

218 R. Wölfel, N. Taccardi, A. Bösmann and P. Wasserscheid, Selective catalytic conversion of biobased carbohydrates to formic acid using molecular oxygen, *Green Chem.*, 2011, **13**, 2759–2763.

219 J. Li, D. Ding, L. Deng, Q. Guo and Y. Fu, Catalytic Air Oxidation of Biomass-Derived Carbohydrates to Formic Acid, *ChemSusChem*, 2012, **5**, 1313–1318.

220 J. Albert, D. Lüders, A. Bösmann, D. M. Guldi and P. Wasserscheid, Spectroscopic and electrochemical characterization of heteropoly acids for their optimized application in selective biomass oxidation to formic acid, *Green Chem.*, 2014, **16**, 226–237.

221 N. I. Gumerova and A. Rompel, Synthesis, structures and applications of electron-rich polyoxometalates, *Nat. Rev. Chem.*, 2018, **2**, 0112.

222 E. Janusson, N. de Kler, L. Vilà-Nadal, D.-L. Long and L. Cronin, Synthesis of polyoxometalate clusters using carbohydrates as reducing agents leads to isomer-selection, *Chem. Commun.*, 2019, **55**, 5797–5800.

223 G. van Meer, D. R. Voelker and G. W. Feigenson, Membrane lipids: where they are and how they behave, *Nat. Rev. Mol. Cell Biol.*, 2008, **9**, 112–124.

224 H. Nabika, Y. Inomata, E. Itoh and K. Unoura, Activity of Keggin and Dawson polyoxometalates toward model cell membrane, *RSC Adv.*, 2013, **3**, 21271.

225 B. Jing, M. Hutin, E. Connor, L. Cronin and Y. Zhu, Polyoxometalate macroion induced phase and morphology instability of lipid membrane, *Chem. Sci.*, 2013, **4**, 3818–3826.

226 H. Nabika, A. Sakamoto, T. Motegi, R. Tero, D. Yamaguchi and K. Unoura, Imaging Characterization of Cluster-Induced Morphological Changes of a Model Cell Membrane, *J. Phys. Chem. C*, 2016, **120**, 15640–15647.

227 D. Kobayashi, H. Nakahara, O. Shibata, K. Unoura and H. Nabika, Interplay of Hydrophobic and Electrostatic Interactions between Polyoxometalates and Lipid Molecules, *J. Phys. Chem. C*, 2016, **2017**(121), 12895–12902.

228 A. Sakamoto, K. Unoura and H. Nabika, Molecular Scale Insights into Activity of Polyoxometalate as Membrane-Targeting Nanomedicine from Single-Molecule Observations, *J. Phys. Chem. C*, 2018, **122**, 1404–1411.

229 X.-X. Han, K.-K. Chen, W. Yan, C.-T. Hung, L.-L. Liu, P.-H. Wu, K.-C. Lin and S.-B. Liu, Amino acid-functionalized heteropolyacids as efficient and recyclable catalysts for esterification of palmitic acid to biodiesel, *Fuel*, 2016, **165**, 115–122.

230 F. Cao, Y. Chen, F. Zhai, J. Li, J. Wang, X. Wang, S. Wang and W. Zhu, Biodiesel production from high acid value waste frying oil catalyzed by superacid heteropolyacid, *Biotechnol. Bioeng.*, 2008, **101**, 93–100.

231 Q. Zhang, X. Liu, T. Deng, Y. Zhang and P. Ma, Recent Progress on Heteropolyacids for Green Fuels Synthesis, *Curr. Green Chem.*, 2020, **7**, 267–281.

232 P. Morin, B. Hamad, G. Sapaly, M. G. Carneiro Rocha, P. G. Pries de Oliveira, W. A. Gonzalez, E. Andrade Sales and N. Essayem, Transesterification of rapeseed oil with ethanol I. Catalysis with homogeneous Keggin heteropolyacids, *Appl. Catal., A*, 2007, **330**, 69–76.

233 A. L. Cardoso, R. Augusti and M. J. Da Silva, Investigation on the Esterification of Fatty Acids Catalyzed by the $H_3PW_{12}O_{40}$ heteropolyacid, *J. Am. Oil Chem. Soc.*, 2008, **85**, 555–560.

234 K. Narasimharao, D. R. Brown, A. F. Lee, A. D. Newman, P. F. Siril, S. J. Tavener and K. Wilson, Structure-activity relations in Cs-doped heteropolyacid catalysts for biodiesel production, *J. Catal.*, 2007, **248**, 226–234.

235 F. Chai, F. Cao, F. Zhai, Y. Chen, X. Wang and Z. Su, Transesterification of vegetable oil to biodiesel using a heteropolyacid solid catalyst, *Adv. Synth. Catal.*, 2007, **349**, 1057–1065.

236 W. Xie, C. Gao and H. Wang, Biodiesel Production from Low-Quality Oils Using Heterogeneous Cesium Salts of Vanadium-Substituted Polyoxometalate Acid Catalyst, *Catalysts*, 2020, **10**, 1060.

237 M. J. Da Silva, C. B. Vilanculo, M. G. Teixeira and A. A. Julio, Catalysis of vegetable oil transesterification by Sn(II)-exchanged Keggin heteropolyacids: bifunctional solid acid catalysts, *React. Kinet., Mech. Catal.*, 2017, **122**, 1011–1030.

238 G. Carta, E. Murru, S. Banni and C. Manca, Palmitic Acid: Physiological Role, Metabolism and Nutritional Implications, *Front. Physiol.*, 2017, **8**, 1–14.

239 Z. Sun, X. Duan, J. Zhao, X. Wang and Z. Jiang, Homogeneous borotungstic acid and heterogeneous micellar borotungstic acid catalysts for biodiesel production by esterification of free fatty acid, *Biomass Bioenergy*, 2015, **76**, 31–42.

240 S. A. Fernandes, A. L. Cardoso and M. J. da Silva, A novel kinetic study of $H_3PW_{12}O_{40}$ – catalyzed oleic acid esterification with methanol via ^{1}H NMR spectroscopy, *Fuel Process. Technol.*, 2012, **96**, 98–103.

241 A. Talebian-Kiakalaieh, N. A. S. Amin, A. Zarei and I. Noshadi, Transesterification of waste cooking oil by heteropoly acid (HPA) catalyst: Optimization and kinetic model, *Appl. Energy*, 2013, **102**, 283–292.

242 M. G. Kulkarni and A. K. Dalai, Waste cooking oil – An economical source for biodiesel: A review, *Ind. Eng. Chem. Res.*, 2006, **45**, 2901–2913.

243 M. G. Kulkarni, R. Gopinath, L. C. Meher and A. K. Dalai, Solid acid catalyzed biodiesel production by simultaneous esterification and transesterification, *Green Chem.*, 2006, **8**, 1056–1062.

244 J. Zhao, H. Guan, W. Shi, M. Cheng, X. Wang and S. Li, A Brønsted–Lewis-surfactant-combined heteropolyacid as an environmental benign catalyst for esterification reaction, *Catal. Commun.*, 2012, **20**, 103–106.

245 K. Srilatha, R. Sree, B. L. A. Prabhavathi Devi, P. S. Sai Prasad, R. B. N. Prasad and N. Lingaiah, Preparation of biodiesel from rice bran fatty acids catalyzed by heterogeneous cesium-exchanged 12-tungstophosphoric acids, *Bioresour. Technol.*, 2012, **116**, 53–57.

246 S. Zhang, Y.-G. Zu, Y.-J. Fu, M. Luo, D.-Y. Zhang and T. Efferth, Rapid microwave-assisted transesterification of yellow horn oil to biodiesel using a heteropolyacid solid catalyst, *Bioresour. Technol.*, 2010, **101**, 931–936.

247 J. Li, X. Wang, W. Zhu and F. Cao, $Zn_{1.2}H_{0.6}PW_{12}O_{40}$ Nanotubes with double acid sites as heterogeneous catalysts for the production of biodiesel from waste cooking oil, *ChemSusChem*, 2009, **2**, 177–183.

248 J. Li, D. Li, J. Xie, Y. Liu, Z. Guo, Q. Wang, Y. Lyu, Y. Zhou and J. Wang, Pyrazinium polyoxometalate tetrakaidecahedron-like crystals esterify oleic acid with equimolar methanol at room temperature, *J. Catal.*, 2016, **339**, 123–134.

249 X.-X. Han, Y.-F. He, C.-T. Hung, L.-L. Liu, S.-J. Huang and S.-B. Liu, Efficient and reusable polyoxometalate-based sulfonated ionic liquid catalysts for palmitic acid esterification to biodiesel, *Chem. Eng. Sci.*, 2013, **104**, 64–72.

250 B. Y. Giri, K. N. Rao, B. L. A. P. Devi, N. Lingaiah, I. Suryanarayana, R. B. N. Prasad and P. S. S. Prasad, Esterification of palmitic acid on the ammonium salt of 12-tungstophosphoric acid: The influence of partial proton exchange on the activity of the catalyst, *Catal. Commun.*, 2005, **6**, 788–792.

251 S. Li, Y. Wang, S. Dong, Y. Chen, F. Cao, F. Chai and X. Wang, Biodiesel production from Eruca Sativa Gars vegetable oil and motor, emissions properties, *Renewable Energy*, 2009, **34**, 1871–1876.

252 J. S. Santos, J. A. Dias, S. C. L. Dias, J. L. de Macedo, F. A. C. Garcia, L. S. Almeida and E. N. C. B. de Carvalho, Acidic characterization and activity of $(NH_4)_xCs_{2.5-x}H_{0.5}PW_{12}O_{40}$ catalysts in the esterification reaction of oleic acid with ethanol, *Appl. Catal., A*, 2012, **443–444**, 33–39.

253 M. Tao, Y. Li, Y. V. Geletii, C. L. Hill and X. Wang, Aerobic oxidation of glycerol catalyzed by M salts of $PMo_{12}O_{40}^{3-}$ ($M = K^+$, Zn^{2+}, Cu^{2+}, Al^{3+}, Cr^{3+}, Fe^{3+}), *Appl. Catal., A*, 2019, **579**, 52–57.

254 M. S. Petronek, B. G. Allen, G. Luthe and J. M. Stolwijk, Polyoxometalate Nanoparticles as a Potential Glioblastoma Therapeutic via Lipid-Mediated Cell Death, *Int. J. Mol. Sci.*, 2022, **23**, 8263.

255 C. Xu, M. Nasrollahzadeh, M. Selva, Z. Issaabadi and R. Luque, Waste-to-wealth: biowaste valorization into valuable bio(nano)materials, *Chem. Soc. Rev.*, 2019, **48**, 4791–4822.

256 R. Fang, A. Dhakshinamoorthy, Y. Li and H. Garcia, Metal organic frameworks for biomass conversion, *Chem. Soc. Rev.*, 2020, **49**, 3638–3687.

257 W. Tu, Y. Xu, S. Yin and R. Xu, Rational Design of Catalytic Centers in Crystalline Frameworks, *Adv. Mater.*, 2018, **30**, 1707582.

258 M. Bilal, M. Adeel, T. Rasheed and H. M. N. Iqbal, Multifunctional metal–organic frameworks-based biocatalytic platforms: recent developments and future prospects, *J. Mater. Res. Technol.*, 2019, **8**, 2359–2371.

259 Y. Li, Y. Wu, K. Liu, S. A. Delbari, A. Kim, A. Sabahi Namini, Q. Van Le, M. Shokouhimehr, C. Xia, H. W. Jang, R. S. Varma and R. Luque, Metal-organic framework-based nanostructured catalysts: Applications in biomass conversion, *Fuel*, 2023, **340**, 127482.

260 H. G. T. Ly, G. Fu, A. Kondinski, B. Bueken, D. De Vos and T. N. Parac-Vogt, Superactivity of MOF-808 toward Peptide Bond Hydrolysis, *J. Am. Chem. Soc.*, 2018, **140**, 6325–6335.

261 S. Dai, C. Simms, I. Dovgaliuk, G. Patriarche, A. Tissot, T. N. Parac-Vogt and C. Serre, Monodispersed MOF-808 Nanocrystals Synthesized via a Scalable Room-Temperature Approach for Efficient Heterogeneous Peptide Bond Hydrolysis, *Chem. Mater.*, 2021, **33**, 7057–7066.

262 H. G. T. Ly, G. Fu, F. de Azambuja, D. De Vos and T. N. Parac-Vogt, Nanozymatic Activity of UiO-66 Metal–Organic Frameworks: Tuning the Nanopore Environment Enhances Hydrolytic Activity toward Peptide Bonds, *ACS Appl. Nano Mater.*, 2020, **3**, 8931–8938.

263 A. Loosen, C. Simms, S. Smolders, D. E. De Vos and T. N. Parac-Vogt, Bimetallic Ce/Zr UiO-66 Metal–Organic Framework Nanostructures as Peptidase and Oxidase Nanozymes, *ACS Appl. Nano Mater.*, 2021, **4**, 5748–5757.

264 A. Loosen, F. de Azambuja, S. Smolders, J. Moons, C. Simms, D. De Vos and T. N. Parac-Vogt, Interplay between structural parameters and reactivity of Zr_6-based MOFs as artificial proteases, *Chem. Sci.*, 2020, **11**, 6662–6669.

265 J. Moons, A. Loosen, C. Simms, F. de Azambuja and T. N. Parac-Vogt, Heterogeneous nanozymatic activity of Hf oxo-clusters embedded in a metal–organic framework towards peptide bond hydrolysis, *Nanoscale*, 2021, **13**, 12298–12305.

266 S. Wang, H. G. T. Ly, M. Wahiduzzaman, C. Simms, I. Dovgaliuk, A. Tissot, G. Maurin, T. N. Parac-Vogt and C. Serre, A zirconium metal-organic framework with SOC topological net for catalytic peptide bond hydrolysis, *Nat. Commun.*, 2022, **13**, 1284.

267 D. Conic, K. Pierloot, T. N. Parac-Vogt and J. N. Harvey, Mechanism of the highly effective peptide bond hydrolysis by MOF-808 catalyst under biologically relevant conditions, *Phys. Chem. Chem. Phys.*, 2020, **22**, 25136–25145.

268 A. Loosen, F. de Azambuja and T. N. Parac-Vogt, Which factors govern the adsorption of peptides to Zr(IV)-based metal–organic frameworks?, *Mater. Adv.*, 2022, **3**, 2475–2487.

269 Y. Chen, V. Lykourinou, C. Vetromile, T. Hoang, L.-J. Ming, R. W. Larsen and S. Ma, How Can Proteins Enter the Interior of a MOF? Investigation of Cytochrome *c* Translocation into a MOF Consisting of Mesoporous Cages with Microporous Windows, *J. Am. Chem. Soc.*, 2012, **134**, 13188–13191.

270 C. Simms, N. D. Savić, K. De Winter and T. N. Parac-Vogt, Understanding the Role of Surfactants in the Interaction and Hydrolysis of Myoglobin by Zr-MOF-808, *Eur. J. Inorg. Chem.*, 2022, e202200145.

271 L. Liu, Z. Chen, J. Wang, D. Zhang, Y. Zhu, S. Ling, K.-W. Huang, Y. Belmabkhout, K. Adil, Y. Zhang, B. Slater, M. Eddaoudi and Y. Han, Imaging defects and their evolution in a metal–organic framework at sub-unit-cell resolution, *Nat. Chem.*, 2019, **11**, 622–628.

272 S. Wang, C. M. McGuirk, A. d'Aquino, J. A. Mason and C. A. Mirkin, Metal–Organic Framework Nanoparticles, *Adv. Mater.*, 2018, **30**, 1800202.

273 A. Solé-Daura, A. Rodríguez-Fortea, J. M. Poblet, D. Robinson, J. D. Hirst and J. J. Carbó, Origin of Selectivity in Protein Hydrolysis by Zr(IV)-Containing Metal Oxides as Artificial Proteases, *ACS Catal.*, 2020, **10**, 13455–13467.

274 M. N. Timofeeva, V. N. Panchenko, I. A. Lukoyanov and S. H. Jhung, Zirconium-containing metal organic frameworks as solid acid catalysts for the N-formylation of aniline with formic acid, *React. Kinet., Mech. Catal.*, 2021, **133**, 355–369.

275 L. T. M. Hoang, L. H. Ngo, H. L. Nguyen, H. T. H. Nguyen, C. K. Nguyen, B. T. Nguyen, Q. T. Ton, H. K. D. Nguyen, K. E. Cordova and T. Truong, An azobenzene-containing metal–organic framework as an efficient heterogeneous catalyst for direct amidation of benzoic acids: synthesis of bioactive compounds, *Chem. Commun.*, 2015, **51**, 17132–17135.

276 F. de Azambuja, A. Loosen, D. Conic, M. van den Besselaar, J. N. Harvey and T. N. Parac-Vogt, En Route to a Heterogeneous Catalytic Direct Peptide Bond Formation by Zr-Based Metal–Organic Framework Catalysts, *ACS Catal.*, 2021, **11**, 7647–7658.

277 R. Fang and J. Liu, Cleaving DNA by nanozymes, *J. Mater. Chem. B*, 2020, **8**, 7135–7142.

278 J. Yang, K. Li and J. Gu, Hierarchically Macro-Microporous Ce-Based MOFs for the Cleavage of DNA, *ACS Mater. Lett.*, 2022, **4**, 385–391.

279 Q. Han, L. Zhang, C. He, J. Niu and C. Duan, Metal–Organic Frameworks with Phosphotungstate Incorporated for Hydrolytic Cleavage of a DNA-Model Phosphodiester, *Inorg. Chem.*, 2012, **51**, 5118–5127.

280 M. Xu, L. Feng, L.-N. Yan, S.-S. Meng, S. Yuan, M.-J. He, H. Liang, X.-Y. Chen, H.-Y. Wei, Z.-Y. Gu and H.-C. Zhou, Discovery of precise pH-controlled biomimetic catalysts: defective zirconium metal–organic frameworks as alkaline phosphatase mimics, *Nanoscale*, 2019, **11**, 11270–11278.

281 J. Dong, H.-D. An, Z.-K. Yue, S.-L. Hou, Y. Chen, Z.-J. Zhang, P. Cheng, Q. Peng and B. Zhao, Dual-Selective Catalysis in Dephosphorylation Tuned by Hf 6 -Containing Metal–Organic Frameworks Mimicking Phosphatase, *ACS Cent. Sci.*, 2021, **7**, 831–840.

282 C. Yang, Z. Jiang, Q. Wu, C. Hu, C. Huang, Y. Li and S. Zhen, One-component nano-metal-organic frameworks with superior multienzyme-mimic activities for 1,4-dihydropyridine metabolism, *J. Colloid Interface Sci.*, 2022, **605**, 214–222.

283 J. Yang, K. Li, C. Li and J. Gu, Intrinsic Apyrase-Like Activity of Cerium-Based Metal–Organic Frameworks (MOFs): Dephosphorylation of Adenosine Tri- and Diphosphate, *Angew. Chem., Int. Ed.*, 2020, **59**, 22952–22956.

284 K. O. Kirlikovali, Z. Chen, T. Islamoglu, J. T. Hupp and O. K. Farha, Zirconium-Based Metal–Organic Frameworks for the Catalytic Hydrolysis of Organophosphorus Nerve Agents, *ACS Appl. Mater. Interfaces*, 2020, **12**, 14702–14720.

285 T. G. Grissom, A. M. Plonka, C. H. Sharp, A. M. Ebrahim, Y. Tian, D. L. Collins-Wildman, A. L. Kaledin, H. J. Siegal, D. Troya, C. L. Hill, A. I. Frenkel, D. G. Musaev, W. O. Gordon, C. J. Karwacki, M. B. Mitchell and J. R. Morris, Metal–Organic Framework- and Polyoxometalate-Based Sorbents for the

Uptake and Destruction of Chemical Warfare Agents, *ACS Appl. Mater. Interfaces*, 2020, **12**, 14641–14661.

286 S. Rojas, A. Rodríguez-Diéguez and P. Horcajada, Metal–Organic Frameworks in Agriculture, *ACS Appl. Mater. Interfaces*, 2022, **14**, 16983–17007.

287 J. E. Mondloch, M. J. Katz, W. C. Isley III, P. Ghosh, P. Liao, W. Bury, G. W. Wagner, M. G. Hall, J. B. DeCoste, G. W. Peterson, R. Q. Snurr, C. J. Cramer, J. T. Hupp and O. K. Farha, Destruction of chemical warfare agents using metal–organic frameworks, *Nat. Mater.*, 2015, **14**, 512–516.

288 M. J. Katz, J. E. Mondloch, R. K. Totten, J. K. Park, S. T. Nguyen, O. K. Farha and J. T. Hupp, Simple and Compelling Biomimetic Metal-Organic Framework Catalyst for the Degradation of Nerve Agent Simulants, *Angew. Chem., Int. Ed.*, 2014, **53**, 497–501.

289 F. A. Son, M. C. Wasson, T. Islamoglu, Z. Chen, X. Gong, S. L. Hanna, J. Lyu, X. Wang, K. B. Idrees, J. J. Mahle, G. W. Peterson and O. K. Farha, Uncovering the Role of Metal–Organic Framework Topology on the Capture and Reactivity of Chemical Warfare Agents, *Chem. Mater.*, 2020, **32**, 4609–4617.

290 Y. Wang, Z. Liu, H. Zhang, J. Liu, H. Dai, T. Ji, F. Liu, P. Cao, J. Zou, S. Wang, L. Wang and Z. Wang, MOF effectively deliver CRISPR and enhance gene-editing efficiency via MOF's hydrolytic activity of phosphate ester bonds, *Chem. Eng. J.*, 2022, **439**, 134992.

291 K. Yu, T. Wei, Z. Li, J. Li, Z. Wang and Z. Dai, Construction of Molecular Sensing and Logic Systems Based on Site-Occupying Effect-Modulated MOF–DNA Interaction, *J. Am. Chem. Soc.*, 2020, **142**, 21267–21271.

292 P. Lenihan, A. Orozco, E. O'Neill, M. N. M. Ahmad, D. W. Rooney and G. M. Walker, Dilute acid hydrolysis of lignocellulosic biomass, *Chem. Eng. J.*, 2010, **156**, 395–403.

293 A. S. da Silva, R. P. Espinheira, R. S. S. Teixeira, M. F. de Souza, V. Ferreira-Leitão and E. P. S. Bon, Constraints and advances in high-solids enzymatic hydrolysis of lignocellulosic biomass: a critical review, *Biotechnol. Biofuels*, 2020, **13**, 58.

294 R. C. Wilhelm, R. Singh, L. D. Eltis and W. W. Mohn, Bacterial contributions to delignification and lignocellulose degradation in forest soils with metagenomic and quantitative stable isotope probing, *ISME J.*, 2019, **13**, 413–429.

295 J. S. Kruger, V. Nikolakis and D. G. Vlachos, Carbohydrate dehydration using porous catalysts, *Curr. Opin. Chem. Eng.*, 2012, **1**, 312–320.

296 F. Valentini, V. Kozell, C. Petrucci, A. Marrocchi, Y. Gu, D. Gelman and L. Vaccaro, Formic acid, a biomass-derived source of energy and hydrogen for biomass upgrading, *Energy Environ. Sci.*, 2019, **12**, 2646–2664.

297 J. Han, Y. Wang, J. Wan and Y. Ma, Catalytic hydrolysis of cellulose by phosphotungstic acid–supported functionalized metal-organic frameworks with different electronegative groups, *Environ. Sci. Pollut. Res.*, 2019, **26**, 15345–15353.

298 J. Chen, K. Li, L. Chen, R. Liu, X. Huang and D. Ye, Conversion of fructose into 5-hydroxymethylfurfural catalyzed by recyclable sulfonic acid-functionalized metal–organic frameworks, *Green Chem.*, 2014, **16**, 2490–2499.

299 Q. Luo, Y. Zhang, L. Qi and S. L. Scott, Glucose Isomerization and Epimerization over Metal-Organic Frameworks with Single-Site Active Centers, *ChemCatChem*, 2019, **11**, 1903–1909.

300 M. Yabushita, P. Li, T. Islamoglu, H. Kobayashi, A. Fukuoka, O. K. Farha and A. Katz, Selective Metal–Organic Framework Catalysis of Glucose to 5-Hydroxymethylfurfural Using Phosphate-Modified NU-1000, *Ind. Eng. Chem. Res.*, 2017, **56**, 7141–7148.

301 R. Oozeerally, D. L. Burnett, T. W. Chamberlain, R. J. Kashtiban, S. Huband, R. I. Walton and V. Degirmenci, Systematic Modification of UiO-66 Metal-Organic Frameworks for Glucose Conversion into 5-Hydroxymethyl Furfural in Water, *ChemCatChem*, 2021, **13**, 2517–2529.

302 K. Liang, R. Ricco, C. M. Doherty, M. J. Styles, S. Bell, N. Kirby, S. Mudie, D. Haylock, A. J. Hill, C. J. Doonan and P. Falcaro, Biomimetic mineralization of metal-organic frameworks as protective coatings for biomacromolecules, *Nat. Commun.*, 2015, **6**, 7240.

303 R. Jiao, Y. Pang, D. Yang, Z. Li and H. Lou, Boosting Hydrolysis of Cellulose at High Temperature by β-Glucosidase Induced Metal–Organic Framework In-Situ Co-Precipitation Encapsulation, *ChemSusChem*, 2022, **15**, e202201354.

304 R. Jiao, Y. Wang, Y. Pang, D. Yang, Z. Li, H. Lou and X. Qiu, Construction of Macroporous β-Glucosidase@MOFs by a Metal Competitive Coordination and Oxidation Strategy for Efficient Cellulose Conversion at 120 °C, *ACS Appl. Mater. Interfaces*, 2023, **15**, 8157–8168.

305 R. Pertiwi, R. Oozeerally, D. L. Burnett, T. W. Chamberlain, N. Cherkasov, M. Walker, R. J. Kashtiban, Y. K. Krisnandi, V. Degirmenci and R. I. Walton, Replacement of Chromium by Non-Toxic Metals in Lewis-Acid MOFs: Assessment of Stability as Glucose Conversion Catalysts, *Catalysts*, 2019, **9**, 437.

306 M. D. de Mello and M. Tsapatsis, Selective Glucose-to-Fructose Isomerization over Modified Zirconium UiO-66 in Alcohol Media, *ChemCatChem*, 2018, **10**, 2417–2423.

307 A. Rapeyko, K. S. Arias, M. J. Climent, A. Corma and S. Iborra, Polymers from biomass: one pot two-step synthesis of furilydenepropanenitrile derivatives with MIL-100(Fe) catalyst, *Catal. Sci. Technol.*, 2017, **7**, 3008–3016.

308 S. Rojas-Buzo, P. García-García and A. Corma, Catalytic Transfer Hydrogenation of Biomass-Derived Carbonyls over Hafnium-Based Metal–Organic Frameworks, *ChemSusChem*, 2018, **11**, 432–438.

309 J. Chen, R. Liu, Y. Guo, L. Chen and H. Gao, Selective Hydrogenation of Biomass-Based 5-Hydroxymethylfurfural over Catalyst of Palladium Immobilized on Amine-Functionalized Metal–Organic Frameworks, *ACS Catal.*, 2015, **5**, 722–733.

310 F. Kerkel, M. Markiewicz, S. Stolte, E. Müller and W. Kunz, The green platform molecule gamma-valerolactone – ecotoxicity, biodegradability, solvent properties, and potential applications, *Green Chem.*, 2021, **23**, 2962–2976.

311 Y. Kuwahara, H. Kango and H. Yamashita, Catalytic Transfer Hydrogenation of Biomass-Derived Levulinic Acid and Its Esters to γ-Valerolactone over Sulfonic Acid-Functionalized UiO-66, *ACS Sustainable Chem. Eng.*, 2017, **5**, 1141–1152.

312 Y. Han, J. Dai, R. Xu, W. Ai, L. Zheng, Y. Wang, W. Yan, W. Chen, J. Luo, Q. Liu, D. Wang and Y. Li, Notched-Polyoxometalate Strategy to Fabricate Atomically Dispersed Ru Catalysts for Biomass Conversion, *ACS Catal.*, 2021, **11**, 2669–2675.

313 M. Cai, Y. Zhang, Y. Zhao, Q. Liu, Y. Li and G. Li, Two-dimensional metal–organic framework nanosheets for highly efficient electrocatalytic biomass 5-(hydroxymethyl)-furfural (HMF) valorization, *J. Mater. Chem. A*, 2020, **8**, 20386–20392.

314 F. Wang, Z. Chen, H. Chen, T. A. Goetjen, P. Li, X. Wang, S. Alayoglu, K. Ma, Y. Chen, T. Wang, T. Islamoglu, Y. Fang, R. Q. Snurr and O. K. Farha, Interplay of Lewis and Brønsted Acid Sites in Zr-Based Metal–Organic Frameworks for Efficient Esterification of Biomass-Derived Levulinic Acid, *ACS Appl. Mater. Interfaces*, 2019, **11**, 32090–32096.

315 P. Shestakova, M. Popova, Á. Szegedi, H. Lazarova, T. K. Nga Luong, I. Trendafilova, J. Mihály and T. N. Parac-Vogt, Hybrid catalyst with combined Lewis and Brønsted acidity based on Zr^{IV} substituted polyoxometalate grafted on mesoporous MCM-41 silica for esterification of renewable levulinic acid, *Microporous Mesoporous Mater.*, 2021, **323**, 111203.

316 Z. Wang and Q. Chen, Conversion of 5-hydroxymethylfurfural into 5-ethoxymethylfurfural and ethyl levulinate catalyzed by MOF-based heteropolyacid materials, *Green Chem.*, 2016, **18**, 5884–5889.

317 J. Cheng, L. Qian, H. Guo, Y. Mao, Y. Shao and W. Yang, A new aminobenzoate-substituted s-triazin-based Zr metal organic frameworks as efficient catalyst for biodiesel production from microalgal lipids, *Fuel Process. Technol.*, 2022, **238**, 107487.

318 J. Cheng, Y. Mao, H. Guo, L. Qian, Y. Shao, W. Yang and J.-Y. Park, Synergistic and efficient catalysis over Brønsted acidic ionic liquid $[BSO_3HMIm][HSO_4]$–modified metal–organic framework (IRMOF-3) for microalgal biodiesel production, *Fuel*, 2022, **322**, 124217.

319 Q. Zhang, X. Liu, T. Yang, C. Yue, Q. Pu and Y. Zhang, Facile synthesis of polyoxometalates tethered to post Fe-BTC frameworks for esterification of free fatty acids to biodiesel, *RSC Adv.*, 2019, **9**, 8113–8120.

320 Q. Zhang, D. Ling, D. Lei, J. Wang, X. Liu, Y. Zhang and P. Ma, Green and Facile Synthesis of Metal-Organic Framework Cu-BTC-Supported Sn(II)-Substituted Keggin Heteropoly Composites as an Esterification Nanocatalyst for Biodiesel Production, *Front. Chem.*, 2020, **8**, 129.

321 W. Xie and F. Wan, Biodiesel Production from Acidic Oils Using Polyoxometalate-Based Sulfonated Ionic Liquids Functionalized Metal–Organic Frameworks, *Catal. Lett.*, 2019, **149**, 2916–2929.

322 W. Xie and F. Wan, Immobilization of polyoxometalate-based sulfonated ionic liquids on UiO-66-2COOH metal-organic frameworks for biodiesel production via one-pot transesterification-esterification of acidic vegetable oils, *Chem. Eng. J.*, 2019, **365**, 40–50.

323 W. Xie and H. Wang, Synthesis of heterogenized polyoxometalate-based ionic liquids with Brønsted-Lewis acid sites: A magnetically recyclable catalyst for biodiesel production from low-quality oils, *J. Ind. Eng. Chem.*, 2020, **87**, 162–172.

324 W. Feng, X. Tie, X. Duan, S. Yan, S. Fang, P. Sun, L. Gan and T. Wang, Covalent immobilization of phosphotungstic acid and amino acid on metal-organic frameworks with different structures: Acid-base bifunctional heterogeneous catalyst for the production of biodiesel from insect lipid, Renew, *Energy*, 2023, **210**, 26–39.

325 M. Han, Z. Gu, C. Chen, Z. Wu, Y. Que, Q. Wang, H. Wan and G. Guan, Efficient confinement of ionic liquids in MIL-100(Fe) frameworks by the ''impregnation-reaction-encapsulation'' strategy for biodiesel production, *RSC Adv.*, 2016, **6**, 37110–37117.

326 M. Han, Y. Li, Z. Gu, H. Shi, C. Chen, Q. Wang, H. Wan and G. Guan, Immobilization of thiol-functionalized ionic liquids onto the surface of MIL-101(Cr) frameworks by S Cr coordination bond for biodiesel production, *Colloids Surf., A*, 2018, **553**, 593–600.

327 C. Chen, Z. Wu, Y. Que, B. Li, Q. Guo, Z. Li, L. Wang, H. Wan and G. Guan, Immobilization of a thiol-functionalized ionic liquid onto HKUST-1 through thiol compounds as the chemical bridge, *RSC Adv.*, 2016, **6**, 54119–54128.

328 C. F. Oliveira, L. M. Dezaneti, F. A. C. Garcia, J. L. de Macedo, J. A. Dias, S. C. L. Dias and K. S. P. Alvim, Esterification of oleic acid with ethanol by 12-tungstophosphoric acid supported on zirconia, *Appl. Catal., A*, 2010, **372**, 153–161.

329 K. N. Rao, A. Sridhar, A. F. Lee, S. J. Tavener, N. A. Young and K. Wilson, Zirconium phosphate supported tungsten oxide solid acid catalysts for the esterification of palmitic acid, *Green Chem.*, 2006, **8**, 790–797.

330 V. Brahmkhatri and A. Patel, Biodiesel Production by Esterification of Free Fatty Acids over 12-Tungstophosphoric Acid Anchored to MCM-41, *Ind. Eng. Chem. Res.*, 2011, **50**, 6620–6628.

331 Zillillah, T. A. Ngu and Z. Li, Phosphotungstic acid-functionalized magnetic nanoparticles as an efficient and recyclable catalyst for the one-pot production of biodiesel from grease via esterification and transesterification, *Green Chem.*, 2014, **16**, 1202–1210.

332 N. Narkhede, S. Singh and A. Patel, Recent progress on supported polyoxometalates for biodiesel synthesis via esterification and transesterification, *Green Chem.*, 2015, **17**, 89–107.

333 M. Stojanović, J. Lalatović, A. Milosavljević, N. Savić, C. Simms, B. Radosavljević, M. Ćetković, T. Kravić Stevović, D. Mrda, M. B. Čolović, T. N. Parac-Vogt and D. Krstić, In vivo toxicity evaluation of a polyoxotungstate nanocluster as a promising contrast agent for computed tomography, *Sci. Rep.*, 2023, **13**, 9140.

334 J. Wang, X. Qu, Y. Qi, J. Li, X. Song, L. Li, D. Yin, K. Xu and J. Li, Pharmacokinetics of Anti-HBV Polyoxometalate in Rats, *PLoS One*, 2014, **9**, e98292.

335 C. Tamames-Tabar, D. Cunha, E. Imbuluzqueta, F. Ragon, C. Serre, M. J. Blanco-Prieto and P. Horcajada, Cytotoxicity of nanoscaled metal–organic frameworks, *J. Mater. Chem. B*, 2014, **2**, 262–271.

336 J. W. M. Osterrieth and D. Fairen-Jimenez, Metal–Organic Framework Composites for Theragnostics and Drug Delivery Applications, *Biotechnol. J.*, 2021, **16**, 2000005.

337 N. I. Gumerova and A. Rompel, Speciation atlas of polyoxometalates in aqueous solutions, *Sci. Adv.*, 2023, **9**, eadi0814.

338 D. E. Salazar Marcano, S. Lentink, M. A. Moussawi and T. N. Parac-Vogt, Solution Dynamics of Hybrid Anderson–Evans Polyoxometalates, *Inorg. Chem.*, 2021, **60**, 10215–10226.

339 Y. Liu, Y. Wu, M. Su, W. Liu, X. Li and F. Liu, Developing Brønsted–Lewis acids bifunctionalized ionic liquids based heteropolyacid hybrid as high-efficient solid acids in esterification and biomass conversion, *J. Ind. Eng. Chem.*, 2020, **92**, 200–209.

340 R. F. Cotta, R. A. Martins, M. M. Pereira, K. A. da Silva Rocha, E. F. Kozhevnikova, I. V. Kozhevnikov and E. V. Gusevskaya, Heteropoly acid catalysis for the isomerization of biomass-derived limonene oxide and kinetic separation of the trans-isomer in green solvents, *Appl. Catal., A*, 2019, **584**, 117173.

341 M. F. M. Gunam Resul, A. M. López Fernández, A. Rehman and A. P. Harvey, Development of a selective, solvent-free epoxidation of limonene using hydrogen peroxide and a tungsten-based catalyst, React, *Chem. Eng.*, 2018, **3**, 747–756.

342 D. C. Batalha, S. O. Ferreira, R. C. Silva and M. J. Silva, Cesium-Exchanged Lacunar Keggin Heteropolyacid Salts: Efficient Solid Catalysts for the Green Oxidation of Terpenic Alcohols with Hydrogen Peroxide, *ChemistrySelect*, 2020, **5**, 1976–1986.

343 M. Daraie, M. Mirzaei, M. Bazargan, V. S. Amiri, B. A. Sanati and M. M. Heravi, Lanthanoid-containing polyoxometalate nanocatalysts in the synthesis of bioactive isatin-based compounds, *Sci. Rep.*, 2022, **12**, 12004.

